Data Rate Enhancement & Interference Mitigation in the Design of Cognitive Radcom

By

Muhammad Fahad Munir

16-FET/Ph.D(EE)/F18

A dissertation submitted to IIU in partial fulfillment of the requirements for the degree of

DOCTOR OF PHILOSOPHY

Department of Electrical & Computer Engineering
Faculty of Engineering and Technology
INTERNATIONAL ISLAMIC UNIVERSITY
ISLAMABAD

2024

LIST OF PUBLICATIONS

1. Munir, Muhammad Fahad, Abdul Basit, Wasim Khan, Athar Waseem, Muhammad Mohsin Khan, Ahmed Saleem, Salman A. AlQahtani, Amil Daraz, and Pranavkumar Pathak. 2023. "Hybrid FSK–FDM Scheme for Data Rate Enhancement in Dual-Function Radar and Communication". Sensors 23, $no.12 : 5440.$ $htt ps : //doi.org/10.3390/s23125440$

2. Muhammad Fahad Munir, Abdul Basit, Wasim Khan, Ahmed Saleem, Aleem Khaliq and Nauman Anwar Baig, "Deep Learning-Enabled Design of Joint Cognitive Radar and Communication System for Interference Mitigation in Noisy Channels", Computers and Electrical Engineering. 2024. DOI: https://doi.org/10.1016/j.compeleceng.2024.109663

3. Muhammad Fahad Munir; Abdul Basit, Wasim Khan, Ahmed Saleem, Abdurrehman Al-Salehi, "A Comprehensive Study of Past, Present, and Future of Spectrum Sharing and Information Embedding Techniques in Joint Wireless Communication and Radar Systems". Wireless Communications and Mobile Computing 2022. DOI: $htt ps : //doi.org/10.1155/2022/9642849$

4. Muhammad Fahad Munir, Abdul Basit, Athar waseem, Mardenee bin Rouslee, Wasim Khan and Ubaid Umar, "Cognitive Fusion of Radar and Communication Functions: Deep Learning Perspectives", The Multimedia University Engineering Conference 2024 (MECON 2024)

5. M. F. Munir, A. Basit, W. Khan, A. Waseem, A. Saleem and A. Al-Salehi, "Frequency Quadrature Amplitude Modulation based Scheme for Dual Function Radar and Communication Systems," 2022 International Conference on Engineering and Emerging Technologies (ICEET), Kuala Lumpur, Malaysia, 2022, pp. $1-5$, doi: $10.1109/ICEET56468.2022.10007302.$

6. Qamar, Muhammad Salman, Ihsan ul Haq, Muhammad Fahad Munir, Athar Waseem, , Mardenee bin Rouslee, Adnan Anwar awan, "Enhancing Energy Efficiency in WSNs with Hybrid LEACH-D and ANN", The Multimedia University Engineering Conference 2024 (MECON 2024)

7. Muhammad Salman Qamar, Ihsan ul Haq, Amil Daraz, Atif M. Alamri, Salman AlQahtani, Muhammad Fahad Munir, "A Novel Approach to Energy Optimization: Efficient Path Selection in Wireless Sensor Networks with Hybrid ANN", CMC-Computers, Materials & Continua, ISSN:1546-2226

8. Ahmed Saleem, Abdul Basit, Muhammad Fahad Munir, Athar Waseem, Wasim Khan, Aqdas Naveed Malik, Salman A. AlQahtani, Amil Daraz, and Pranavkumar Pathak. 2023. "Alternating Direction Method of Multipliers-Based Constant Modulus Waveform Design for Dual-Function Radar-Communication Systems" Entropy 25, no. 7 : 1027. *https://doi.org/*10.3390/*e*25071027

9. Muhammad Salman Qamar, Shanshan Tu, Farman Ali, Ammar Armghan, Muhammad Fahad Munir, Fayadh Alenezi, Fazal Muhammad, Asar Ali, and Norah Alnaim. 2021. "Improvement of Traveling Salesman Problem Solution Using Hybrid Algorithm Based on Best-Worst Ant System and Particle Swarm Optimization" Applied Sciences 11, no. 11 : 4780.. *https://doi.org/*10.3390/*app*11114780

10. Ahmed Saleem, Abdul Basit, Muhammad Fahad Munir, Athar Waseem, Wasim Khan, Aqdas Naveed Malik, "Optimizing Penalty Parameter Selection of Alternating Direction Methods of Multipliers for an Improved Joint Radar-Communication Waveform Design" (Submitted to Digital Signal Processing. revision Submitted)

11 : Ahmed Saleem, Abdul Basit, Muhammad Fahad Munir, Athar Waseem, Wasim Khan, Aqdas Naveed Malik, "Beam space Design for Joint Radar-Communication Systems", (sub-

mitted to " Wireless Personal Communications", Springer Limited.)

12. Muhammad Salman Qamar, Ihsan ul Haq, Muhammad Fahad Munir, Aimal Daraz, Adnan Anwar Awan, Baitullah Bareer, "Innovative Approaches for Energy efficiency in WSN; LEACH-D and ANN integration", (submitted to IEEE Access. Revision Submitted)

13. Elahi, A., Qureshi, I.M., Zaman, F. et al. Techniques for the suppression of sidelobes in a non-contiguous orthogonal frequency division multiplexing framework. Appl Inform $3,6(2016)$. $https://doi.org/10.1186/s40535-016-0022-1$

14. A. Waseem, A. Khaliq, R. Ahmad and M. F. Munir, "Channel equalization for MIMO-FBMC systems," 2016 International Conference on Intelligent Systems Engineering (ICISE), Islamabad, Pakistan, 2016, pp. $272-277$, doi: $10.1109/INTELSE.2016.7475133$.

15. A. Khaliq, A. Waseem, M. F. Munir and R. Ahmad, "Comparison of adaptive noise cancelers for ECG signals in wireless biotelemetry system," 2016 International Conference on Intelligent Systems Engineering (ICISE), Islamabad, Pakistan, 2016, $pp.181-184$, $doi: 10.1109/INTELSE.2016.7475117$.

16. Z. -U. Khan, A. Naveed, F. Munir and F. Zaman, "Efficient sidelobe suppression by matching beams in two polynomial technique," 2016 International Conference on Intelligent Systems Engineering (ICISE), Islamabad, Pakistan, 2016, $pp.345-349$.
doi: $10.1109/INTELSE.2016.7475147$.

17. Atif Elahi,Ijaz Mansoor Qureshi,Fawad Zaman,Fahad Munir,"Reduction of out of band radiation in NonContiguous OFDM based cognitive radio system using heuristic techniques", Volume 32, Issue 2, Pages $349-364$, Journal of Information, Science and Engineering.

18. Fawad Zaman, Ijaz Mansoor Qureshi, Fahad Munir, Zafar Ullah Khan,"Four-dimensional parameter estimation of plane waves using swarming intelligence". Chinese Physics B, Volume 23, Number 7. Published 22 May 2014. $DOI 10.1088/1674-1056/23/7/078402$.

This dissertation includes the research articles from S. No 1 to 5.

Copyright © 2024 by Muhammad Fahad Munir

All rights reserved. It is declared that the research work presented in this dissertation "Data Rate Enhancement & Interference Mitigation in the Design of Cognitive Radcom", is solely my work.

DEDICATION

My respected teachers, parents, brothers, sisters, wife, kids and friends.

Abstract

In dual-function radar and communication (DFRC) systems, radar and communication functionalities utilize the same hardware and frequency band. Typically, radar operations take place in the main lobe, while communication tasks are performed in the side lobes. However, situations may arise where both the radar target and the communication receiver are located within the main lobe or side lobes. Such scenarios lead to interference and a consequent reduction in data rates.

Two approaches are proposed to enhance communication data rates. The first combines Frequency Shift Keying (FSK) with Quadrature Amplitude Shift Keying (QASK) or Quadrature Amplitude Modulation (QAM), termed FQAM, which improves performance by embedding information in both frequency and constellation number. The second approach, FSK-FDM, combines FSK and Frequency Division Multiplexing (FDM) to modulate multiple FSK symbols for higher data rates, improving bit rate and reducing bit error rate (BER) via waveform and frequency selection, independent of receiver position.

A deep learning-based approach is employed to enhance data rates and mitigate interference. The method selects the optimal waveform from a pool of orthogonal waveforms, using adaptive constellation and QASK/QAM waveforms when both the radar and receiver are in the main lobe, and PSK-based waveforms when the receiver is in the side lobe. The receiver transmits signal-

to-noise ratio (SNR) and data to the DFRC fusion center, which adjusts the waveform, data rate, and constellation for the next Pulse Repetition Interval (PRI). This cognitive technique optimizes spectrum usage, radar tracking, and security.

The proposed methods were simulated across various scenarios, demonstrating superior performance in data rate and interference mitigation compared to existing techniques. Simulation results validate the effectiveness of these approaches.

Acknowledgements

Allah, The Most Merciful, The Most Gracious, I would like to express my gratitude to Allah for granting me the stamina and endurance to complete this research. All praise and thanks to Allah for His last Prophet Muhammad (Sallulahu 'Alayhi wa Sallam) and all of His Sahaba (Razi-Allahu 'Anhu) who dedicated their lives to Dawah and the dissemination of knowledge.

I extend my profound gratitude to my Supervisor, Dr. Abdul Basit, and my Co-Supervisor, Dr. Wasim Khan, for their unwavering support, inspiration, innovative ideas, and invaluable guidance throughout my PhD journey. Their dedication ensured consistent progress, as they never allowed me to miss a weekly presentation or meeting, always taking time to discuss and review my work. Moreover, Dr. Abdul Basit's prompt responses to my messages on WhatsApp further exemplified his commitment, ensuring I always had the support I needed. Without their continuous efforts and kind mentorship, this PhD would not have been possible.

Special thanks to my teacher, Prof. Dr. Ijaz Mansoor Qureshi (late), who always encouraged me and provided the spirit and guidance necessary for this research. I express my heartfelt thanks to my colleague, Dr. Ahmad Saleem, who consistently assisted me in times of need.

My Father, Mother (Late), brother, sisters, wife, kids, other family members, and friends deserve my gratitude. Their prayers, love, and unwavering support

throughout my education were among the strongest motivators.

("Muhammad Fahad Munir")

Contents

List of Tables

List of Figures

List of Abbreviations

Abbreviation	Full Form
AM	Amplitude Modulation
ACM	Automatic Modulation Classification
ANN	Artificial Neural Network
ATC	Air Traffic Control
AWGN	Additive White Gaussian Noise
BN	Batch Normalization
BER	Bit Error rate
BPSK	Binary Phase Shift Keying
BP	Backpropagation
CAESAR	Carrier AgilE phaSed Array Radar
CNN	Convolutional Neural Network
CR	Cognitive Radio
CSK	Code Shift Keying
CU	Communication User
CRSS	Communication and radar spectrum sharing
DFRC	Dual Function Radar and Communication
DFT	Discrete Fourier Transform
DL	Deep Learning

DNN	Deep Neural Network
DPSK	Differential Phase Shift Keying
DSP	Digital Signal Processing
ECC	Error-Correcting Code
EDGE	Enhanced Data rates for GSM Evolution
FFT	Fast Fourier Transform
FM	Frequency Modulation
FSK	Frequency Shift Keying
FQAM	Frequency Quadrature Amplitude Modulation
GAN	Generative Adversarial Network
GRU	Gated Recurrent Unit
GSM	Global System for Mobile Communications
GPRS	General Packet Radio Service
HMM	Hidden Markov Model
ICSI	interference channel state information
I/Q	In-phase/Quadrature
IF	Intermediate Frequency
ISI	Inter-Symbol Interference
ISAC	Integrated sensing and communication
INR	Interference to noise ratio
IoT	Internet of Things
ITU	International Telecommunication Union
JRC	Joint Radar and Communication
KNN	K-Nearest Neighbors
LFM	Linear Frequency Modulation
LSTM	Long Short-Term Memory

LPI	Low Probability of Intercept
LTE	Long-Term Evolution
MAC	Medium Access Control
MAPAR	Multi-carrier Agile Phased Array Radar
MIMO	Multiple Input Multiple Output
ML	Maximum Likelihood
MMSE	Minimum Mean Square Error
MLP	Multi-Layer Perceptron
MSE	Mean Squared Error
NTIA	National Telecommunications and Information Administration
NN	Neural Network
NR	New Radio
OFDM	Orthogonal Frequency Division Multiplexing
OOK	On-Off Keying
PARP	Peak-to-Average Power Ratio
PCM	Pulse Code Modulation
PRF	Pulse Repetition Frequency
PSD	Power Spectral Density
PSK	Phase Shift Keying
QAM	Quadrature Amplitude Modulation
QPSK	Quadrature Phase Shift Keying
RMSE	Root Mean Square Error
RCC	Radar-communication coexistence
RNN	recurrent neural network
SAR	synthetic aperture radar

SNR	Signal-to-Noise Ratio
SDR	Software Defined Radio
STFT	Short-Time Fourier Transform
SVM	Support Vector Machine
TDMA	Time Division Multiple Access
TDOA	Time Difference of Arrival
UAV	Unmanned Aerial Vehicle
V2C	vehicle to cloud
V2N	vehicle to network
V2P	vehicle to Pedestrian
V2V	vehicle to vehicle
WCDMA	Wideband Code Division Multiple Access
WiFi	Wireless Fidelity
WRC	World Radio Communication Conference
WLAN	Wireless Local area network

Chapter 1

INTRODUCTION

To ensure a high data rate and improved quality of service, increasing bandwidth is mandatory for wireless communication. Consequently, the growth of wireless communication applications with these properties has led to a tremendous rise in the auction price of the available frequency spectrum. Given the increasing demand for data rates, network providers are constrained to consider the reuse of available spectrum currently allocated to other technologies. Radar spectrum emerges as a prime candidate for integration into different communication systems, as substantial portions of the spectrum are readily accessible at radar frequencies. Conventional radar applications worldwide encompass air traffic control (ATC), geophysical monitoring, climate observation, and security exploration, among others. However, radar systems designated for monitoring purposes are now being adopted for communication by sharing the spectrum. Currently, the allocated frequency bands can be broadly categorized into two groups: radar systems and communication systems. Although a significant portion of the frequency bands from 1 to 10 GHz is primarily allocated to radar operations, new collaboration opportunities with communication systems such as 5G NR, LTE, and Wi-Fi are paving the way for novel possibilities. On one hand, sharing high-frequency bands, such as the millimeter-wave band, benefits

both communication and radar platforms by enabling high data rates and improved target tracking. On the other hand, there are concerns about interference from both military and civilian applications, particularly for critical radar operations. In the past decade, radars have evolved with increased precision and a broader range of capabilities, including surveillance, clutter management, back scanning, and handling false alarms simultaneously. Therefore, they require higher frequency bands compared to traditional radars. Moreover, the growth of civil activities and the emergence of new technologies in social media have dramatically increased, putting strong pressure on the bandwidth allocation board. Since higher bandwidth for radar, as well as standalone communication designs, is the need of the day, it also warrants the hybridization of both designs (i.e., radar and communication) to attain joint benefits at higher bandwidths. However, all the aforementioned challenges need to be addressed properly. This includes identifying frequency bands that could be made available for wireless broadband, which is necessary for the improved overall performance of joint radar and communication designs. The International Telecommunication Union (ITU) and the World Radio Communication Conference (WRC) review the allocation of the frequency spectrum annually, and in the United States of America, the National Telecommunications and Information Administration (NTIA) has dedicated its efforts to identifying frequency bands that could be made available for wireless broadband service provision alongside radar operations. It has been reported in the literature that in the L band, the GSM system (GPRS, EDGE) can overlap with UHF radars operating between 1 to 2 GHz, whereas in the S-band, Long Term Evolution (LTE) and WiMax overlap with Airport Surveillance or Air Traffic Control (ATC) radar within a frequency range between 2 to 4 GHz. Other examples of WiMax and radar overlap are

mentioned by several researchers. Finally, millimeter waves, which are used for Orthogonal Frequency Division Multiplexing (OFDM), single carrier, WLAN, ranging from 11 ft to 33 ft, are used for indoor communication and overlap with high-resolution imaging radar. Similarly, the same OFDM-based Wireless LAN (WLAN) used for outdoor activities, ranging from 100 m to 5 km using OFDM, overlaps with weather radar operating between 2 to 4 GHz in the C band. Thus, to fulfill the need for extra bandwidth for wireless communication, further exploration of spectrum sharing is needed. Notably, the enhanced data rates and interference mitigation capabilities warrant a thorough investigation to meet the need of modern day technologies i.e., 5G and beyond. Therefore, innovative solutions for effective and reasonable spectrum sharing is needed.

1.1 Background

Previously, various authors utilized their expertise to explore the performance of radar and communication systems as independent entities for an extensive period. Radar experts and specialists have been engaged in endeavors aimed at identifying and enhancing various parameters, including but not limited to range estimation, velocity, target speed, angle of arrival, scanning and tracking surveillance, radar cross-section, and other metrics. Additionally, efforts have been focused on angle-to-range fixation calculations, as observed in phased array radar systems. Moreover, cognitive methodologies, as proposed by Simon Haykin, have been adopted to equip radar systems with the ability to perceive their environment through feedback mechanisms derived from their surroundings. In comparison to the swift advancements observed in radar technology, the field of communication technologies is experiencing rapid progress

across various formats and applications. Scholars and professionals are dedicated to exploring methods for augmenting data transmission rates, minimizing interference, and refining signal-to-noise ratio parameters. This focus extends to contemporary developments within communication technologies, including the evolution of 4th and 5th-generation systems, where researchers are particularly concerned with optimizing both the speed and integrity of data transmission in these systems. In both radar and communication systems, similar mathematical principles and the electromagnetic spectrum are employed, along with the utilization of single and multiple antenna arrays. Moreover, advancements in digital signal processing serve to bridge the divide between these two technological domains. These developments have given rise to a novel breed of radar with adaptive capabilities and the capacity for coexistence, allowing it to function alongside other systems and derive mutual benefits. This innovative hybrid radar paradigm has been characterized by various names and configurations, empowering researchers and experts to address the fundamental objectives of both systems.

1.2 Significance of Research

The proposed research is highly significant in the DFRC field due to its open-ended nature, and very little work has been done to date, to the best of my knowledge. Concerns about spectrum overcrowding and limitations in frequency bands have encouraged researchers to focus more on spectrum management. This has led us to use the concept of Cognitive Dual Function Radar and Communication (Cognitive DFRC). On the other hand, developing new schemes for coexistence among the diverse facilities has increased competi-

tion. Thus, the need to design a new transceiver, along with their temporal or spatial degrees of freedom, including techniques for improved data rates and interference mitigation abilities are employed to achieve the goals for DFRC systems.

1.3 Problem Statement

Recent literature shows that multiple sidelobe levels have been used to transmit binary bits using either ASK or PSK without disrupting main radar operations. However, the data rate achieved is very low, as it is constrained by the Pulse Repetition Frequency (PRF), ranging from KHz to a few MHz. This low data rate results from embedding only one or two bits (symbols) per radar pulse. Additionally, the combined radar and communication design, which uses the same transmit array, reduces overall efficiency in DFRC systems. This reduction affects Signal-to-Noise Ratio (SNR) levels, target estimation/detection, and Bit Error Rate (BER) on both the radar and communication sides. Another significant concern is interference detection and mitigation, which limits the performance of both radar and communication receivers. Interference can be intentional (e.g., clutter, self-introduced jamming) or unintentional (e.g., microwaves, X-rays/MRI, high-voltage lightning), leading to spectrum congestion. New methods for data rate enhancement and interference mitigation are needed to be thoroughly investigated to explore potential degrees of freedom in DFRC systems.

1.4 Objectives of Research

In light of the above discussion, the primary objective of this research is to develop an advanced cognitive architecture for DFRC systems to enhance communication data rate and interference mitigation to significantly enhance overall system performance. The key objectives have been listed below:

- **Data Rate Enhancement for DFRC**: The first objective is to implement different strategies to optimize data transmission rates within DFRC systems, overcoming traditional limitations imposed by Pulse Repetition Frequency (PRF) and ensuring the efficient utilization of available bandwidth.
- **Interference Mitigation Between Target and Communication User**: The second objective is to deploy sophisticated interference mitigation techniques to minimize the impact of both intentional and unintentional interference sources in DFRC systems, thereby improving target detection accuracy and ensuring robust communication reliability, simultaneously.
- **Increased Efficiency with Joint Platform Utilization at Transmitter through Perception-Action Cycle**: The third objective is to optimize the integration of a joint platform at the transmitter level to maximize system efficiency based on perception-action cycle i.e. Cognitive DRFC system. This approach aims to achieve superior SNR levels for enhanced data rates, reduced Bit Error Rate (BER) and precise target estimation for communication and radar operations, respectively.

1.5 Contribution of the Research

The main contributions can be summarized as follows:

1 **Frequency Quadrature Amplitude Modulation based technique**: The first contribution of this research is the proposed Frequency Quadrature Amplitude Modulation (FQAM) technique, which utilizes both Frequency Shift Keying (FSK) and Quadrature Amplitude Shift Keying/Quadrature Amplitude Modulation (QASK/QAM) to enhance the data rate of a DFRC system. This novel technique embeds information in both the frequency and amplitude of constellation symbols, thereby increasing the data rate. The method improves interference mitigation by safeguarding against intercepts from directions other than the pre-assigned communication directions, allowing for the transmission of information to single or multiple communication directions regardless of their location (e.g., whether the communication receiver is in the main or side lobe of the generated beam pattern). Additionally, the decoding of each FQAM symbol by each communication receiver is independent of neighboring symbols in the sequence.

2 **A Hybrid Frequency Shift keying and Frequency Division Multiplexing based Approach**: The second contribution of this research is the introduction of a new approach that combines Frequency Shift Keying (FSK) with Frequency Division Multiplexing (FDM) for embedding information into radar-based waveforms. In this approach, multiple orthogonal communication symbols are modulated within a single pulse using FDM. This design improves the bit rate (BR) and reduces the bit error rate (BER) for communication receivers, regardless of their location within the radar's main lobe or side lobe regions. Additionally, it minimizes inter-symbol interference by ensuring that the decoding of each composite symbol at any communication receiver is independent of neighboring symbols.

3 **Deep Learning-Enabled Cognitive Design for DFRC**: The third contribution of this research is the proposed cognitive DFRC architecture, which employs a pool of orthogonal waveforms at the transmitter. Utilizing a perception-action cycle, this technique adapts to QAM, QASK, and PSK-based waveforms and constellation numbers based on feedback from the DFRC receiver. Importantly, the cognitive DFRC structure incorporates a Convolutional Neural Network (CNN) architecture designed to autonomously learn and extract features from received signals with varying SNRs, enabling the transmitter to adapt to changing scenarios.

1.6 Thesis Organization

This doctoral thesis explores the integration of radar and communication functionalities within a single system, with the goal of enhancing data rate and interference mitigation capabilities. The research is organized into four main chapters, each addressing key aspects of the DFRC system and contributions. Chapter One provides an introduction to the motivation, objectives, and scope of the study. It highlights the increasing demand for multifunctional systems and outlines the challenges and opportunities in the field of radar-communication integration.

Chapter Two presents a comprehensive literature review, synthesizing existing research on dual-function radar and communication systems. The review covers various aspects, including waveform design, interference mitigation, and modulation techniques, providing a solid foundation for the proposed methodologies.

Chapter Three, a novel FQAM modulation-based technique is introduced

for information embedding and interference mitigation in dual-function systems. This technique aims to optimize spectral efficiency while ensuring robust communication and radar performance. The proposed method is thoroughly analyzed through theoretical modeling and simulation results.

Chapter Four focuses on deep learning-based techniques for communication receivers in dual-function systems. Specifically, an approach for received signal identification and automatic modulation classification is proposed. The effectiveness of the proposed method is validated through extensive simulation experiments, demonstrating its potential for real-world applications.

The thesis concludes with a summary of key findings and discussion of future research direction. The potential for further advancements in dual-function radar and communication systems is highlighted, emphasizing the importance of continued research in this rapidly evolving field.

Chapter 2

Literature Review: Spectrum Sharing and Information Embedding Techniques

This section aims to thoroughly evaluate recent advancements in CRSS (Communication and Radar Spectrum Sharing) and DFRC (Dual-Functional Radar-Communication). This thesis investigates the latest trends in DFRC design, focusing on data embedding techniques. The discussion begins with an overview of various spectrum-sharing techniques, followed by an explanation of the DFRC data model. Then different methods of embedding information in radar waveforms, such as amplitude and phase shift keying, phase rotation invariance method, and time modulation arrays, are explored. Subsequently, various techniques for modifying communication waveforms to support radar functions and beam pattern-based modulation techniques like sub-beam sharing are explored. Furthermore, the performance of different DFRC information embedding methods are compared in terms of interference mitigation, secure communication, improved bit error rate (BER), and data rate enhancement. Lastly, different research challenges in the field are highlighted and directions for future studies are suggested.

2.1 Spectrum Sharing Approaches for DFRC

The crowding of the spectrum cannot be addressed by traditional communication techniques and beamforming approaches [1–4]. Therefore, the co-existence of both radar and communication designs is highly necessary for radar emission and communication on the available spectrum [5–8]. In a broader sense, this co-existence can occur either through time-based sharing or by embedding information into radar emissions for the same spectrum. The following subsections provide details about integrating radar-communication designs and diverse spectrum-sharing methods.

2.1.1 Time Sharing Approach

One of the simple methods to integrate radar with communication is to use time-based sharing of resources [9–11]. A strobe switch is used for switching between radar and communication users [12] as shown in Figure 2.1.

Note that, when a communication process is required, the strobe switch will turn OFF the radar operation and allow the communication modem to transmit and receive and vice versa for the radar operation. For this purpose, some protocols need to be devised so that enabling and disabling communication links does not affect the radar performance. This type of system is also known as the radar system joined with the communication [12]. The design of such a system is simple but it degrades the radar efficiency. The radar operation utilizes the frequency-modulated continuous wave (FMCW), while the commu-

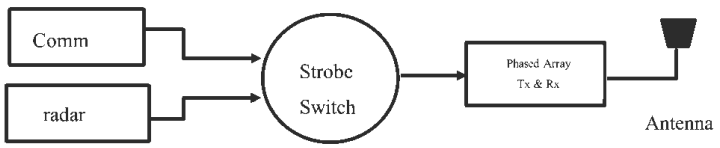

Figure 2.1: Time sharing strobe switch

nication symbol is encoded by using either ASK, FSK, or PSK, while higher order schemes can also be used e.g., QAM. The limitation of this technique is the reduced efficiency and less time slot allocation for radar and communication users, respectively. Thus, this technique is only feasible when small bursts of data are used.

The authors in [13] used different waveforms for radar and communication to mitigate the interference issues. The $M_T \times 1$ transmitted signal can be written as

$$\mathbf{s}(\mathbf{t}) = \mathbf{s}_r(t) + \mathbf{s}_c(t) \tag{2.1}$$

Where, $\mathbf{s}_r(t)$ is radar based waveform while $\mathbf{s}_c(t)$ communication based waveform respectively. The system resources are distributed between radar and communication in the time domain, which results in performance degradation [14]. To allocate the resources in different time domains by using nonoverlapping frequency is studied in [15], while random antenna switching in [16] and media access control in [17]. Similarly, the sub-carrier approach of OFDM in time sharing is also implemented in [18] and in [19] optimized the subcarrier by using a-priory knowledge target and statistical model is studied.

2.1.2 Spectrum Sharing Approach

Contrary to the previous approach, both radar and communication operations work simultaneously in spectrum sharing all the time [20].

This sharing leads us to the new paradigm of research, which is called communication and radar spectrum sharing (CRSS) or integrated sensing and communication (ISAC). This CRSS is further divided into two broad categories, one is temporal coexistence or joint radar and communication (JRC), while the

other is dual function radar and communication (DFRC).

2.1.2.1 Joint Radar and Communication Coexistence

This is the first type of CRSS which is also called radar-communication coexistence (RCC), where the same frequency band is used to perform radar operations as well as communication operations. Furthermore, it does not require common transmitting hardware as shown in Figure 2.2. This type of system is also called an opportunistic system or joint radar and communication (JRC). In this technique, the spectrum sensing (i.e., radar operation) acts as a primary user, while the communication operations are performed on a secondary basis. In this arrangement, the radar transmitter scans the entire environment and tracks its target. During the scanning process, the signals received by both the communication transmitter and receiver are considered interference. Moreover, during communication activity, the signal received by the radar receiver from the communication transmitter is considered interference and will be mitigated. Authors of [21] divided the concept of JRC into three broad categories, i.e. coexistence, cooperation, and co-design.

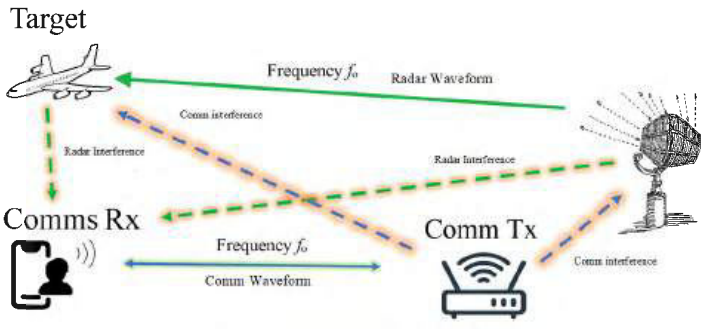

Figure 2.2: Radar and Communication Coexistence

Coexistence & Cooperation

In co-existence, interference is mitigated without exchanging information [21], while in co-operation, information is explicitly shared with beneficiaries i.e. radar and communication system [20]. In later cases, both systems improve the system performance by using shared knowledge. Interference is mitigated jointly and this level of collaboration is the first step towards joint architecture and attempting RF convergence. This branch leads towards cognitive behavior between radar and communication systems, which is explained in the next section.

Codesign

Eventually, in co-design both systems need to be designed jointly. There are two possibilities, either by using the same hardware at the transmitter side or by using the same waveform [22]. To avoid interference, the communication devices need to keep their power levels under certain threshold levels. Authors in [23–25] studied that communication is only allowed if it will not compromise the radar operation. The performance merit for communication is set under the following three constraints, which are: i) average data rate for a small distance between radar and communication receiver, ii) half duplex communication only, and iii) percentage of time that communication user can transmit. Similarly, in [26], another scenario is studied where the radar senses the entire spectrum periodically, while the cellular base station (BS) is only allowed to communicate if it lies in sidelobes of the main radar beam. In this case, the performance will be evaluated by keeping the minimum tolerable distance in terms of interference-to-noise ratio (INR). The main drawback of this technique is that the communication receiver cannot fully utilize the spectrum and it must

keep its power below certain levels. Mis–detection due to spectrum sharing between an American integrated naval weapons system and with a cellular system including 100 base stations operating at $3.5GHz$ in S-Band, which raised the interference management and power allocation respectively is investigated in [27]. Thus, to improve the above-mentioned drawbacks, authors in [28] studied the regulatory policies for 10 GHz band where sharing occurs between radar and communication users in terms of sensing and relocation techniques. In the same line of action, [29] discussed sharing the spectrum with rotating radar in detail and authors in [30; 31] studied the spectrum sharing when the distance between radar and communication is fairly large given that performance is not affected. Another study is carried out by [32] to investigate the performance of shared spectrum in the L band for rotating radar and fixed communication users. In their study, the communication user is supposed to limit its transmit power when it senses the radar main beam.

Precoder-based design is another solution to this problem, which uses interference channel state information (ICSI). In this case, the radar transmitter first estimates the information of the pilot signal being transmitted by the communication receiver and maintains a given ratio of INR [33]. This technique mitigates the interference efficiently. However, it can only be applied in scenarios where radar has primary privileges. Another drawback to this scheme is its computational complexity cost at the radar transmitter. Likewise, the communication receiver first identifies the mode of the radar (i.e., either probing or scanning) and then starts its communication. The other solution is to build an efficient receiver for improved interference mitigation. The primary task of such a receiver is to evaluate the target parameters in the existence of the BS interference. This receiver can either be at the radar side or the BS side. In [34], a

null-space precoder-based approach is used on radar waveform by using singular value decomposition (SVD), this results in zero-forced interference to communication user. The system is further improved by using optimization-based techniques in precoder design in [35] and [36] in the presence of clutter. The overall drawback of the aforementioned precoder-based techniques is they rely on the knowledge of the interfering channel between the radar and the communication user. One way to have such information is by sending training signals by DFRC transmitter to all communication receivers or by getting through the coordination office connected to both radar and communication system [35], this burdens the system in terms of spectrum and computational complexities. It is concluded by [37] that those communication users who are trying to obtain the spectrum initially allocated to radar must guarantee the target detection rather than obtaining ICSI.

2.1.2.2 Cognitive Radar and Communication

Making devices capable of dual functionality can lower prices and improve spectrum management. To address interference and high data rate needs for both systems, communication receivers should be adaptable to sense the radar environment, and radars should be modified to detect communication signals. Cognitive behavior must be implemented on both the transmitter side and the radar and communication receivers [38; 39]. Thus, by upgrading the radars and communication users to do cognition, i.e., the ability to make their own decisions according to needs has been warranted. However, without any central administration, all the networks will face chaos and congestion. Note that a modified version of JRC, incorporating cognition between radars and multiple communication users, is discussed in [40]. Centralized control is utilized to

assign thresholds to power levels for communication users. In [39], similar concepts are applied to the DFRC network, as depicted in Figure 2.3.

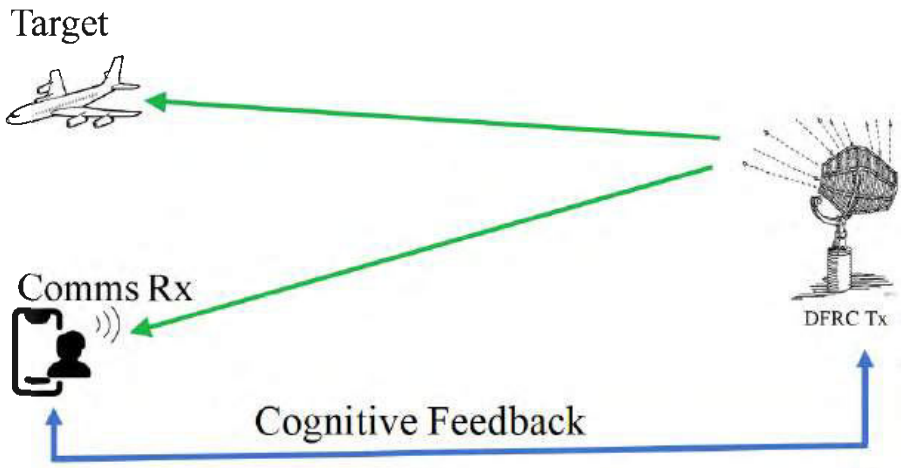

Figure 2.3: Cognitive behaviour for Radar & Communication

This approach employs a single hardware to transmit a dual-nature waveform, benefiting both radar operations and communication users. Likewise, the efficient utilization of bandwidth through dynamic frequency allocation is explored in [41; 42]. In [43; 44] Lagrangian optimization techniques have been applied to obtain solutions for power allocation to communication users. Furthermore, [45] studied dynamic power allocation to communication users while maintaining a satisfactory threshold level for transmission. In [46], the authors investigated how communication users can adaptively adjust their transmit power to maximize the data rate. Optimal power control and adaptive data rate were proposed in [47; 48] to maximize the capacity of communication users capacity while maintaining average interference power and peak transmission power constraints. Additionally, [49] studied fast power allocation to communication users with a constraint on low computational complexity to achieve an optimal solution.

2.1.2.3 Dual Function Radar Communication (DFRC)

The other major branch of CRSS is DFRC [50; 51]. In this category, the radar and communication systems work on a single hardware at the transmitter side for both functions as shown in Figure 2.4.

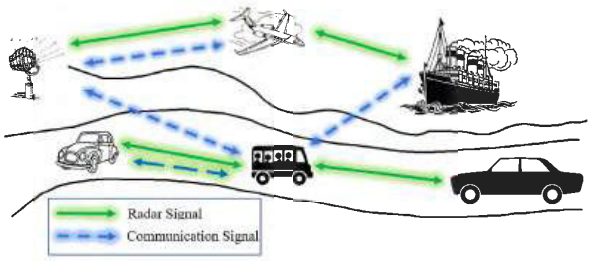

Figure 2.4: Dual Function Radar and Communication

This technique is also called intentional modulation on a pulse [52] or a Co–Radar [53]. This joint approach provides efficient utilization of power [54], less weight, and reduced system size on one hand and provides compatibility to avoid spectrum congestion's on the other hand as studied by [15; 55; 56]. The DFRC system performs radar operations and communication tasks simultaneously by using a dual-nature waveform. The overreaching objective of the DFRC is to utilize the radar spectrum to capitalize on the resources by using existing infrastructure. These resources may include multi-sensor beamforming, high power and high-gain antennas, and large bandwidth.

Keeping in mind the smart nature of the DFRC to sense the nearby environment, these are employed in synthetic aperture radar systems (SAR) designs, vehicle-to-vehicle (V2V) communication, vehicle to network, (V2N), vehicle to pedestrian (V2P) and vehicle to cloud (V2C) communication designs as mentioned by [57]. These features enable the DFRC to be the most suitable candidate for vehicular network applications. The main aim of successful communication is to maximize the data rate by embedding information in the transmitted

waveform [58], while radar waveforms focus on maximizing detection performance [59–61]. Thus, a dual-function system that performs radar and communication operations simultaneously involves a performance trade-off between these functions.

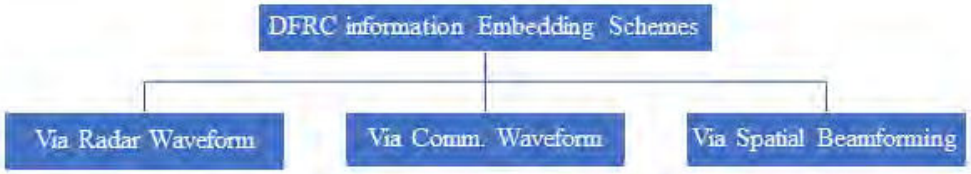

Figure 2.5: Information Embedding Tree diagram

Three different methods are devised to embed information bits in the waveform of a DFRC transmitter side. 1^{st} is embedding communication bits into radar waveform [62–64] while 2^{nd} is using communication waveform for radar operations as well [65; 66] and 3^{rd} is by using beamforming-based approaches [67; 68] as shown in hierarchical structure Figure 2.5.

To flourish the DFRC systems, researchers needed to devise signaling strategies vigorously and materialize the modulation schemes of the radar, which would lead to integrating and improving the use of the existing radio spectrum.

The following section presents an overview of DFRC systems from the information-embedding perspective in terms of data model, data rate, computational complexities, and radar capabilities. Note that, it discusses the various techniques and implementation strategies that define the state-of-the-art DFRC designs.

2.2 Radar waveform for information embedding

Information bits are embedded into radar waveforms. Radar operation is performed in the main lobe, while the communication receiver operation is

performed only in the side lobe regions [69]. To embed information into radar waveform-based DFRC, the following techniques are reviewed.

2.2.1 ASK Based Method

The most popular among all methods for information embedding in radar waveform is ASK-based waveform design [55] in which the communications bits are mapped to the side lobe levels of the received signal at the communication receiver. Two sets of weight vectors are used for this purpose. If the received signal has higher power than the predefined threshold ε, it will be considered as binary one and if the received power is below a certain threshold, it is considered as a binary zero as shown in Figure 2.6.

$$sidelobelevel = \begin{cases} \Delta_H = |\mathbf{w}^H \mathbf{a}(\theta_j)| \geq \varepsilon \\ \Delta_L = |\mathbf{w}^H \mathbf{a}(\theta_j)| < \varepsilon \end{cases} \tag{2.2}$$

The overall form of a radar waveform with information embedded to it at the transmitter of the DFRC is

$$\mathbf{s}(t,\tau) = \sqrt{\frac{M_T}{L_B}} \sum_{g=1}^{L_B} (B_L(\tau)\mathbf{w}_L^* + (1 - B_L(\tau))\mathbf{w}_H^*)\psi_g(t) \tag{2.3}$$

Similarly, the signals in Equation 2.4 are considered for the communication receiver.

By performing a simple ratio test,

$$\widehat{B}_L(\tau) = \begin{cases} 0, if|y_j(t,\tau)| \geq T \\ 1, if|y_j(t,\tau)| \leq T \end{cases} \tag{2.5}$$

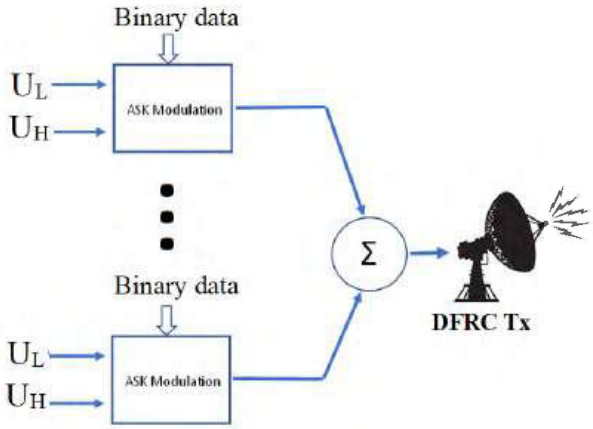

Figure 2.6: Amplitude Shift Keying based Information Embedding

$$y_j(t,\tau) = \begin{cases} \sqrt{\frac{M_T}{L_B}}\alpha_j \mathbf{c}_j(\phi_j)\sum_{g=1}^{L_B}[B_L(\tau)\mathbf{w_L}^H\mathbf{a}(\theta_j) + (1-B_L(\tau)\mathbf{w_H}^H\mathbf{a}(\theta_j))]\psi_g(t) + \mathbf{n_j}(t,\tau), B_L(\tau) = 1 \\ \sqrt{\frac{M_T}{L_B}}\alpha_j \mathbf{c}_j(\phi_j)\sum_{g=1}^{L_B}[B_L(\tau)\mathbf{w_L}^H\mathbf{a}(\theta_j) + (1-B_L(\tau)\mathbf{w_H}^H\mathbf{a}(\theta_j))]\psi_g(t) + \mathbf{n_j}(t,\tau), B_L(\tau) = 0 \end{cases} \tag{2.4}$$

Where, T is the threshold.

ASK is used to modulate the data in sidelobes [70]. Using the same analogy in [71] for multi-waveform, multi-user communication is used by creating multiple sidelobes levels (SLL). This uses an optimization technique to embed binary information. On one hand, this technique is simple to implement but on the other hand, it has a limited data rate. For a DFRC system to be more effective, the information embedding is secure against non-legitimate users located in directions. Another prominent scheme is devised by using side lobe AM-based communication, having the main lobe dedicated to radar operations, while the side lobe is dedicated to communication purposes. This sidelobe AM-based information embedding is achieved by two methods, The first is by use of time modulated array (which is explained in a subsequent section later), while the second approach is based on convex optimization. That is, K distinct SLLs are achieved by solving a convex beamforming problem to obtain weight vectors. During each radar pulse, one of the k^{th} weight vectors is utilized to transmit the

signal, where each weight vector represents a unique binary symbol.

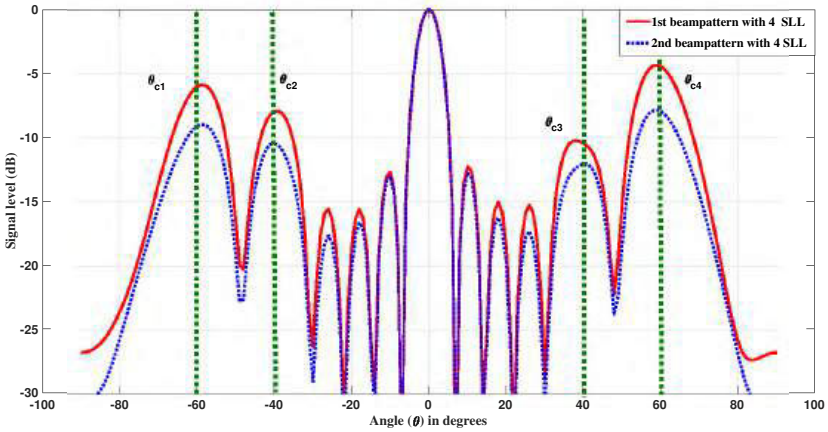

Figure 2.7: 4 Side Lobe Levels with 2 beams

Moreover, a generalized side lobe canceller method is implemented in [72], by using both the active and the listening modes of the radar. In active mode, the main lobe is used for radar operations while side lobes are dedicated for communication. In listening mode, there is no radar operation and the entire duration is dedicated for the communication. Eight SLLs are achieved by the author as shown in Figure 2.7. Two beampatterns with the same power in the main lobe are used for radar operations while variable sidelobes are used to accommodate four communication receivers. The Communication receivers were located at $\theta_{c1} = -60^o, \theta_{c2} = -40^o, \theta_{c3} = 40^o and \theta_{c4} = 60^o$. The red beampattern represents binary zero, while the blue beampattern represents binary one respectively. The first beampattern having red color has four sidelobe levels starting from $SLL_1 = -6$ dB, $SLL_2 = -7$ dB, $SLL_3 = -10$ dB, and $SLL_4 = -5$ dB respectively. Similarly, for 2^{nd} beampattern blue color line having the following SLLs which are $SLL_1 = -11$ dB, $SLL_2 = -9dB$, $SLL_3 = -8$ dB and $SLL_4 = -12$ dB . Thus to increase the number of communication receivers, the SLL must be increased.

2.2.2 PSK Based Method

Another technique is devised in [73], which uses a PSK modulation scheme to embed information. The phase shift will let us know whether the embedded bit is 1 or 0. Similarly, authors in [69] proposed phase modulation (PM) for embedding information into radar waveforms. Binary data is mapped with the phase of the signal, which is decoded by using a phase detector at the receiver side. PM-based information embedding provides more accurate results as compared to AM and multi-waveform ASK-based methods. Another advantage of the said scheme is that it can be used for both directional and broadcast modes and for coherent and non-cohere detection. In [74] authors claim that the PSK-based method is more secure as compared to the ASK based method because interference can disintegrate the SLL as compared to the phases of the waveform. If the communication is coherent, only one waveform is used with 1 beamforming weight vector, and if the communication is incoherent, a pair of waveforms and beamforming weight vectors are required, as shown in Figure 2.8. Communication symbols that are embedded into the phase of the signal equals the total number of waveforms minus one.

To ensure the radar operation, a unity power weight vector has to be used.

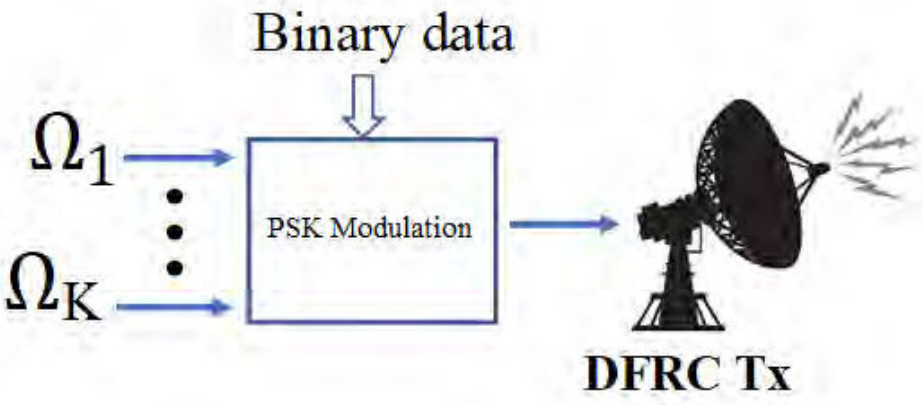

Figure 2.8: Phase Shift Keying based Information Embedding

The model of the DFRC radar waveform-based signal is as follows

$$\mathbf{s}(t,\tau) = \sqrt{\frac{P_T}{2}}[\mathbf{w_g}^* \psi_p + \mathbf{w_g}^* \psi_q] \tag{2.6}$$

Similarly, the model of the signal received at the communication receiver is given as

$$\mathbf{y_p}(\tau) = \sqrt{\frac{P_T}{2}}[\alpha_j(\mathbf{w_p}^H \mathbf{a}(\theta_j))] + \mathbf{n}_p(\tau) \tag{2.7}$$

and

$$\mathbf{y_q}(\tau) = \sqrt{\frac{P_T}{2}}[\alpha_j(\mathbf{w_q}^H \mathbf{a}(\theta_j))] + \mathbf{n}_q(\tau) \tag{2.8}$$

Where P_T is the power of the signal, $\psi_p(t)$ and $\psi_q(t)$ are two orthogonal radar waveforms with unity power, and $\mathbf{w_g}$ is the weight vector. α_j is the channel coefficient, $\mathbf{a}(\theta_j)$ is the steering vector towards the direction of j^{th} communication receiver and $\mathbf{n}_q(\tau)$ is AWGN. During each radar pulse, only one bit of information is embedded in the form of a phase symbol. The embedded phase symbol can be extracted using

$$\widehat{\phi}(\tau) = angle|\frac{\mathbf{y}_p(\tau)}{\mathbf{y}_q(\tau)}| \tag{2.9}$$

It is important to note that both waveforms $\psi_p(t), \psi_q(t)$ will be transmitted simultaneously. Hence at the receiver side, the difference between both waveform phases will determine the phase symbol. The common terms between both phases will be cancelled out and this extracted phase value will be compared with the original dictionary. Therefore, phase synchronization is not required. Moreover, it is also worth mentioning that if the entire process is non-coherent, and channel coefficient α_j is correctly estimated, then two symbols can also be transmitted, and this leads to double the data rate. This technique can hold

the benefits of MIMO radar but lacks the dual functionality of MIMO radar and MIMO communication. As with the increase in the in-constellation size, the exact correlation on the phase symbol becomes difficult at the receiver end, affecting the communication process.

2.2.3 Phase Rotation Invariance Method

In [55], a phase rotation invariance-based scheme is used. This technique uses two waveforms to embed one bit of information. This technique is easy to implement and gives a better data rate, but it needs a minimum of two matched filters at the communication end. The phase rotation is direction θ_j dependent, hence only the intended communication receiver will receive embedded information that is located at θ_j. In this case, the communication process is directional. In those situations, where the communication receiver location is not known in advance or the communication receiver is moving rapidly, either iteratively calculating the communication receiver location or broadcast mode will be used. During each PRI, information is embeded in the form of binary 0 or binary 1 by employing a pair of beamform weight vectors. $\mathbf{w_1}, \tilde{\mathbf{w}}_\mathbf{1}$... $\mathbf{w_k}, \tilde{\mathbf{w}}_\mathbf{k}$. Let $\phi_1, ..., \phi_k$ be the K dimensional phase rotation alphabet associated with the K pairs:

$$\tilde{\varphi} = \angle \left(\frac{\mathbf{w}^H \mathbf{a}(\theta_c)}{\tilde{\mathbf{w}}^H \mathbf{a}(\theta_c)} \right) \tag{2.10}$$

where, $k = 1, ..., K$ phase rotational coded. It is important to note that only one of the k^{th} code is embeded in each PRI to deliver Q bits of information. The shape of the transmitted signal is:

$$s(t, \tau) = \mathbf{w_k} \psi(t) + \tilde{\mathbf{w}}_\mathbf{k} \tilde{\psi}(t). \tag{2.11}$$

Unlike the traditional PSK method, this proposed scheme embeds information in the phase difference between two waveforms. This technique simplifies phase detection and requires less computation. The signal received at the communication receiver will have the following form:

$$x_c(t,\tau) = \tilde{\alpha}_c(\tau)\left(\mathbf{w_k^H} a(\theta_c)\psi(t) + \tilde{\mathbf{w}}_\mathbf{k} a(\theta_c)\tilde{\psi}(t)\right) + n_c(t,\tau) \tag{2.12}$$

The signal components associated with $\psi(t)$ and $\tilde{\psi}(t)$ at the output of the matched filter in the communication receiver can be expressed as:

$$y(t) = \tilde{\alpha}_c(\tau)\mathbf{w_k^H} a(\theta_c) + n(t) \tag{2.13}$$

$$\tilde{y}(t) = \tilde{\alpha}_c(\tau)\tilde{\mathbf{w}}_k^H a(\theta_c) + \tilde{n}(t) \tag{2.14}$$

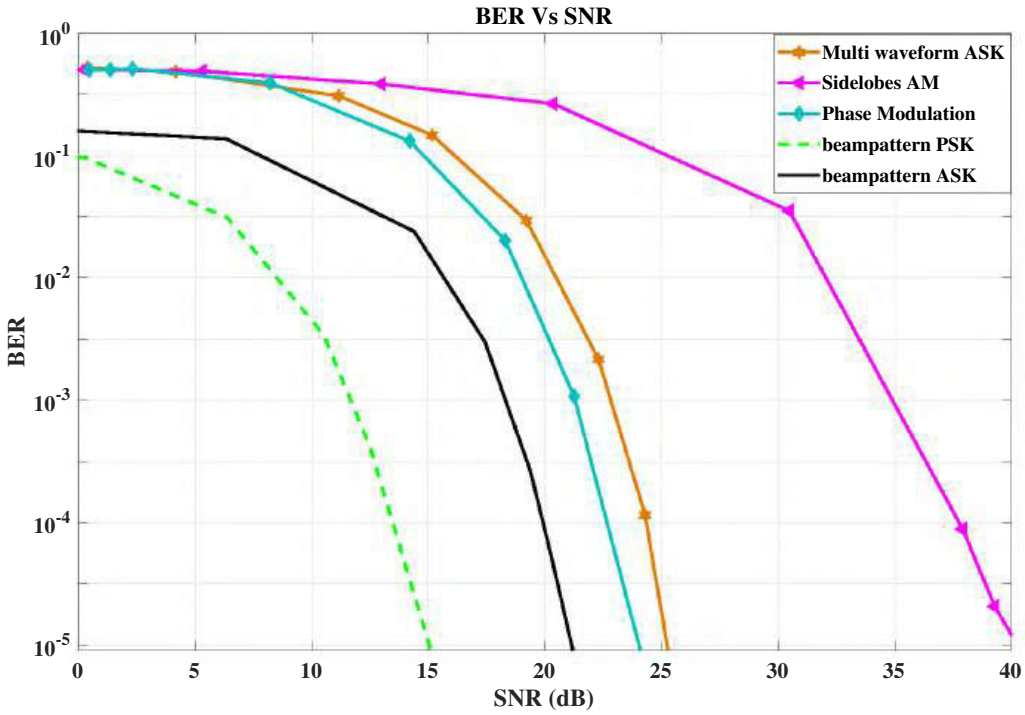

Figure 2.9: BER vs SNR of Phase Rotation Invariance based scheme.

Therefore, the phase rotation embedded in the received signal can be esti-

mated as:

$$\tilde{\varphi} = \angle \left(\frac{\mathbf{w}^H \mathbf{a}(\theta_c)}{\tilde{\mathbf{w}}^H \mathbf{a}(\theta_c)} \right) \tag{2.15}$$

The embedded binary sequence can be determined by comparing $\tilde{\varphi}$ obtained in Equation 2.15 with the phase dictionary. Furthermore, it is important to note that the selected waveforms remain constant throughout the PRI but change on a pulse-by-pulse basis.

Figure 2.9 shows the comparison of different schemes studied so far in terms of SNR and BER. For $\theta_c = 50^o$ and $\theta_r = 0^o$, the performance of sidelobes AM-based approach shows the worst results as compared to beampattern AM and multi waveform ASK. Similarly, the beampattern PSK outperforms beampattern ASK, phase modulation, and aforementioned techniques.

2.2.4 Index Modulation Based Method

Previous techniques discussed so far were either using amplitudes of waveform or using the phase of transmitter waveform to embed information. Now, consider another domain of information embedding which is called index modulation (IM). Index modulation methods use the index or number of antenna elements to convey additional information bits [75]. Multi-carrier Agile Phased Array Radar (MAPAR) is used to embed information bits for the remote user by using the same technique in [76]. Thus, integrating index modulation into a DFRC transmitter side by using radar waveform leads to a high spectral and energy efficient system, without degrading radar performance [77]. The sparse array is used by [78] to embed information into an orthogonal waveform and permutation of the antenna element. However, this reduces transmit power and antenna gain, thus degrading the target detection and overall performance. In [79] propose Carrier Agile Phased Array Radar (CAESAR), which can achieve

wideband performance by using narrow band signals. The above-mentioned performance is achieved by applying the concept of Frequency Agile Radar (FAR) in which carrier frequency changes from pulse to pulse, thus a combination of the unique frequency with different antenna elements provides more degrees of freedom as shown in Figure 2.10.

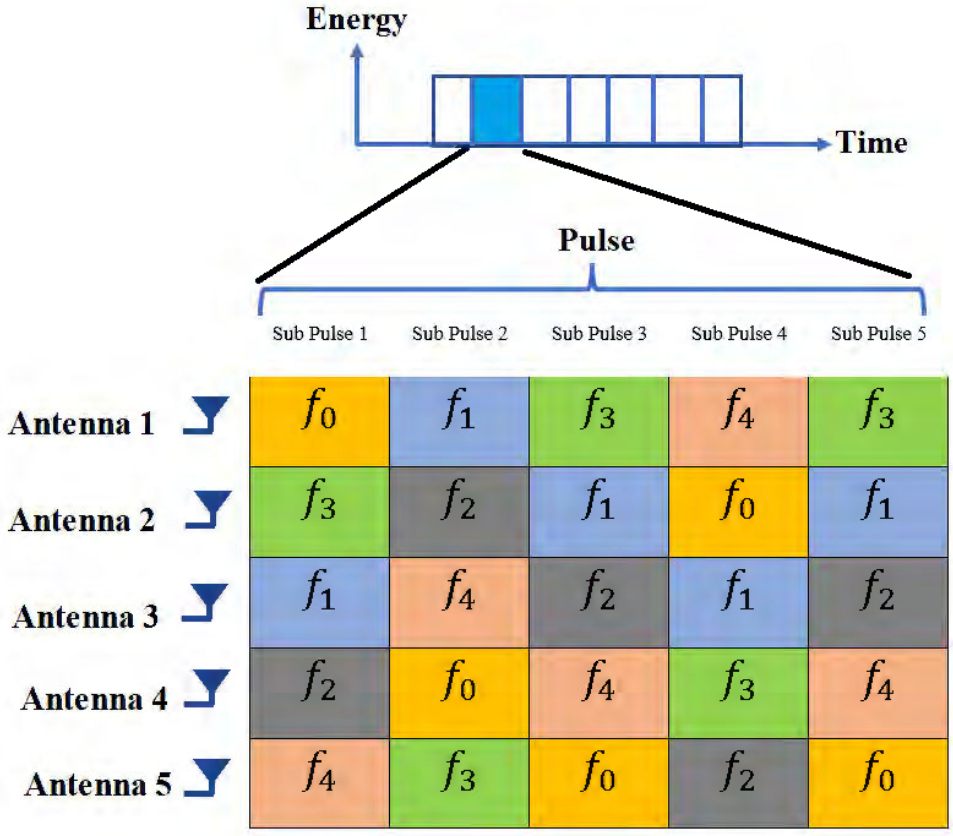

Figure 2.10: Index Modulation based Information Embedding

Index modulation can be achieved by pairing antenna elements with unique waveforms. This pairing is known to both the transmitter and receiver. In the case of MIMO radar, there is no fixed binding between waveforms and antenna elements. The system model swaps the antenna elements and waveforms randomly. This swapping does not affect the performance of the system. Let us consider MIMO with M_T antenna elements and G orthogonal waveforms, this pairing provides a constellation effect in terms of factorial i.e., $G!$ and the total

bit rate becomes

$$bitrate(R) = [log_2(G!)](f_{PRF}) \tag{2.16}$$

signal at the transmitter of DFRC having form in MIMO

$$s(t,\tau) = \sqrt{\frac{P}{M_T}}\mathbf{W}\psi(t) \tag{2.17}$$

$$\psi(t) = \mathbf{P}\phi(t) \tag{2.18}$$

$$\psi(t) = \mathbf{P}\phi(t) \tag{2.19}$$

where, $\mathbf{P}$ is the permutation matrix of $M_T \times M_T$, W is the beamforming weight matrix, $\psi(t)$ shuffled waveform matrix and $\phi(t)$ is wave form matrix.

The received signal at the communication receiver with index-modulated waveform is

$$\mathbf{y}_j(t) = \alpha_j \mathbf{P}^T \mathbf{W}^H \mathbf{a}(\theta_j) + \mathbf{n}(t) \tag{2.20}$$

where α_j is channel coefficient, $\mathbf{a}(\theta_j)$ is steering vector in the direction of j^{th} communication receiver(θ_j)

Comparison is provided for symbol decoding in [75] by using maximum likelihood (ML) based decoder, noniterative sub-optimal decoder, and iterative low complexity decoder as shown in Figure 2.11, among all, the computationally complex optimal ML decoder achieves the lowest BER values. As the number of messages is increased, N_b grows, however, the overall BER performance degrades as shown in Figure 2.12.

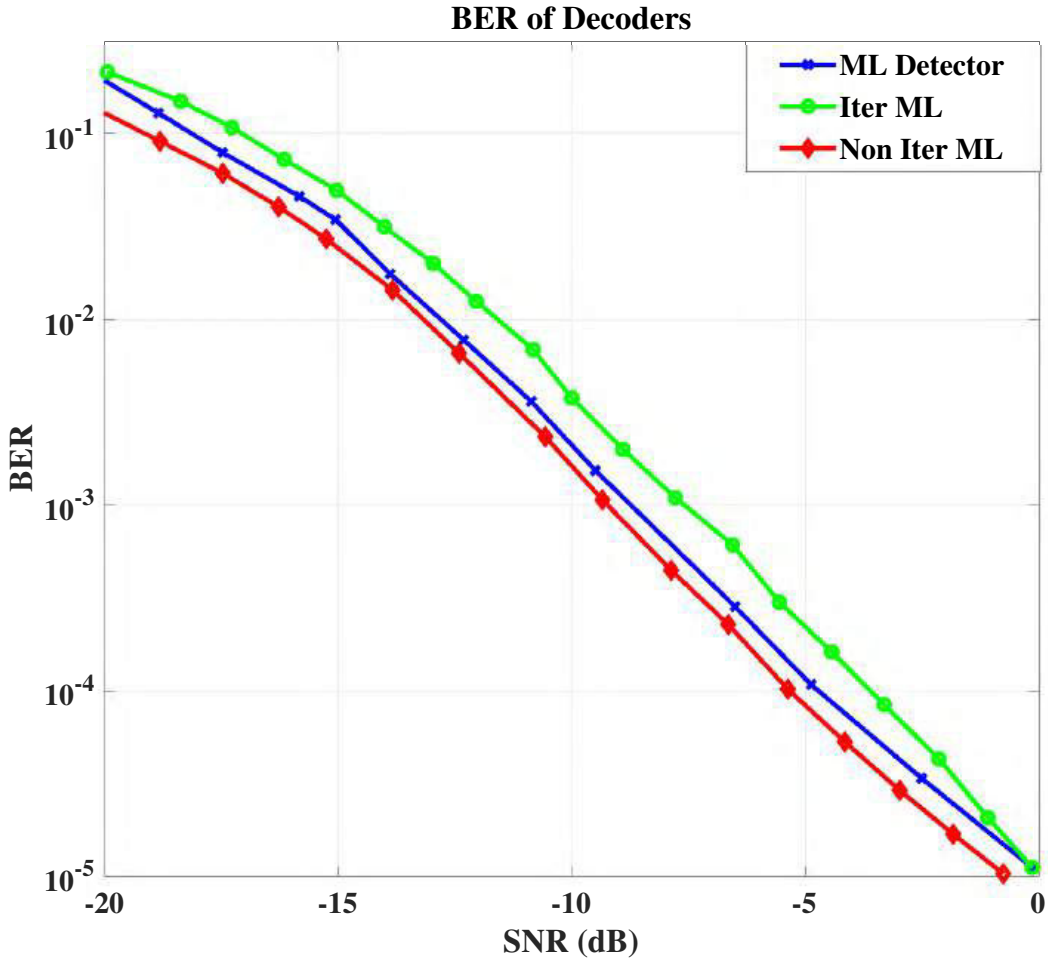

Figure 2.11: Index Modulation-based Bit Error Rate

2.2.5 Code shift keying-Based Method

Changing radar waveform on a pulse-to-pulse basis introduced a new horizon for researchers [80]. This technique enables us to assign numbers to the waveform and at the receiver decoding the waveform will give extra information. This is itself an information embedding technique because each waveform represents a unique symbol. In this technique, binary data is mapped to Gold codes or Kasami codes, initially, and then embedded to the waveform from the dictionary as shown in Figure 2.13.

By using this technique, the interference between radar and communication user and due to other targets is minimized to a remarkable level because they

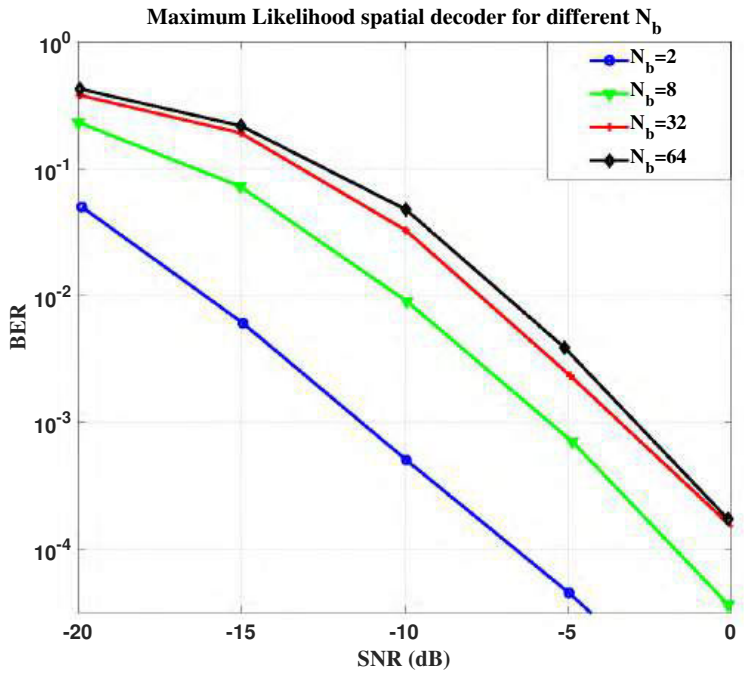

Figure 2.12: BER vs SNR of ML decoder

provide a low probability of intercept (LPI) [81]. Monte Carlo simulations were used to check the performance of the communication receiver by using various code lengths for both gold and Kasami codes. PSK modulation can be used to increase the bit rate. At DFRC, CSK-based waveform is transmitted via an omnidirectional antenna, at the radar receiver, a narrow beam width is required to achieve scanning by a phased array radar (PAR) antenna. Suppose, there is a dictionary of G waveforms, with G assumed to be the power of 2, then by assuming each waveform as a communication symbol, the bit rate R_{bit} of the transmitted waveform can be written as

$$R_{bit} = [log_2 G] \tag{2.21}$$

If the code length is N_c chips, and the duration of each chip is tc the maximum bit rate to be achieved can be obtained by $R = R_{bit} f_{PRF}$. Similarly, for

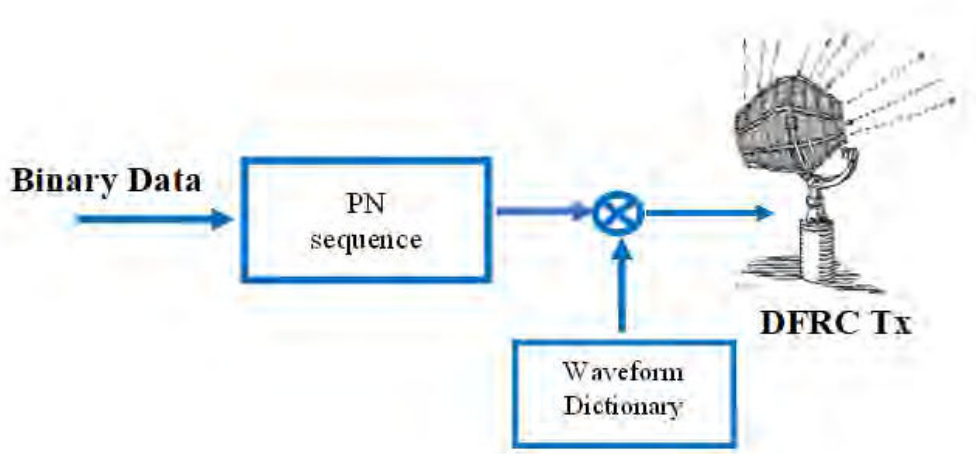

Figure 2.13: Code Shift Keying based Information Embedding

binary PSK modulated waveform, the bit rate can be achieved by

$$R_{bit} = [log_2 G + 1] f_{PRF} \tag{2.22}$$

Furthermore, now the symbol error rate is determined by using Gold codes and Kasami codes in [81],1x10^7 trials of Monte Carlo simulations were conducted by using code length of $M = 32$ bits, $M = 64$, $M = 128$, and $M = 512$ bits by using QPSK modulation respectively.

For $M = 32$ and $M = 64$, small Gold codes and Kasami codes were used while for $M = 128$, and $M = 512$, large codes are used. It is concluded that Gold codes for $M = 64$ perform well as compared to Kasami codes for $M = 64$ bits shown in Figure 2.14.

2.2.6 Frequency Hopping Based Method

Authors of [82–84] used frequency hoping waveform for radar purposes only. Keeping the success rate for radar only, they now utilize the same concept in DFRC.

In this approach, the author of [85] used the PSK symbol in radar waveform

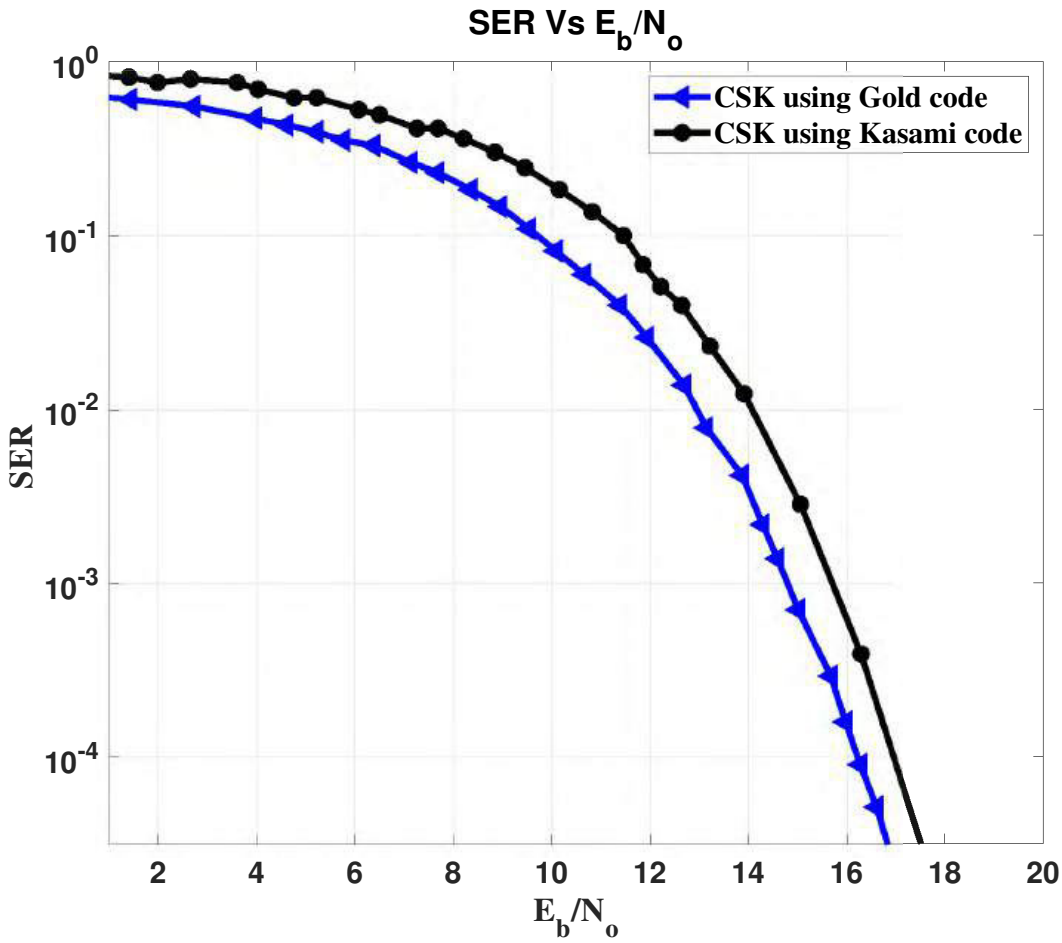

Figure 2.14: Symbol Error rates for Code shift keying for $M = 64$

to embed information. Sub-pulse-based architecture is used to cipher the information. The waveform is divided into multiple segments called hops as shown in Figure 2.15. To decode the PSK symbol, the communication receiver needs accurate information about the channel and frequency hopping sequence (FHS). This technique improves the data rate because pulse repetition frequency (PRF) is improved, but on the other hand, the requirements of multiple hops, accurate channel estimation, and multiplicative clutter effect due to timing offsets increase the computational complexity. The MIMO-based DFRC by using FH waveforms is proposed in [86]. This architecture uses radar as the primary function, while communication is on a secondary basis. During each FH interval, only one bit of information is embedded by using PM. However, due to

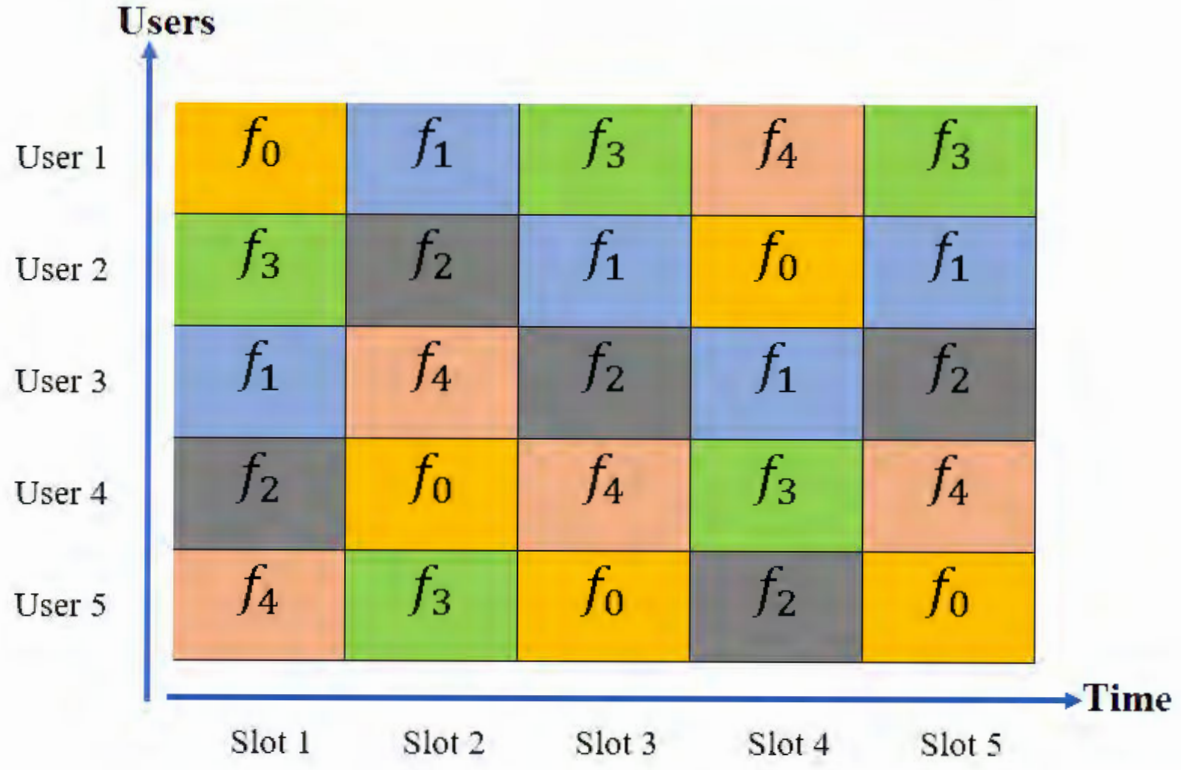

Figure 2.15: Frequency Hopping based Information Embedding

the time-variant nature of the channel, waveform optimization needs to be done successively to obtain target information and other features as well.

These features and target information are later on used to increase the MI between the target response and the target returns. Author of [87] used PSK and DPSK-based symbols for FH waveforms. In this proposed technique, M_T antenna elements and K frequencies to generate Frequency Hopped waveform were used. The greater the number of frequencies, the greater the number of hops (Q) and hence, the higher the number of symbols (L) per pulse. The number of symbols can be achieved by using

$$symbol(L) = {}^{M_T}C_K = \left(\frac{M_T!}{K!(M_T-K)!}\right) \tag{2.23}$$

$$bitrate = [log_2 L](Q)(f_{PRF}) \tag{2.24}$$

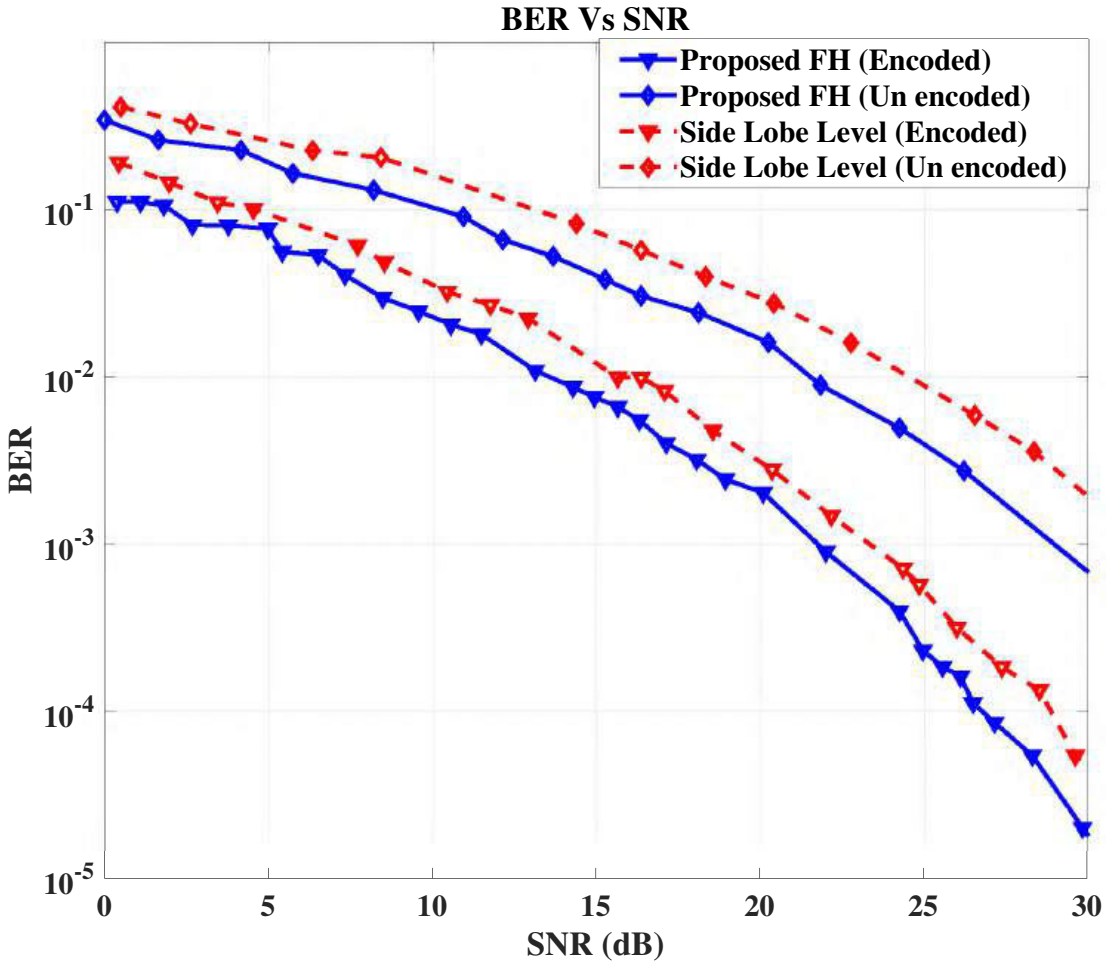

Figure 2.16: Frequency Hopping based BER Vs SNR

This is the simplest method to implement and it gives a higher bit rate (R) as compared to previous approaches.

Numerical results are based on Monte Carlo simulations to validate the effectiveness of this method i.e., frequency hopping-based waveform design in [39]. A high PRF is used in the X band, which in return gives a data rate of megabits, respectively.

Figure 2.16 shows the performance in terms of BER vs SNR for frequency hopping in phase-modulated waveform (uncoded) and convolutional encoder of rate $2/3$ in waveform (encoded) compared with $method1$ i.e., controlling side lobe levels (SLL) for communication users in [88], respectively.

2.2.7 Chirp Slope Keying (CSK) Based Method

In this technique, information is embedded into radar emission by using chirp sub-carriers [89]. These chirps are generated by using Fractional Fourier Transform (FrFFT) [90]. Linear Frequency Modulated (LFM) pulse is used to preserve the radar performance. This type of information embedding is used to mitigate the inter-channel interference (ICI) caused by Qausi chirp subcarriers [91]. Authors of [70; 92] used the slope of chirps to represent the digital modulating data i.e., 1 and 0. A rising slope or up-chirp means bit equals 1, while a falling slope or down-chirp means bit is zero. Higher constellation can be achieved by using a large number of up/down chirp levels [93]. Additionally, Direct Sequence Code Division Multiple Access (DS-CDMA) proposed by [94] avoids mutual interference between communication user and radar. In [95] achieved orthogonality between radar and communication signals by implementing up-chirps and down-chirps. [96] implemented Stepped Frequency Continuous Waveforms (SFCW) and [97] used BPSK signal modulated by LFM. Similarly, [98] used saw chirp for communication purposes.

2.2.8 Time Modulated Array Based Method

Time Modulated array or 4-dimension antenna array uses a pre-defined time sequence programmed at the transmitter to radiate beampattern [99]. Initially, TMA was limited to the field of radio astronomy only [100] due to slow FR switches, nonavailability of ad-hoc design methodologies for on-off sequence of antenna elements, and inefficient implementation of time modulation [101]. From the beginning of the new century, the demand for TMA increased, when low-priced array structure, irregularly shaped geometry, and low SLL became the demand of industry with unconventional radiation characteristics [102]. Re-

cent developments of TMA in DFRC with each beampattern represent unique binary information. One of the main advantages of using TMA is the use wide-band instead of narrow-band signals. Authors in [103] used ULA at DFRC transmitter side, similarly, another study is carried out by [104–107] to implement TMA for harmonic beamforming, multiprogramming in [108], angle diversity in [109] and [110] conducts a quantitative study on the energy efficiency of the radar and communications integration. The overall efforts were made to reduce the power losses in terms of sideband radiation.

The basic idea of TMA is to use the radar Integration Time (IT) by dividing it into time slots according to modulation. A specific number of antenna elements were turned off several times instant to achieve a higher data rate. This switching of antenna element represents 1 bit ON or OFF as shown in Figure 2.17. To keep radar operations uninterrupted, a Genetic Algorithm (GA) based optimization technique is used [9] and 4 different beampatterns were designed to transmit binary information.

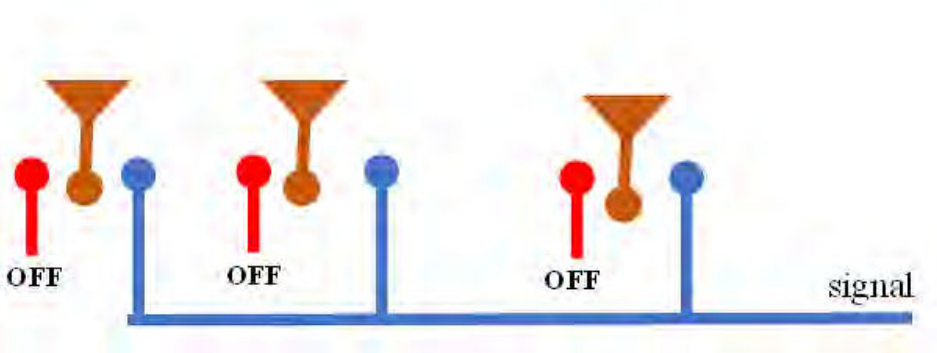

Figure 2.17: Time Modulated Array for Information Embedding

In the above methods, the data rate is highly dependent on the PRF of the radar and can be achieved only when a line-of-sight (LOS) channel is used. Similarly, time modulated linear array (TMLA) is utilized for information embedding by [111], these obtain low SLL by using single and multiple frequen-

cies in different designs. It is concluded that only by controlling time-based sequence, diverse power levels, and different beampatterns can be achieved. [112] used TMA for information embedding by proposing two different architectures which are, Sparse TMA (STMA) in which phase angle is set to zero while power is set to unity, and second is Phase Only Synthesis TMA (POSTMA), in which phase is optimized by using GA.

So far, an overview of different strategies for radar-embedded communication signals has been presented. Such strategies are key to establishing dual-function systems that permit the simultaneous execution of both radar and communication functions from a shared platform. A balanced and complete account of existing methods has been provided and their respective advantages and disadvantages are discussed. In the following section, the methods that use communication signals for radar operations are overviewed.

2.3 Communication waveform for radar operations

A DFRC system shares its resources like spectrum, power, and antenna elements to transmit such a signal which suits both the radar and communication receivers [113–120]. Now methods are analyzed, that utilize the communication-based waveforms that scan the target without any degradation in system efficiency by simply doing small alterations in the actual waveform. This approach utilizes digital multiplexing techniques to encode digital data into multiple orthogonal frequency carriers called sub-carriers. By using OFDM-based waveform for DFRC, better characteristics of low side lobes, high Doppler tolerance and information transmission capacity are achieved, as reported in [17; 121–126]. Decoding at the receiver side is done by using the Fast Fourier Trans-

form (FFT). Because of the diverse nature and wide range of applications, the OFDM-based waveform became a feasible option to attract researchers as an alternate solution to fulfill the requirements of the industry [127].

2.3.1 Mutual Information Based Design

Mutual information between radar and communication plays a vital role in terms of channel capacity and radar performance [128–131]. In this technique, Mutual Information (MI) between the communication user and radar target is used as an optimization objective for radar at the transmitter side [132]. Radar MI is used to evaluate the radar performance, while channel capacity calculation is used as performance measure of the communication system. The impact of SNR and the number of antenna elements on MI and channel capacity is calculated in [133].

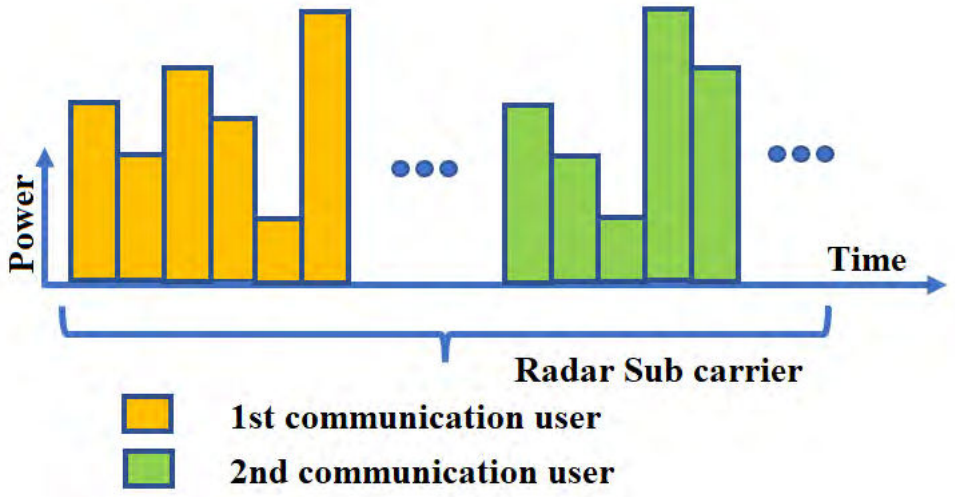

Figure 2.18: OFDM based subcarrier approach for different communication users

An adaptive OFDM (AOFDM) design-based approach is proposed in [130] in which the conditional MI between the radar and the received signal is used to calculate the data information rate (DIR) in a frequency selective channel. Similarly, Inner bounds on the performance of DFRC in terms of DIR and

estimation information rate at receiver is also investigated in [134]. Afterward, the MI maximization is further explored in [135] to minimize the minimum mean square error (MMSE) in terms of the target impulse response. Moreover, for communications-based waveform design, a litmus test is to maximize the data rate by adaptively assigning the transmit power according to the CSI [136].

To summarize the discussion, by using OFDM-based waveforms, MI maximization can be solved as a convex optimization problem. Therefore, it becomes an attractive measure as compared to other optimization criteria, like the probability of detection and Cramer-Rao bound, which are generally non-convex problems [19]. In OFDM-based systems, the entire bandwidth is divided into K subcarriers and it is important to note that each subcarrier uses a unique frequency. Similarly, each communication receiver utilizes one sub-channel only, while radar utilizes all subcarriers for estimation purposes as shown in Figure 2.18. DFRC transmitter and communication receiver need to be synchronized in terms of frequency [137]. The signal at the output of the transmitter of dual function antenna array is:

$$\mathbf{x} = \mathbf{F}\mathbf{s} \tag{2.25}$$

where, $\mathbf{x}$ contains L symbols and K subcarriers and $K \leq L$.

$\mathbf{F}$ is an Inverse Discrete Fourier Transformed matrix and each row represents the OFDM sub-carrier.

$\mathbf{s} = [s_1, s_2, \ldots, s_K]^T$ having length$Kx1$ vector, represents the amplitudes and phases of each sub–carrier.

The signal at the radar receiver is given as

$$\mathbf{y}_{Radar} = \mathbf{H}\mathbf{s} + \mathbf{n} \tag{2.26}$$

where **H** contains all the diagonal values of channel impulse responses, **n** is AWGN vector. Similarly, the signal received at the communication receiver is given as

$$\mathbf{y}_{comm,j} = \mathbf{G_j s} + \mathbf{m_j} \tag{2.27}$$

Where, $G_j = diag(g_j)$ and $g_j = [g_(j,1), g_(j,2), \ldots, g_(j,K)]^T$ denotes channel coefficients for the K subcarrier, which are associated with J^{th} communication receiver.

Information is embedded into this OFDM waveform by using the QPSK phase as explained in [137]. Each communication receiver is allotted a unique subcarrier, which uses using unique frequency. Hence, at the communication end, the interference is minimal. The main task in OFDM-based waveform design is to manage the transmit power of each sub-carrier such that radar target identification is improved. The power of each phase can be calculated by $p_k = |s_K|^2$. Hence, the overall transmit power of the transmitted signal is

$$P_{total} = \mathbf{x^H x} \Rightarrow \mathbf{s^H F^H F s} \Rightarrow \mathbf{s^H s} = \sum_{k=1}^{K} P_k = tr(P) \tag{2.28}$$

where, $tr(.)$ represents the trace of matrix. The maximum power allocated to k^{th} sub–carrier is represented as $p_{(k,max)}$, hence the

$$p_{max} = [p_{(1,max)}, p_{(2,max)}, \ldots, p_{(K,max)}]^T$$

The following optimization gives us acceptable radar objectives

$$\sum_{j=1}^{J} \sum_{k=1}^{K} \mathbf{w}_{j,k} log(1 + \frac{p_k \sigma^2_{gj,k}}{\sigma^2_{mj,k}}) \tag{2.29}$$

such that

$$\sum_{k=1}^{K} \mathbf{w}_{j,k} log(1 + \frac{p_k \sigma_{gj,k}^2}{\sigma_{m_{j,k}}^2}) \leq -\gamma \alpha_{opt}$$

where $\sigma_{g_{j,k}}^2$ is normalized channel gain for communication receiver and $\sigma_{h_k}^2$ is normalized channel gain for radar target, $\sigma_{n_k}^2$ is noise components in the K sub-carriers at radar receiver and $\sigma_{m_{j,k}}^2$ is noise components in the K sub-carriers at J^{th} communication receiver. α_{opt} represents the MI level of the radar and communication users and γ is the flexibility of radar towards communication users. The value of γ ranges between 0 and 1. For better radar operations, the value of γ is more inclined towards 1.

$$1^T p \leq P_{total,max} \tag{2.30}$$

$$0 \leq p \leq P_{max} \tag{2.31}$$

Radar function allows the dual-purpose transmitter to vary the power allocation such that the radar mutual information does not fall below $\gamma \alpha_{opt}$.

Figure 2.19 shows power allocation for communication user by assigning 29 subchannels to user 1 shown by red color while 3 subchannels to user 2 shown by blue color, respectively. Only one radar target is present utilizing all 32 subchannels. The maximum power normalization for each subcarrier is set to 10 units. Maximizing the overall communication mutual information is done by using eq (14) in [137]. It is observed that three subchannels that are assigned to user 2 are low-powered, which results in better MI. Similarly, for the worst case scenario, 8 subcarriers are assigned to user 1, while 16 subcarriers are assigned to user 2. The mutual information is degraded with poor channel conditions than the communication receiver 1 in radar-favored sub-carriers.

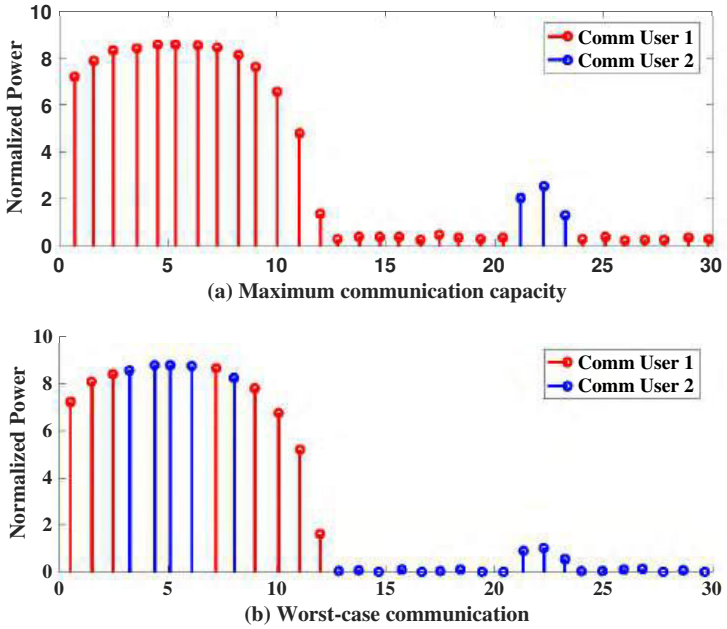

Figure 2.19: Power allocation for Mutual Information based OFDM subcarriers for Radar centric design

2.3.2 Index Modulation Based Design

Authors in [138] used index modulation for increasing data rate by using OFDM waveform. Information is encoded into waveform by using quadrature amplitude modulation (QAM) as well as by using the indices of antenna elements in the DFRC transmitter.

These two parameters help us to improve the efficiency as compared to the traditional OFDM [139–142], and the advantages observed are mentioned in [143]. This presented technique gives good results for radar scanning in terms of energy efficiency, reduced PAPR, robustness to ICI, and improved BER respectively. Similarly, [75] used different antenna elements and frequencies of subcarrier, which act as constellation space. In this technique, authors split the information bits by using a bit splitter module, where each bit is mapped to the index selector and Golay code sequence inserter module. Afterward, sub-blocks or sub-carriers are created in the OFDM block creator. All the sub-

carriers undergo the IFFT and cyclic prefix (CP), then data is further converted from parallel to serial and transmitted through the DFRC transmitter as shown in Figure 2.20.

The m^{th} OFDM symbol, which is generated by applying IFFT is given below:

$$\mathbf{x_m} = IFFT((\mathbf{X_m}) = [X_{m,1}, X_{m,2}, ..., X_{m,N}]^T \tag{2.32}$$

where, matrix $\mathbf{X}$ contains frequency domain transmitted symbols and $X_{m,n}$ represents m^{th} symbol transmitted over n^{th} sub–carrier.

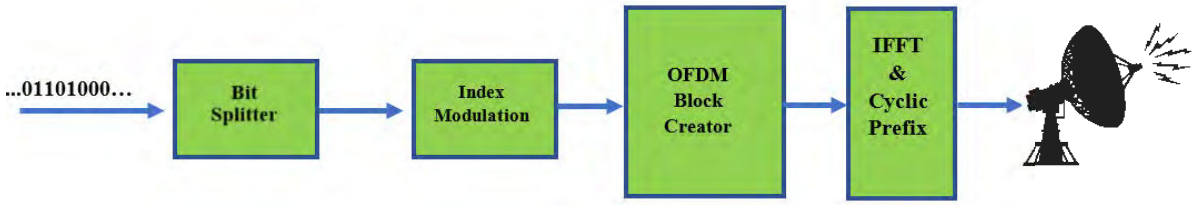

Figure 2.20: OFDM based Index Modulation at DFRC Tx

The cyclic prefix of C samples is added to the beginning of the OFDM symbol after applying IFFT as below,

$$\mathbf{x} = [x_{m,(N-C+1)}, x_{m,(N-1)}, ..., x_{m,N}]^T \tag{2.33}$$

This baseband discrete signal is processed with a digital-to-analog converter and up-converted to the desired carrier frequency. The signal to be transmitted through the DFRC transmitter becomes

$$\widetilde{x}(t) = real[\mathbf{x}(t)e^{j(2\pi f_c t + \overline{\theta})}] \tag{2.34}$$

Here, f_c is the carrier frequency and $\overline{\theta}$ is the initial phase of the transmitted signal. The channel through which this transmitted signal propagates introduces Doppler shift and delay to each subcarrier in each path. The channel is

modeled as

$$c(t,\tau) = \sum_{p=1}^{P} \alpha_p e^{-j(2\pi v_p \tau)} \delta(\tau - \tau_p) \tag{2.35}$$

where α_p represents attenuation factor, τ_p is radar time delay and v_p is doppler frequency shift for p^{th} target. The signal received at the radar in the frequency domain is given as

$$\mathbf{y}[n] = \sum_{p=1}^{P} \alpha_p x(\frac{n}{F_s} - \tau_p) e^{j(2\pi n \frac{v_p}{F_s})} + \mathbf{w}[n] \tag{2.36}$$

where, $F_s = N\Delta f$ is the sampling frequency upon which the received signal is sampled, and $\mathbf{w}[n]$ represents the AWGN vector.

At the communication receiver, the null subcarrier is used to identify the location of the communication receiver and then well known maximum likelihood (MLL) approximation is used to decode the QAM modulation. The performance of radar is calculated in terms of the MSE, while the performance of the communication receiver is calculated in terms of BER.

2.4 Beampattern Modulation

Since existing literature mostly focuses on the scheme of using a single beam for communication and sensing [144–147], beamforming-based approaches for radar and communication are reviewed in this section. The aim is to study the performance parameters of separate beams for radar operations as well as communication systems generated by a single aperture by using signal processing algorithms [148]. It is important to note that both radar and communication systems have different requirements for beamforming [149; 150]. Working on high frequencies, radio system encounters propagation loss, therefore, the communication system on the one hand requires stable and LOS beams for large gain,

while radar on the other hand requires time-varying and directional scanning beams.

2.4.1 Sub-beam sharing Design

The concept of 3-dimensional multibeam is presented by [151] for radar in terms of a narrow beamwidth in azimuth, circular or rectangular shape in elevation, and low SLL from a single aperture. Similarly, authors in [152] used the same concept for 5G communication systems, and [153] for a two-channel selectable down converter for interference mitigation in radar operations, respectively. Recent developments for unified hardware-based radar and communication multibeam is studied in [154–160].

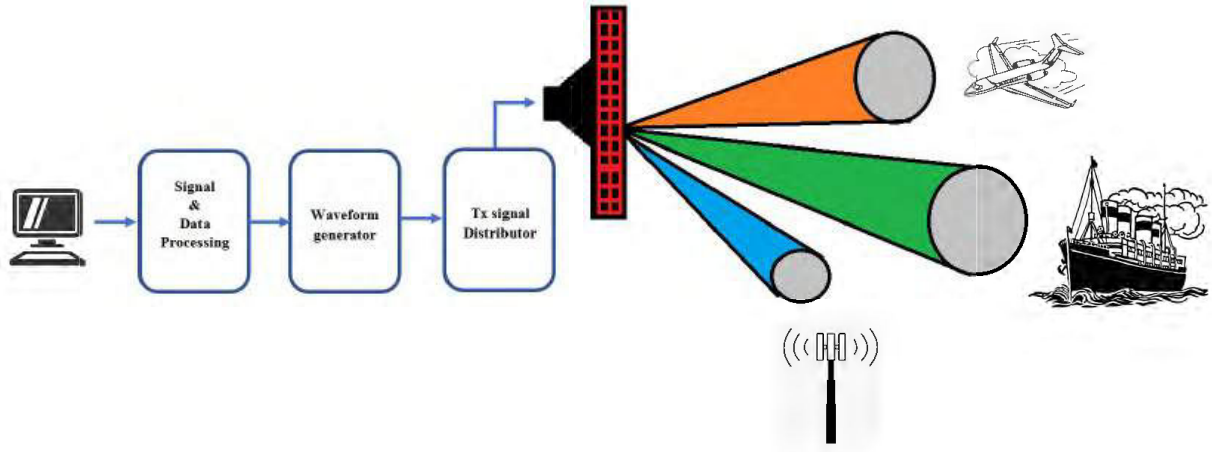

Figure 2.21: Multiple Beams Concept

The entire spectrum is divided into portions called subbeam, one portion is utilized by the communication receiver all the time while the remaining portion is used for different radar operations as shown in Figure 2.21. Phased array radars can scan in 2 dimensions to fully utilize the available spectrum. This system is capable of transmitting and receiving simultaneously and multiple beams are generated using the same transmitter. The general drawback of mul-

tiple beams is that total power is divided into multiple beams and the scan range is reduced. [148] proposed the idea of splitting the transmitter antenna array into two parts for joint radar and communication for interference mitigation. The proposed framework implements time division duplex (TDD) for radar operations while OFDM for communication systems respectively. The parameter estimation is done by an on-grid compressed sensing-based algorithm.

2.5 Feature Based Estimation

The feature-based estimation technique extracts multiple features from the received signal to estimate the characteristics of the transmitted signal, such as its range, velocity, amplitude, phase frequency, and modulation type [161]. By using FB estimation techniques, cognitive radio systems can determine if a signal is legitimate or not and thus help prevent false alarm detection [162]. Ultimately, FB estimation is essential for reliable spectrum sharing and efficient cognitive radio networks. Additionally, with improved communications performance and efficient spectrum exploitation, FB estimation can provide a valuable tool for interference avoidance in wireless networks [163]. The FB classification can be implemented by Combining with Kalman Filtering [164] or Hidden Markov Models (HMM) to improve the efficacy of results and prevent false detections [165].

The suboptimal Feature-based method is developed to classify signals by identifying useful features before the classification process [166]. These features can include instantaneously calculated values, transformed representations, statistical measures, or characteristics derived from constellation shapes. Extensive research has been conducted on both methods, revealing that the LB

method offers the most effective solution but demands significant computational resources and prior knowledge of the signal. On the other hand, although less optimal in terms of accuracy, the FB method provides a faster response time due to its lack of dependence on prior information. In ML-based techniques, feature extraction becomes a task requiring expertise when employing these methods. To overcome this challenge in FB methods and enhance their efficacy in recognizing complex patterns effectively compared to shallow models do deep learning approaches have drawn considerable attention for reducing reliance on traditional feature engineering methodologies. Due to the rapid advancements in DL technologies, numerous methods have been developed to self-learn the features, and DL is preferred because it requires large datasets, which are easily obtained from communication systems. The complexity of DL is a major concern since it involves training and testing phases, many applications have utilized depthwise convolutional networks. As a result of depth-wise convolutions, the model size is reduced significantly, but accuracy remains the same. Compared to conventional convolution, this model has fewer parameters, making it suitable for small devices in cognitive environments. In [167], authors applied Markov-based decision process and Deep Q network to estimate the target parameters for cognitive radar. The main achievement is to minimize the interference between radar and the communication user. In [168] separable convolutional neural network (CNN) is applied to estimate features of the received signal at the communication receiver. The authors have applied CNN architecture to the signal received from a high noise-impaired channel. Similarly, in [169] long short-term memory (LSTM) with a gated recurrent unit (GRU) layer is applied to obtain higher accuracy for B5G wireless networks and Internet of Things (IoT) networks. The efficacy of results is measured in

terms of accuracy, training loss, and confusion matrix. The value of SNRs is used between -20dB to 20 dB. A few more models based on CNN architectures are studied in [170–172]mainly focusing on extraction of features, calculating the computational complexity and accuracy of proposed models. In [173; 174], researchers skipped the features extraction step to further reduce the computational complexities. Similarly, to increase the performance while keeping low computational complexities, the combination of CNN with recurrent neural network (RNN) is presented in [175; 176]. More details about the use of CNN, RNN, and other variants of DL algorithms have been widely discussed in literature by [177; 178].

2.6 Summary

In summary, dual-function radar and communication systems use two main approaches: likelihood-based and feature-based estimation. They share the same hardware, with radar operations mainly in the main lobes and communication in the side lobes.

Furthermore, the selection of waveforms plays a critical role in dual-function systems, with radar-based waveforms commonly employing ASK or PSK modulation, while communication-based waveforms utilize OFDM, frequency hopping, and index modulation techniques. Additionally, the utilization of multiple beams allows for dedicated operations in various scenarios.

In feature-based approaches, neural network-based architectures are applied to either the communication receiver, radar receiver, or both, to estimate the received signal accurately. This integration of advanced techniques enhances the performance and versatility of dual-function radar and communication systems,

enabling them to adapt to diverse operational requirements efficiently. As these technologies continue to evolve, they hold immense potential for addressing the complex challenges of modern communication and surveillance applications.

Chapter 3

Modulation-Based Information Embedding and Interference Mitigation for the Design of DFRC

In today's world, where versatile systems are crucial, combining radar and communication on one platform is a big focus of research. Therefore, Frequency Shift Keying (FSK)-based methods are employed to encode information for both radar and communication. This chapter of the dissertation closely examines how these methods can be optimized, with a particular emphasis on two novel approaches: Frequency Quadrature Amplitude Modulation (Freq QAM) and a hybrid approach combining Frequency Shift Keying with Frequency Division Multiplexing (FSK-FDM). The integration of FSK-based strategies presents promising opportunities for the implementation of dual-function radar and communication systems. Moreover, the strengths and weaknesses of the proposed schemes are discussed in the subsequent section by presenting a variety of examples and Monte Carlo simulations.

3.1 Frequency Quadrature Amplitude Modulation based technique

A new approach is introduced in this section for information embedding by using the FQAM method for DFRC. Information is embedded in the radar-based waveform in the form of symbols. Each symbol is composed of orthogonal frequency using M-ary FSK and binary information encoded by M-ary QAM. All the mapping is done in the Lookup table, which is shared with the communication receiver in advance. Once the symbols are composed by keeping orthogonality constraints, they are transmitted in each radar pulse. Each pulse contains only one symbol, which changes on a pulse-to-pulse basis. The receiver transcribes each accompanying bit with a unique frequency as 0 or 1 based on whether that constellation and frequency are radiated. The proposed technique has the following attributes:

- The communication message shall be transmitted to single or multiple communication directions regardless of their location, whether they are located in the main lobe or sidelobes.
- This process is secure against intercepts from directions other than the pre-assigned communication directions.
- The decoding of each FQAM symbol at each communication receiver is independent of another neighboring symbol in the sequence.

The remainder of the proposed scheme is structured as follows: Section 3.1.1 introduces the proposed DFRC Data Model, while Section 3.1.2 presents the Frequency QAM-based information embedding scheme. Additionally, the key advantages are discussed in Section 3.1.3, and the receiver designs for both

the radar and the communications are discussed in Section 3.1.4. Furthermore, simulation results are compared in Section 3.1.5, and finally, Section 3.3 concludes the FQAM scheme.

3.1.1 Proposed DFRC Data Model for FQAM Methodology

Consider a uniform linear array (ULA) used at the transmitter side of the dual-function array. The inter-element distance between the antenna element is set to half of the wavelength. The array's length at the transmitter is represented by M_T, while M_R and N_R denote the length of radar and communication receiver arrays, respectively. The length of the DFRC transmitter and radar receiver are set equal. The radar receiver is placed with a DFRC transmitter array such that both observe the same spatial angle. In contrast, the communication array is placed in a far field at some arbitrary location. One of the key objectives of the DFRC transmitter is to generate signals with high target tracking capabilities and embed the binary information into the waveform without degrading the system performance. The signals at the input of the DFRC transmitter are given as:

$$\mathbf{s}(t,\tau) = \sum_{g=1}^{G} \lambda(\tau)\mathbf{w_g}^{*} x_g \tag{3.1}$$

where, t represents the time within each radar pulse or fast time index, while τ represents pulse number or slow time index. $\lambda(\tau)$ is Uniform power assigned to each beamforming weights, $(.)^*$ denotes the complex conjugate and $\mathbf{w_g}(t)$ is Uniform Transmit array beamforming weight vector having dimensions $M_T \times 1$. $x_g(t), g = 1,2,3,..,G$ are G orthogonal waveforms that contain the embedded sequence of binary data. It is assumed that waveforms must

fulfill the conditions of orthogonality with no time delay and can be written mathematically as:

$$\int_T x_g(t)x'_g(t)dt = 0 \tag{3.2}$$

and

$$g \neq g', \tag{3.3}$$

where T is the pulse width.

For error-free communication, all the waveforms must be orthogonal to each other, but in reality, perfectly orthogonal waveforms are difficult to construct due to time delay and phase shifts. Therefore, waveforms with low cross-correlations and less spectral overlap are used. The problem of waveform design lies beyond the scope of this study.

3.1.2 The Frequency QAM-based information embedding scheme

During each radar pulse, one frequency will be selected from the pool of $M-FSK$ which is mapped to one constellation symbol of $M-QAM$. The $M-FQAM$ symbol contains information

$$N = \log_2 M, \tag{3.4}$$

Where M is the combination of M_f and M_q. Let us denote M_q QAM symbols as $\{x_1, x_2, ..., x_{M_q}\}$, where $x_k = A_k e^{j\phi_k}$ The mathematical form of the proposed information embedding scheme is as follows:

$$x_{(m,k)} = \sqrt{2\lambda} A_k e^{(j(2\pi f_m + \phi_k))} \tag{3.5}$$

Where, $m = 0, 1, ..., M_f - 1$ represents frequency and $k = 1, 2, ..., M_q$ represents data symbol, λ is the uniform transmit power and A_k is the amplitude of each symbol. Figure 3.1 illustrates the proposed mapping rule.

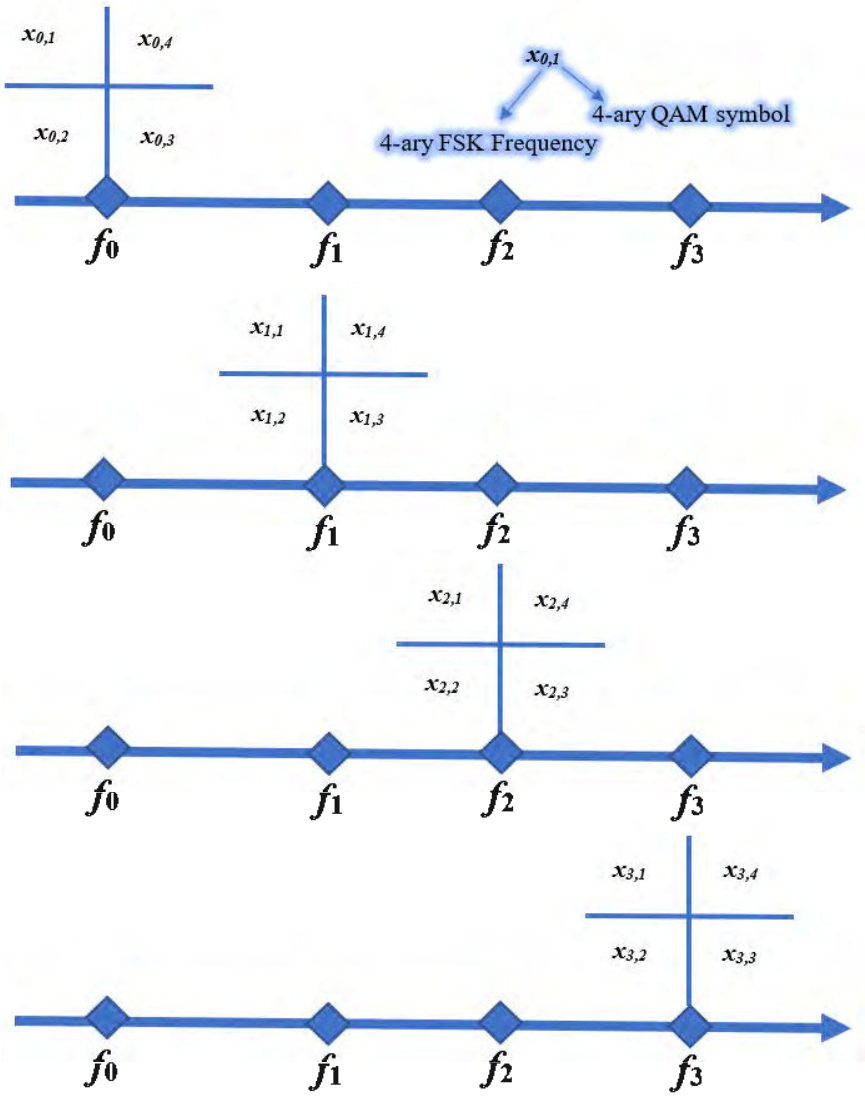

Figure 3.1: FQAM Proposed Methodology

Four frequencies were implemented to construct a $4-$ary Frequency Shift Keying (FSK) system, each represented by two bits, alongside four Quadrature Amplitude Modulation (QAM) symbols, each also represented by two bits, as illustrated in the Table. 3.1.

Table 3.1: $16-ARY$ **FQAM bits mapping,** $4-ARYFSK$ **frequency and** $4-ARYQAM$ **data symbol**

Binary Input data	Data Sequence		Frequency Sequence				FQAM Symbol
0000	0	0	0	0	X1	F1	x(1,0)
0001	0	0	0	1	X2	F2	x(1,1)
0010	0	0	1	0	X3	F3	x(1,2)
0011	0	0	1	1	X4	F4	x(1,3)
0100	0	1	0	0	X1	F1	x(2,0)
0101	0	1	0	1	X2	F2	x(2,1)
0110	0	1	1	0	X3	F3	x(2,2)
0111	0	1	1	1	X4	F4	x(2,3)
1000	1	0	0	0	X1	F1	x(3,0)
1001	1	0	0	1	X2	F2	x(3,1)
1010	1	0	1	0	X3	F3	x(3,2)
1011	1	0	1	1	X4	F4	x(3,3)
1100	1	1	0	0	X1	F1	x(4,0)
1101	1	1	0	1	X2	F2	x(4,1)
1110	1	1	1	0	X3	F3	x(4,2)
1111	1	1	1	1	X4	F4	x(4,3)

3.1.3 Key Advantage of the Proposed Scheme

The key advantage of the proposed scheme is that it is the merger of two technologies, as explained earlier. On the one hand, it utilizes the benefits of frequency diversity and digital modulation schemes, and on the other hand, it gives a higher data rate. The 4 QAM allows us to transmit 2 bit of information while the proposed scheme 4 FQAM allows us to transmit 3 bits. Similarly, using traditional 8 QAM, 3 bits can be transmitted, but with the proposed 8 FQAM, 4 bits can be sent using the same computational complexities. For the case of 16 QAM, 4 bits can be transmitted while 16 FQAM sends 5 bits of information.

This study considers the DFRC transmitter beampattern with four communication receivers to assess efficacy in broadcast mode, whereas it is tested with a single communication receiver for the dedicated link. The radar target is sit-

uated at an angle of $\theta_r = 0^o$. The first communication receiver is positioned at $\theta_{c1} = 30^o$, while the second is at $\theta_{c2} = 50^o$. Additionally, the third receiver is located at $\theta_{c3} = -30^o$, and the fourth at $\theta_{c4} = -50^o$, as illustrated in Figure 3.2.

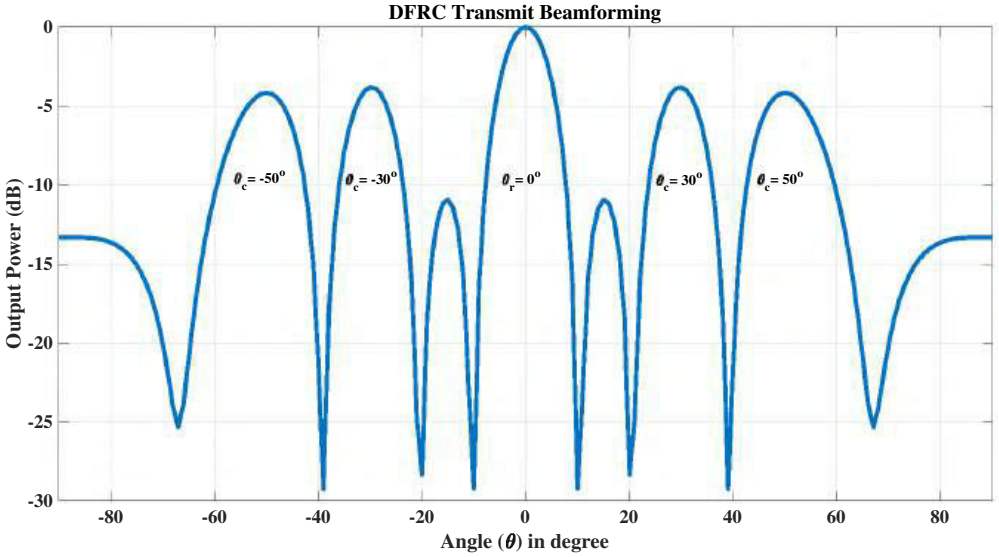

Figure 3.2: DFRC transmit array beampattern with one Radar target at $\theta_r = 0^o$ while four Communication receivers at an angle of $\theta_{c1} = 30^o, \theta_{c2} = 50^o, \theta_{c3} = -30^o, and \theta_{c4} = -50^o$

3.1.4 Receiver Design

In this study, two types of receivers are studied: the radar receiver and the communication receiver. The radar receiver determines the direction of arrival, i.e., the angle DOA θ of the target, while at the communication receiver, the frequency and the modulation scheme of the transmitted symbol is analyzed.

3.1.4.1 Performance of the Communication Receiver

This section presents the decoding methodology of the proposed FQAM at the communication receiver under the AWGN channel. The location of the communication receiver is assumed to be stationary during the entire commu-

nication interval. A matched filtering-based soft decoding methodology is applied at the receiver side. Let us consider L communication receivers, located somewhere in the far field. It is assumed that the dictionary of orthogonal waveform at dual function transmitter is known to each of the communication receivers. Assume that the j^{th} communication receiver with Uniform linear shape array antennas having dimension N_R receive the following baseband signal

$$\mathbf{y}_j(t,\tau) = \alpha_j c_j(\phi_j)(\mathbf{a}^T(\theta_j)s(t,\tau))\mathbf{b}(\theta_m) + \mathbf{n}_j(t,\tau) \tag{3.6}$$

where, α_j = channel coefficient constant from transmitter array towards J^{th} communication receiver

$c_j(\phi_j)$ = steering vector from receive array in direction of ϕ_j communication receiver

$\mathbf{n}_j(t,\tau)$ = Additive white Gaussian noise with variance σ^2 I

(ϕ_j) = direction of j^{th} communication receiver. The information is decoded in two simple steps, as explained below:

Frequency Content Decoding

At the beginning, the beamforming operation is executed to remove the steering vector from the received signal. Additionally, the matched filtering technique is employed to extract the frequency component embedded in the received signal. This includes convolving the received signal with a matched filter kernel designed to maximize the signal-to-noise ratio (SNR) of the desired frequency component.

$$\hat{\mathbf{x}}_f(t) = \hat{\mathbf{y}}_{com}(t,\tau) * \mathbf{h}(t) \tag{3.7}$$

where $\hat{\mathbf{x}}_f(t)$ is the filtered frequency content and $\mathbf{h}(t)$ represents the matched filter kernel for frequency extraction. Both the signals are in the time domain representation.

QAM Symbol Decoding

Subsequently, after extracting the frequency contents, the received signal will be matched and filtered with the QAM symbol dictionary. This involves aligning the received signal with a template waveform representing each possible QAM symbol and maximizing the correlation between the received signal and the template waveform.

$$\hat{\mathbf{x}}_q(t) = \hat{\mathbf{y}}_{com}(t,\tau) * \mathbf{g}(t) \tag{3.8}$$

Whereas, $\mathbf{g}(t)$ is the template waveform for QAM symbol extraction.

Therefore, the use of matched filtering for both frequency component extraction and QAM symbol extraction enables the communication receiver to accurately demodulate and decode the transmitted information.

3.1.4.2 Performance of the Radar Receiver

In this section, the performance of the radar receiver is evaluated in the far field at $\theta_r = 0^o$. The number of antenna elements at the radar receiver is set to M_R. The beamforming-based algorithm is used for the direction of arrival (DOA) estimation. Consider, there are M far-field targets within the radar main beam; the vector form of the baseband signal received by the radar receiver is expressed as:

$$\mathbf{x}_{radar}(t,\tau) = \sum_{m=1}^{M} \mathbf{B_m}(\tau)(\mathbf{a}^T(\theta_m)s(t,\tau))\mathbf{b}(\theta_m) + \mathbf{e}(t,\tau) + \mathbf{n}(t,\tau) \tag{3.9}$$

where, $B_m(\tau)$ is the reflection coefficient of the m^{th} target that obeys the Swerling II target model, $b(\theta_m)$ is the steering vectors of the receiver array in the direction of θ_m. Similarly, $a(\theta_m)$ is the steering vector of the transmitter array in the direction of θ_m and $e(t,\tau)$ is the $M_R \times 1$ vector comprises the signals that impinge on the receive array from the sidelobe region also called as interference vector and $n(t,\tau)$ is the AWGN with variance σ^2 I.

The results are shown in terms of power and theta as shown in Figure 3.3.

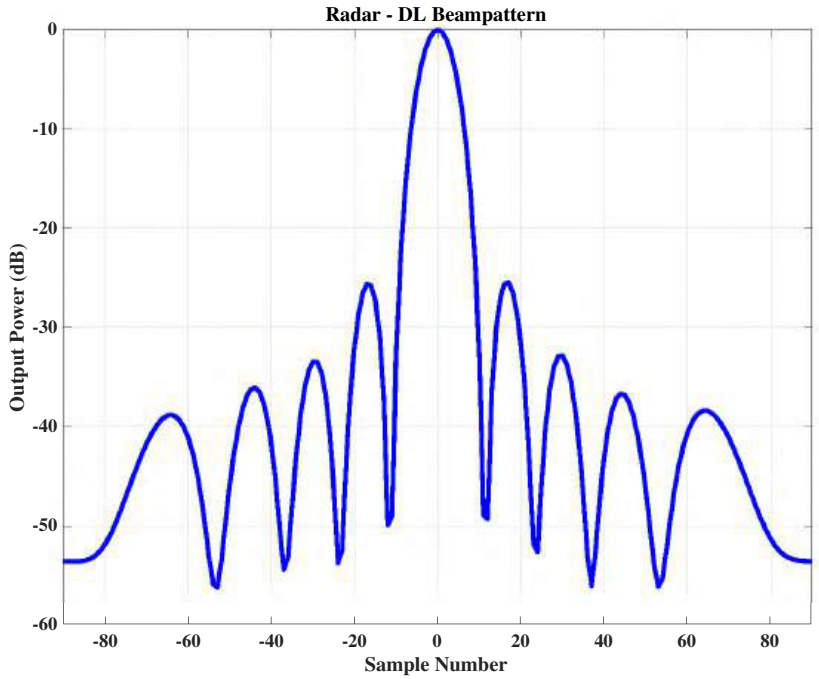

Figure 3.3: Radar receiver at $\theta_r = 0^o$

3.1.5 Results and Discussion

Consider a uniform linear array with $M_T = 24$ antenna elements at the DFRC transmitter and $M_R = 24$ antenna elements at the radar receiver. During each radar pulse, the binary information encoded in the FQAM symbol is transmitted from the DFRC transmitter and delivered to the communication receiver and radar receiver, respectively. It is important to note that only one waveform

will be transmitted during each radar pulse, and it changes from pulse on pulse basis.

3.1.5.1 Example 1: Single Communication Receiver

In the 1^{st} case, one radar receiver and one communication receiver is considered. The communication receiver is located at $\theta_c = 20^o$ while the radar receiver is located at $\theta_r = 0^o$ as shown in Figure 3.4. The objective is to minimize the out-of-sector radiation while maintaining the distortion-less response towards θ_r. Additionally, a sidelobe level (SLL) is enforced towards the communication receiver. Here it is important to tell that a constraint is imposed upon the communication receiver that the number of communication receivers (J) must be less than the antenna elements (M_T) at the DFRC transmitter. Thus the overall optimization problem can be written as:

$$\begin{aligned} \min_{\mathbf{w}} \max_{\theta} \quad & |\mathbf{w}^H a(\theta)\ |, \ \ \theta \in \widetilde{\Theta} \\ \text{such that} \quad & \mathbf{w}^H a(\theta_r) = 1 \\ \text{and} \quad & \mathbf{w}^H a(\theta_{c_j}) = \triangle_j \quad j = 1, ..., J \end{aligned} \tag{3.10}$$

The constraint defended in Equation 3.10, $\widetilde{\Theta}$ represents the sidelobes other than those of the communication receiver, while $\triangle_j$ represents the predefined power level allocated to sidelobes containing the communication receiver. The same weight vector is assigned to the communication receiver during the entire pulse duration. A lookup table is shared with each communication receiver in advance containing the power of SLL and Mainlobe. The following power allocation formula is used to convert from linear scale to dB scale.

$$\triangle_j = 10 \log 10 (\frac{(\gamma_j)^2}{\sigma^2}) \tag{3.11}$$

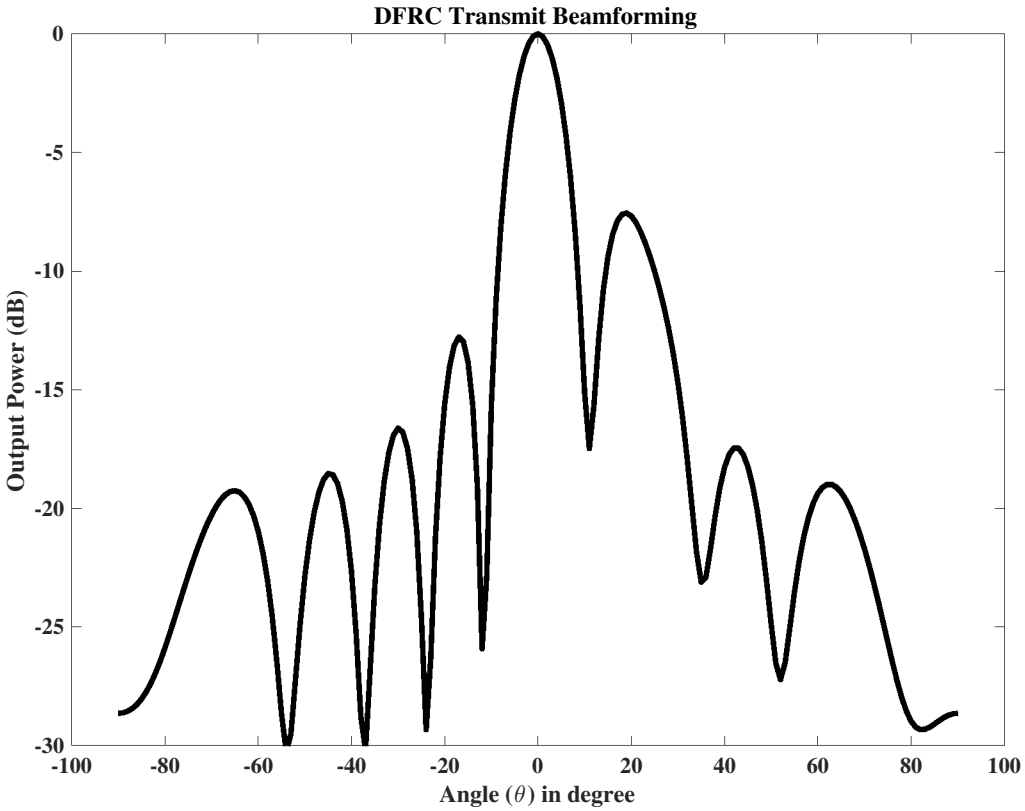

Figure 3.4: Example 1: Beam pattern of transmitter array with $\theta_r = 0^o$ and single communication receiver at $\theta_c = 20^o$

where σ represents the variance of noise and γ_j represents linear power of the sidelobes. In this case, the main lobe power is set to maximum, while the sidelobe containing communication receiver is set to $\triangle_1 = 7dB$. The linear power allocated to sidelobe is $\gamma_1 = 0.1995$. The signal received by the communication receiver located at $\theta_c = 20^\circ$ is shown in Figure 3.5.

3.1.5.2 Example 2: Multiple Communication Receivers

In the 2^{nd} case, a single radar target is considered along with four communication receivers. In this scenario, two distinct sidelobe levels were selected. As the placement of communication receivers lies $\pm 30^\circ$ and $\pm 50^\circ$, Therefore, the following arrangements were made. The 1^{st} and 3^{rd}communication receivers

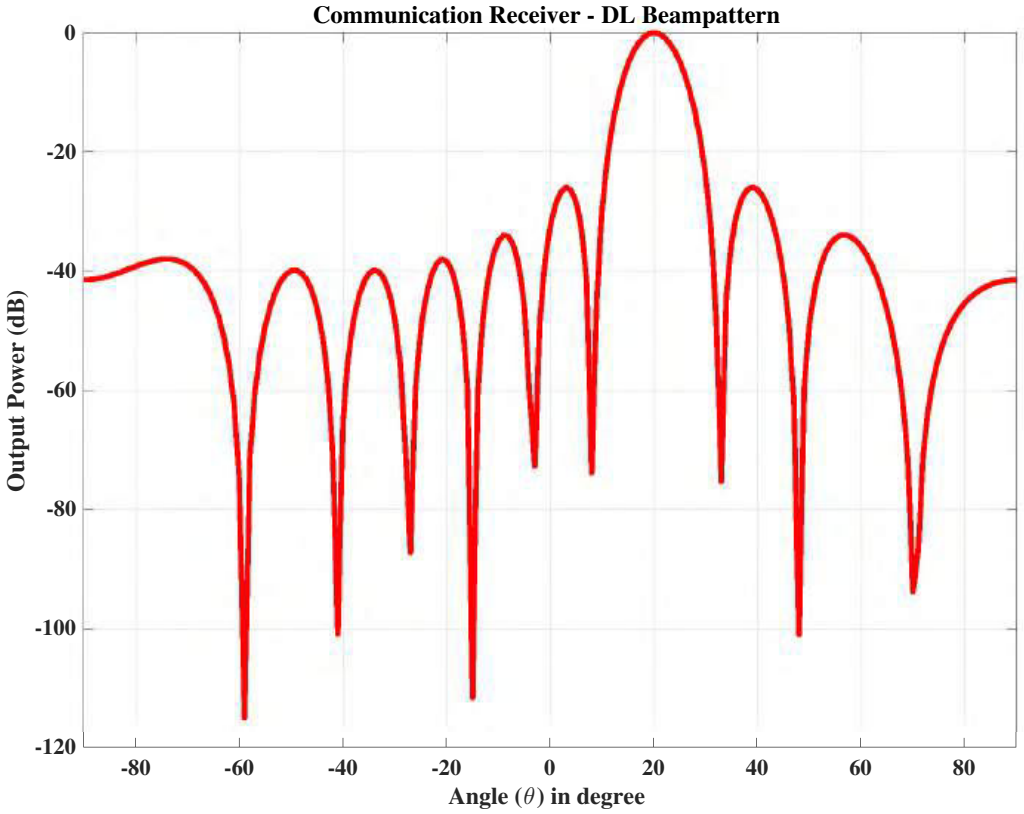

Figure 3.5: Example 1: Single communication Receiver at $\theta_c = 20^o$

were located at an angle of $\theta_{c1} = 30^\circ$ and $\theta_{c3} = -30^\circ$ with allocated power of $\triangle_1 = -8dB$. Similarly, the 2^{nd} and 4^{th} communication receivers were located at position $\theta_{c2} = 50^\circ$ and $\theta_{c4} = -50^\circ$ with allocated power of $\triangle_2 = -7dB$ as shown in Figure 3.6. In this example, main lobe is set with maximum power, while 1^{st} SLL is selected as $\gamma_1 = 0.1585$ and 2^{nd} SLL is selected as $\gamma_2 = 0.1995$.

It is important to note that all the constraints used in Equation 3.10 were observed. Moreover, the conversion from linear scale to dB scale is done by using Equation 3.11. In this case, broadcast mode is used, and all communication receivers receive the same data. The beamforming-based approach is applied to decode the baseband signal, and then the decoding of bits is done as per the scheme discussed above. From Figure 3.7, it can be observed that at the communication receiver, whether it is a single case or a broadcast case, the received

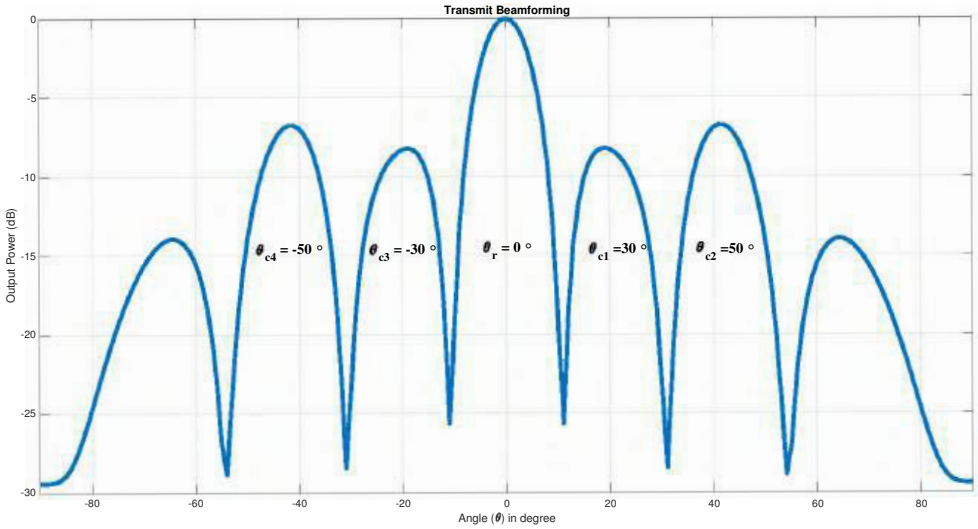

Figure 3.6: Different sidelobe Levels for each Communication receiver.

signal main lobe is approximately 25 dB higher than the sidelobes.

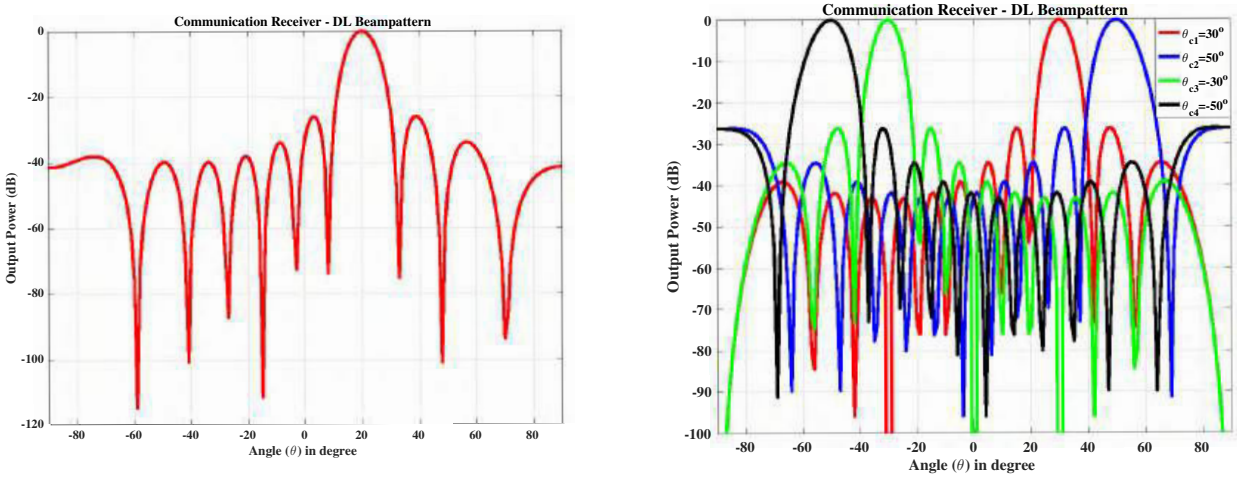

(a) Single Communication Receiver

(b) Multiple Communication Receiver

Figure 3.7: Received signal power at communication receiver under optimized weights

3.1.5.3 Example 3: Performance Analysis of the proposed scheme

In the 3^{rd} case, the radar receiver is placed at the same point, i.e. $\theta_r = 0^o$, while a single communication receiver is used and placed near the radar's main lobe, i.e. $\theta_c = 5^o$. In this example, as the target and the communication receiver lie very close to each other, a wider main lobe accommodates both entities.

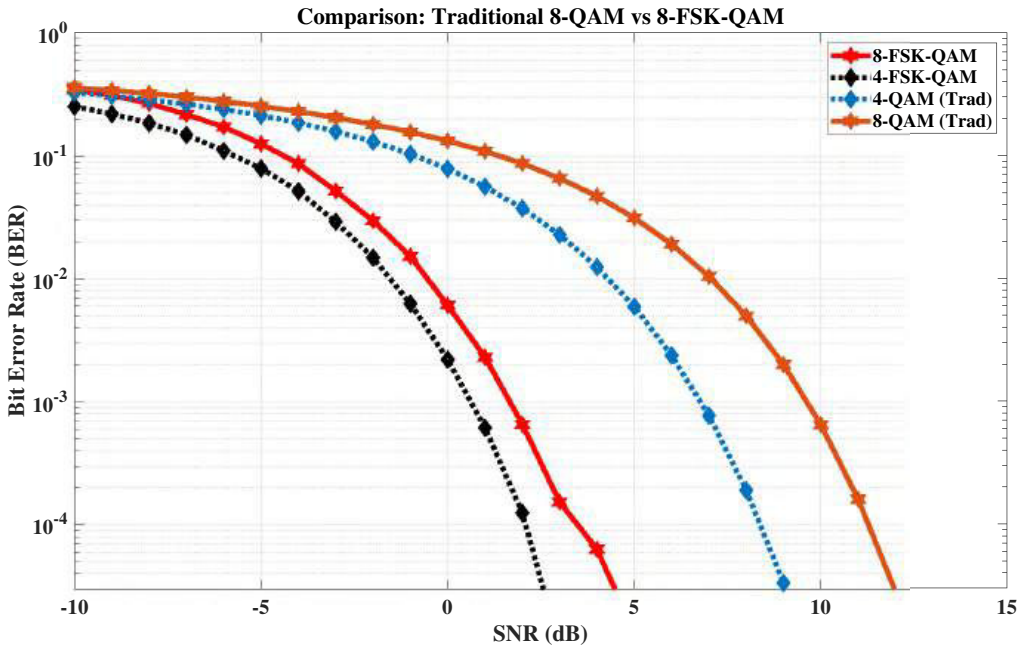

Figure 3.8: Example 3: Performance comparison of the proposed FQAM technique with existing techniques

The width of the main lobe can be controlled by $\Theta = [\theta_{min}, \theta_{max}]$. One of the objectives is to provide higher power to the wider main lobe and suppress the sidelobes. The following optimization problem is developed for this scenario.

$$\begin{aligned} \min_{\mathbf{w}} \max_{\theta} \quad & |\mathbf{w}^H a(\theta) \mid \ \theta \in \Theta \\ \text{such that} \quad & \mathbf{w}^H a(\theta_r) = \varepsilon \\ \text{and} \quad & \mathbf{w}^H a(\theta_{c_j}) = \triangle_j \quad j = 1, ..., J \end{aligned} \tag{3.12}$$

The power level of the main lobe can be controlled by ε, while communication receivers that lie outside the wider main lobe can be calculated by γ. Performance degradation is not observed at the radar receiver or the communication receiver. This experiment concluded that the proposed techniques perform well in the main and side lobes. Also, it is important to note that there is no impact of a wider main lobe on radar performance. The performance comparison of the proposed scheme with traditional QAM is calculated in terms of BER and

SNR. The proposed $4-FQAM$ scheme outperforms $4-QAM(Trad)$, while $8-FQAM$ gives better SNR compared to tp $8-QAM(Trad)$ as shown in Figure 3.8. As the size of the constellation increases from $4-QAM$ to $16-QAM$, the probability of error increases, and the efficiency of the system decreases. One of the key parameters is the selection of the orthogonal frequencies and the sampling frequency.

3.2 A Hybrid Frequency Shift Keying and Frequency Division Multiplexing-based Approach

This section of the chapter presents a new approach to embedding information in radar waveforms by a hybrid FSK–FDM technique, which enjoys the benefits of both modulations and multiplexing techniques. Note that AM-based techniques are used when the communication receiver resides in the side-lobe region of the radar. In contrast, PM techniques perform better on communication receivers in the main lobe region. However, the proposed design facilitates the delivery of information bits to the communication receivers with an improved bit rate (BR) and bit error rate (BER) regardless of their locations in the radar's main lobe or side lobe regions. Initially, a lookup table is maintained that contains the symbols mapped against the possible combination of two information bits. Since each symbol contains information on the orthogonal waveforms and frequencies, a composite signal is generated by adding multiple symbols using a linear adder. Eventually, the overall data rate significantly increased when adding the symbol through a linear adder in each PRI. Next, this composite signal is modulated at an intermediate frequency upon which the radar operates. Finally, the received signal at the communication

receiver is passed through the bandpass filtering procedure to extract the individual symbol. Each combination of waveform and frequency is decoded using matched filtering. The main attributes of this study are summarized as follows:

- The proposed design facilitates the delivery of information bits to the communication receivers with an improved bit rate (BR) and bit error rate (BER) regardless of their locations in the radar's main lobe or side lobe regions.
- The proposed method offers reduced inter-symbol interference as the decoding of each composite symbol at any communication receiver is independent of other neighboring symbols.

The rest of the chapter is organized as follows. The section 3.2.1 explains the signal data model, while Section 3.2.2 presents the proposed information embedding approach at the transmitter side. Furthermore, communication receiver design is discussed in Section 3.2.3.2, while Section 3.2.4 presents the simulation results, followed by the conclusion in Section 3.3.

3.2.1 Proposed Data Model

A signal data model is developed in the following sections for the DFRC design, using FSK and FDM techniques. The DFRC transmitter, the radar receiver, and the communication receiver are all equipped with uniform linear arrays (ULAs) using M_T, M_R, and N_R antenna elements, respectively.

In general, all arrays maintain a half-wavelength spacing between the elements. In this study, it is considered that the DFRC transmitter and radar receiver are placed so close to each other that they receive the same angle of radiation from each other. The transmitter array mainly generates pulses for

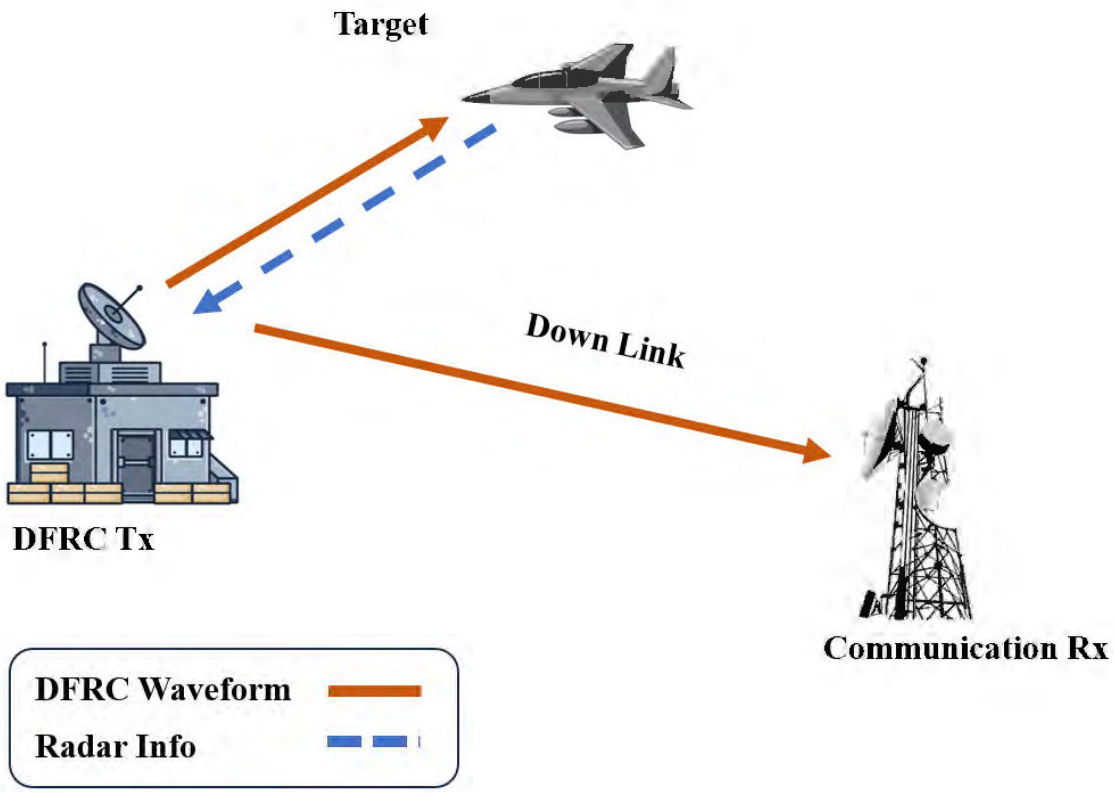

Figure 3.9: Data model for the DFRC.

detecting and tracking radar targets. The secondary objective of the transmitter array is to embed communication bits in the pulses without affecting the radar operation. The DFRC transmitting array steers the transmitted power within the main beam, where radar operation occurs. The proposed data model is shown in Figure 3.9. The $M_T \times 1$ vector form of the baseband signal for the τ^{th} radar pulse at the input of the transmit antenna [71] is:

$$\mathbf{s}(t,\tau) = \lambda(\tau)\mathbf{w}^*(t)\mathbf{x}_{fdm}(t) \tag{3.13}$$

where time within each radar pulse is represented by t, and the pulse number is represented by τ. For each transmitted waveform, $\lambda(t)$ determines how much power is assigned to each waveform such that the total transmitted power is fixed. This vector is primarily designed to focus the transmitted power inside the main beam of the radar while minimizing the power radiated outside

the main beam. Similarly, $\mathbf{w}(t)$ represents the uniform transmit array beamforming weight vector with dimensions $M_T \times 1$ for all waveform combinations, $(.)^*$ denotes the complex conjugate and $\mathbf{x}_{fdm}(t)$ is the composite vector developed by adding multiple FSK-modulated symbols. Each FSK symbol represents two bits of information based on multiple orthogonal waveform combinations. More details about the construction of $\mathbf{x}_{fdm}(t)$ are discussed in Section 3.2.2. It is assumed that the proposed waveform vectors must be orthogonal to be effective, but this is not necessarily true of the baseband signals $\mathbf{s}(t, \tau)$.

3.2.2 Proposed Transmit Signalling Strategy for Information Embedding

Every transmitted orthogonal JWF combination is used during each radar pulse to deliver two information bits to the communication receivers. Binary information is embedded in radar signals in the form of waveform numbers and frequencies. These signals are sent from a DFRC transmitter and received by both a radar and communication receiver.

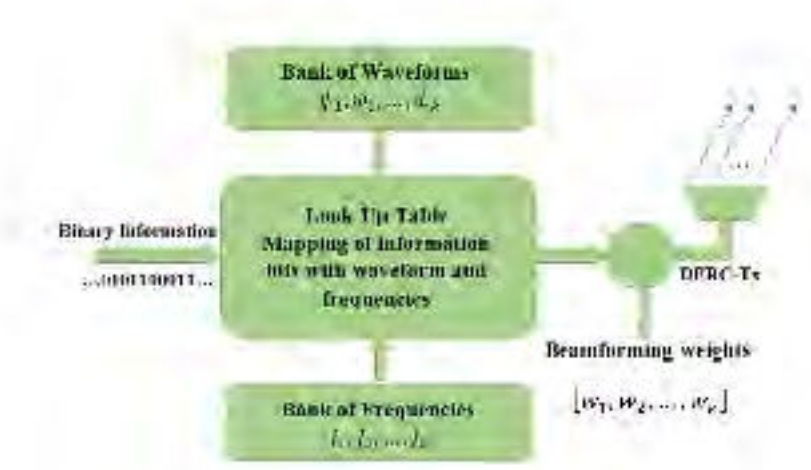

Figure 3.10: The proposed information embedding methodology at the DFRC transmitter.

The data is then extracted from the signal, allowing the radar receiver to determine the objects' direction and velocity. Two bits of information are mapped

during each radar transmit pulse, whereas two frequencies are used in this technique to represent either binary 0 or binary 1, as shown in Figure 3.10. The two frequencies are selected from a pool of available frequencies, depending on the information the transmitter wants to communicate. The communication receiver then decodes the frequencies and extracts the binary information from the signal. Similarly, the two waveforms represent binary 0 or binary 1. This information mapping is performed through FSK. This method is based on the fact that different frequencies can be easily distinguished and used to represent different binary values. In FSK, two different frequencies are assigned to represent the binary digit 0 and digit 1. The transmitter then sends these frequencies, one after the other. The receiver decodes the frequencies to extract the binary data from the signal. Thus, employing FSK modulation, two bits can be represented by distinct frequencies and waveforms, as shown in Table 3.2.

Table 3.2: The lookup table.

$m_1(t) = \xi_{00}(t) = \psi_{0,f_0}(t)$	$m_2(t) = \xi_{01}(t) = \psi_{0,f_1}(t)$
$m_3(t) = \xi_{10}(t) = \psi_{1,f_0}(t)$	$m_4(t) = \xi_{11}(t) = \psi_{1,f_1}(t)$

Each communication symbol encodes two bits of information using a waveform and frequency combination. Consider the random bits pattern shown in Table 3.3. By mapping each bit pattern to a specific waveform and frequency combination, it is possible to construct two distinct symbols that can be sent over a communication channel. These symbols can then be decoded back to the corresponding bit pattern on the receiver side. The pattern selector selects a suitable combination of waveform and frequency to be transmitted.

For example, for $B_l(t) = 00$, the joint waveform and frequency (JWF) combination of $\xi_{00}(t)$ has been selected from the lookup table. Moreover, multiple JWF combinations are added to make a composite signal using FDM. This sig-

Table 3.3: Random information bit mapping to a JWF combination.

...	0	1	1	1	1	0	0	0	...
	$\xi_{01}(t)$		$\xi_{11}(t)$		$\xi_{10}(t)$		$\xi_{00}(t)$		

nal is then transmitted from the DFRC transmitter as shown in Figure 3.11.

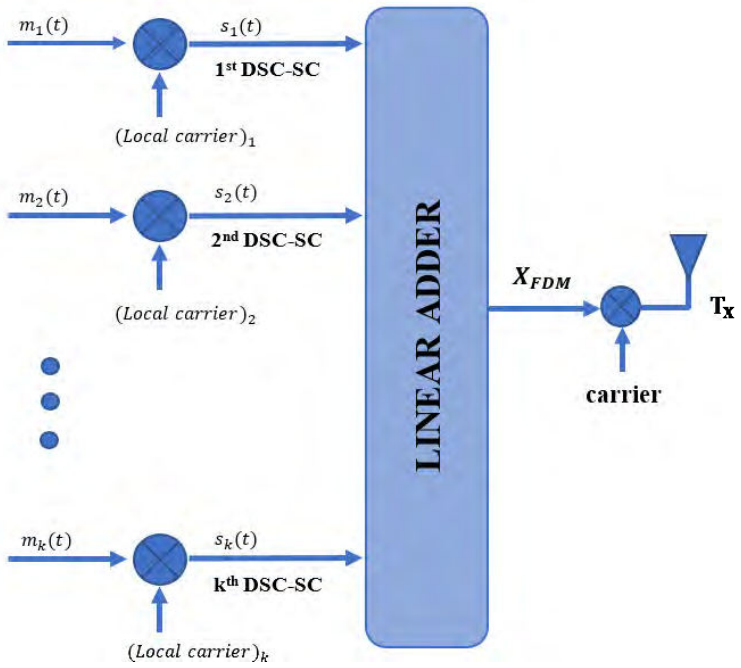

Figure 3.11: The proposed composite information embedding methodology using frequency division multiplexing at the DFRC transmitter.

Next, the modulated symbols are added together to achieve a double data rate using the FDM technique. The composite signal is received by the communication receiver, where the JWF symbols are separated via a frequency demodulator. The pattern selector then decodes these JWF combinations into the corresponding bit patterns. These bit patterns can then be converted back to the symbols originally sent by the transmitter. The symbols are then converted to binary data, which can be used for further processing. The mathematical description of a composite signal is given as:

$$\mathbf{x}_{fdm}(t) = \sum_{j=1}^{J} \mathbf{m}_j(t,\tau) \tag{3.14}$$

where, $\mathbf{m}_j$, $j = 1,...,J$ is the JWF symbol added together to double the data rate in the proposed scheme. The overall form of the JWF sample with allocated power can be written as:

$$\mathbf{m}_{i,j}(t) = \sqrt{\frac{M_T}{L_B}}(t)\xi_{i,f_j}(t) \tag{3.15}$$

Note that all waveforms must be mutually orthogonal for improved communication with less inter-waveform interference.

3.2.3 Receiver Design

This study examines two types of receivers: the radar receiver and the communication receiver. At the radar receiver, the direction of arrival (DOA) of the target, represented by angle θ, is determined, along with the probability of target detection and receiver operation characteristics. Furthermore, at the communication receiver, the demodulation of information and the security of communication transmission are analyzed.

3.2.3.1 Radar Receiver

Assume that the radar main beam contains M far-field targets. The vector form of the baseband signal received by the radar receiver is expressed as

$$\mathbf{x}_r(t,\tau) = \sqrt{\frac{M_T}{L_B}} \sum_{m=1}^{M} \beta_m(\mathbf{a}^T(\theta_m)\mathbf{s}(t,\tau))\mathbf{b}(\theta_m) + \mathbf{e}_r(t,\tau) + \mathbf{n}_r(t,\tau) \tag{3.16}$$

where $\sqrt{\frac{M_T}{L_B}}$ is the received signal power, β_m is the reflection coefficient of the mth target, $\mathbf{a}(\theta_m)$ is the steering vector in the direction θ_m from the dual-function transmitter, $\mathbf{s}(t,\tau)$ is the base band signal, $\mathbf{b}(\theta_m)$ is the steering vector in the direction θ_m at the receiver, $\mathbf{e}_r(t,\tau)$ is the interference vector at the radar receiver, and $\mathbf{n}_r(t,\tau)$ is the AWGN vector zero mean with variance $\sigma^2\mathbf{I}$ at the radar receiver. The reflection constant, β_m, remains constant during each pulse but varies on a pulse-to-pulse basis, obeying the Swerling II model. Similarly, $\mathbf{e}_r(t,\tau)$ is the interference vector that impinges on the receiver array from the side lobes. It is important to note that processing is performed directly on the receiver array $M_T \times 1$ vector $\mathbf{x}_r(t,\tau)$ without going into waveform diversity at this stage.

3.2.3.2 Communication Receiver

There are K communication receivers in the far field, each having an array of N_R elements. For ease and convenience and a priory communication, the lookup table containing the dictionary of the orthogonal JWF made using FSK modulation and FDM symbols at the dual-function transmitter is known to each communication receiver. Assume that the kth communication receiver, equipped with N_R antenna elements arranged uniformly in a linear shape, receives the following FSK–FDM composite signal.

$$\mathbf{y}_{k_{fdm}}(t,\tau) = \sqrt{\frac{M_T}{L_B}}\alpha_k(\mathbf{a}^T(\phi_i)\mathbf{s}(t,\tau))\mathbf{c}_k(\phi_i)\mathbf{x}_{fdm}(t,\tau) + \mathbf{n}_{k_{fdm}}(t,\tau) \qquad (3.17)$$

where $\sqrt{\frac{M_T}{L_B}}$ is the received power at the communication receiver, α_k is the channel coefficient constant from the transmitter array towards the kth commu-

nication receiver which summarize the propagation environment, $\mathbf{a}(\phi_i)$ is the steering vector in the direction θ_m from the dual-function transmitter, $\mathbf{s}(t,\tau)$ is the baseband signal, $\mathbf{c}_k(\phi_k)$ is the steering vector from the receive array in the direction ϕ_k from the communication receiver, $\mathbf{x}_{fdm}$ is the composite FSK–FDM signal, $\mathbf{n}_k(t,\tau)$ is the AWGN vector zero mean with variance $\sigma^2\mathbf{I}$ at the communication receiver, and (ϕ_k) is the direction of the kth communication receiver.

As a first step, the beam-forming operation is applied to the received signal. The steering vector is separated from it by multiplying the beam-forming weights at the communication receiver. This allows for the extraction of the desired signal from the received signal, allowing the receiver to focus on the direction of the signal and ignore signals from other directions. This reduces interference from other sources and improves the signal-to-noise ratio (SNR) at the receiver. The beam-forming operation is mathematically expressed by Equation (3.18).

$$\mathbf{g}_{k_{fdm}}(t,\tau) = \mathbf{c}_k^H(\phi_j)\mathbf{y}_{k_{fdm}}(t,\tau) \tag{3.18}$$

The next step in this process is to apply bandpass filtering techniques to the received FDM composite signal.

The bandpass filter is implemented as a digital finite impulse response (FIR) filter and configured to have a passband with the desired bandwidth. The filtered signal is then demodulated to recover the original transmitted information. A mathematical description is given in Equation (3.19) and a graphic representation is shown in Figure 3.12

$$\mathbf{r}_k(t,\tau) = \mathbf{v}(\vartheta)\mathbf{g}_{k_{fdm}}(t,\tau) \tag{3.19}$$

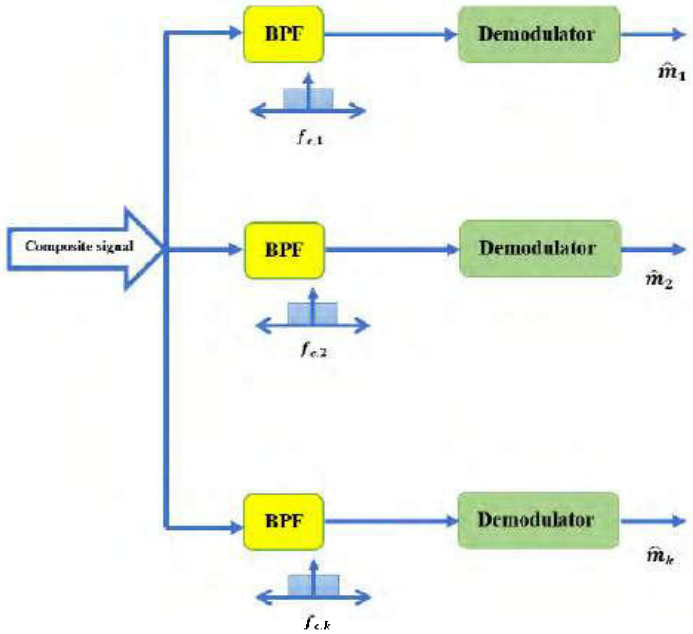

Figure 3.12: The proposed composite information decoding methodology at the communication receiver.

where $\mathbf{v}(\vartheta)$ is the bandpass filtering coefficients at the kth communication receiver.

Matched filtering is then applied to the signal, Equation (3.19), to identify the actual binary information transmitted. This involves multiplying the signal by a reference signal delayed by the same amount of time as the original signal. The multiplication results are then accumulated over a period of time. The accumulated signal can be used to identify the binary information transmitted. Matched filtering is mathematically described by Equation (3.20).

$$\mathbf{y}_{k,l}(t,\tau) = \begin{cases} \sqrt{\frac{M_T}{L_B}}\mathbf{r}_1(t,\tau) + \mathbf{n}_1(t,\tau), & if \quad B_l = 00 \\ \sqrt{\frac{M_T}{L_B}}\mathbf{r}_2(t,\tau) + \mathbf{n}_2(t,\tau), & if \quad B_l = 01 \\ \sqrt{\frac{M_T}{L_B}}\mathbf{r}_3(t,\tau) + \mathbf{n}_3(t,\tau), & if \quad B_l = 10 \\ \sqrt{\frac{M_T}{L_B}}\mathbf{r}_4(t,\tau) + \mathbf{n}_4(t,\tau), & if \quad B_l = 11 \end{cases} \tag{3.20}$$

The overall process of match filtering and information decoding at the com-

munication receiver is shown in Figure 3.13. Furthermore, by performing the simple ratio test on the output of the filter in Equation (3.18), the following is obtained

$$\widehat{B}_l(\tau) = \begin{cases} 0 & if \quad |y_{k,l}| \geqslant T \\ 1 & if \quad |y_{k,l}| \leq T \end{cases} \tag{3.21}$$

where T is the threshold constant of frequency separation for orthogonality.

It is important to note that multiple waveforms are selected at a time, and they change on a pulse-to-pulse basis. The data rate is given as a product of the number of bits per pulse and the PRF, i.e.,

$$\text{Data Rate} = \text{PRF} \times \text{bits per composite symbol.} \tag{3.22}$$

The probability that 00 is transmitted and 01 is received can be written as $P(01|00)$. Similarly, when 10 is received, it can be written as $P(10|00)$ and the overall equation with error function can be modeled as:

$$P(00|00) = 1 - \{P(01|00) + P(10|00) + P(11|00)\}. \tag{3.23}$$

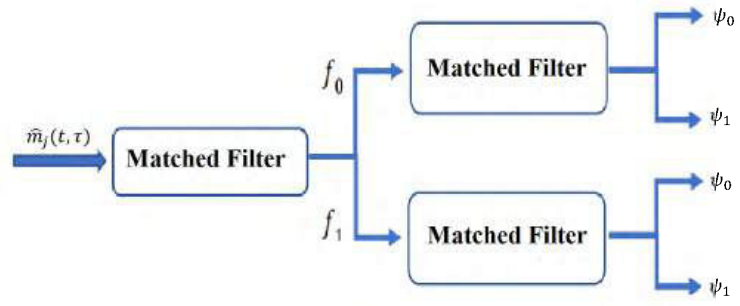

Figure 3.13: Detailed demodulator design in terms of matched filtering after the bandpass filter at the communication receiver.

3.2.4 Results and Discussion

Consider a uniform linear transmit array consisting of $M_T = 24$ antenna elements spaced one-half wavelength apart. The purpose of this array is to maximize the directivity of the transmitted signal and minimize interference at the same time. In addition to the radar operation within the main beam, it is assumed that a communication message of two FSK symbols is added cooperatively during each radar pulse. This is performed to develop a composite signal containing four bits of information transmitted through the channel. The baseband signals with FSK modulation are generated using the frequencies $f_1 = 100$ Hz and $f_2 = 200$ Hz in these simulations. The main beam is fixed in a specified direction. All simulations are performed using Matlab, on a system with an Intel microprocessor 11^{th} generation, 8 GB RAM, and 2 GB graphics memory.

In the following sections, the simulation results are presented with different illustrative examples for clarity and manageable acquaintance.

3.2.4.1 Example 1: Single Communication Receiver

In the 1^{st} case, the radar target is fixed at $\theta_r = 0^\circ$ and the communication receiver is placed at $\theta_c = -50^\circ$ as shown in Figure 3.14, while the signal received at the communication receiver is shown in Figure 3.15.

3.2.4.2 Example 2: Multiple Communication Receiver

At the communication receiver, an $N_R = 24$ antenna elements with the same arrangements as used for the radar receiver. In the 2^{nd} case one radar target is considered which lies in the main beam fixed at $\theta_r = 0^\circ$, while four communication receivers are located in the side lobes at $\theta_{c1} = 20^\circ$, $\theta_{c2} = 40^\circ$, $\theta_{c3} = -20^\circ$ and $\theta_{c4} = -40^\circ$, as shown in Figure 3.16.

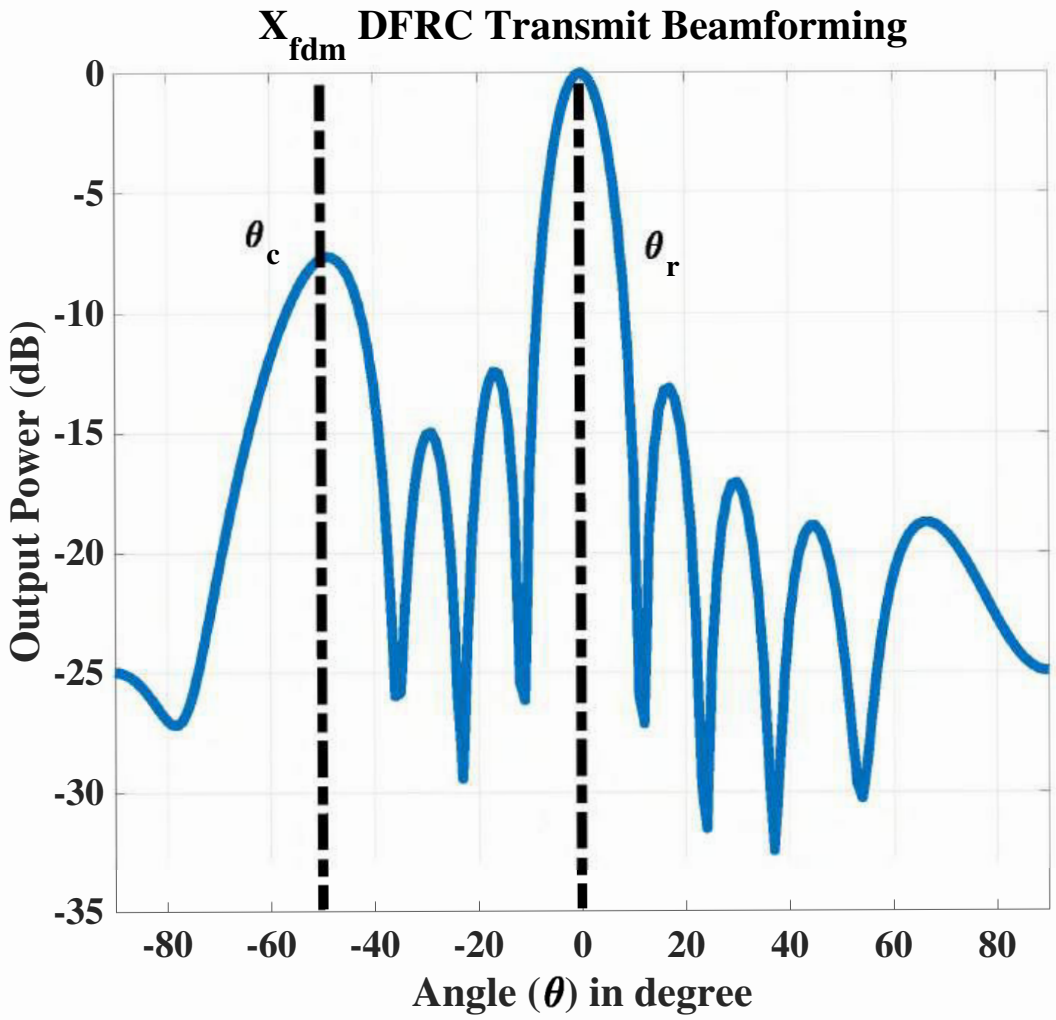

Figure 3.14: Example 1: The transmitted signal with radar $\theta_r = 0^\circ$ and the single communication receiver at $\theta_c = -50^\circ$.

The data is transmitted to the communication receivers using the broadcast mode. The signal received at each communication receiver is shown in Figure 3.17.

3.2.4.3 Example 3: Bit Error Rate Comparison of the Proposed Scheme

In this study, it is assumed that the average transmit power of each transmit antenna is normalized to 1, i.e., the total transmit power is fixed to $P_{total} = 1$. For each method considered, the total transmitted power is distributed evenly among the number of waveforms. To calculate the BER, 10^6 pulses are considered in the embedding process. As a result, the performance of the various

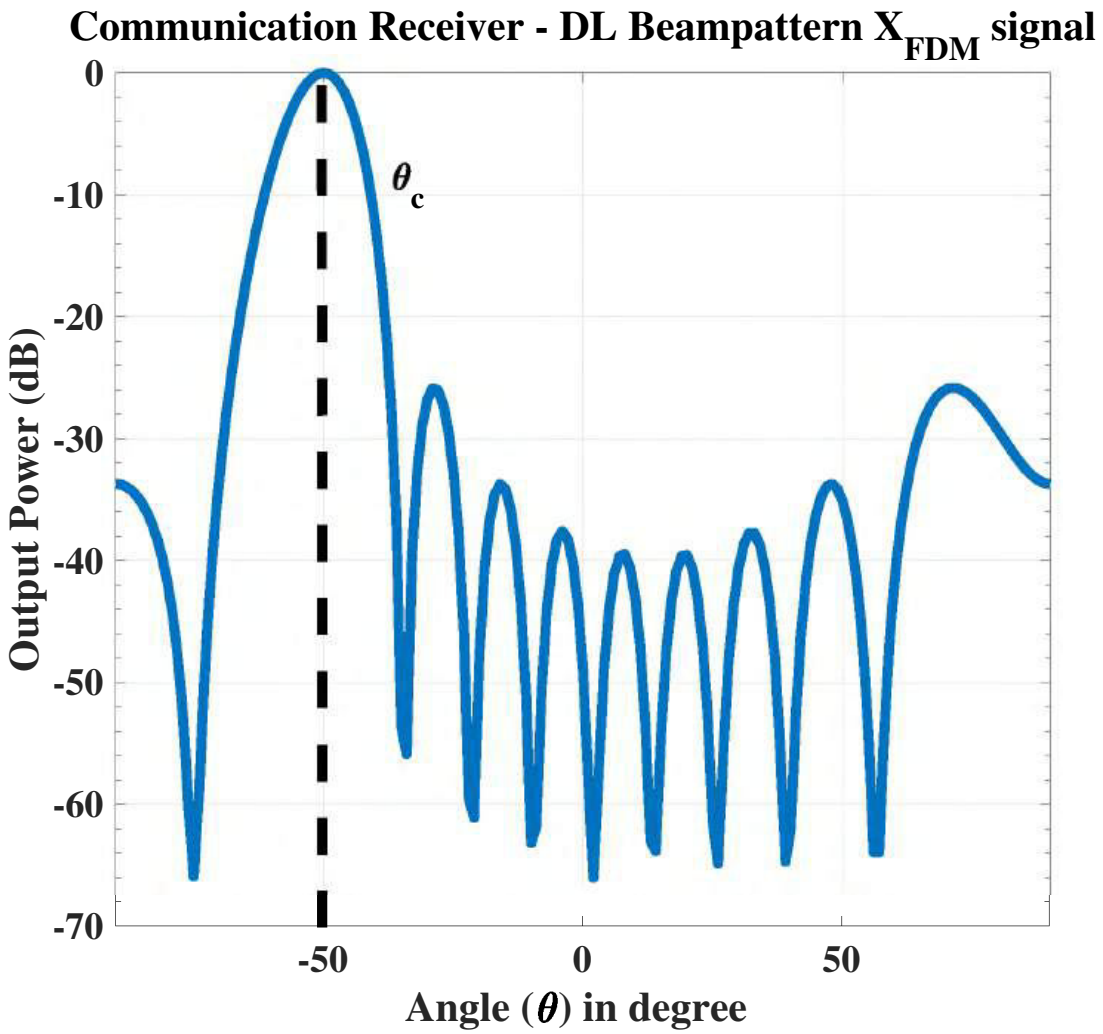

Figure 3.15: Example 1: The proposed composite FDM signal received at the communication receiver.

methods can be compared objectively and fairly. This ensures that the methods are evaluated based on the same SNR and that the average power of each transmit antenna remains the same.

The performance of both cases explained in examples 1 and 2 of the proposed scheme remains the same, and no degradation is observed. For the case of four communication receivers as shown in example 2, there is a slight degradation in the BER compared to the single communication receiver due to interference. The performance of the proposed scheme, for a single communication receiver with side lobe control, is compared with waveform diversity

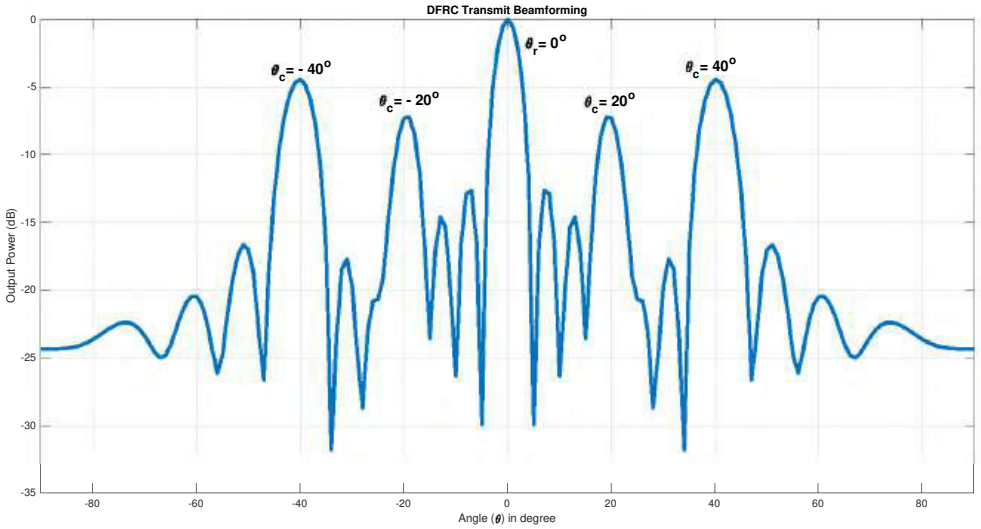

Figure 3.16: Example 2: The transmitted signal with the single radar receiver at $\theta_r = 0^\circ$ and the four communication receivers at $\theta_{c1} = 20^\circ$, $\theta_{c2} = 40^\circ$, $\theta_{c3} = -20^\circ$ and $\theta_{c4} = -40^\circ$.

cited in [71] and achieved improved BER performance. Moreover, the proposed scheme outperforms the ASK-based information embedding technique as cited in [74]. It can also be observed from the results shown in Figure 3.18, that the proposed scheme converges more quickly with the safe margin of $3dB$ when compared with the beam pattern PSK-based approach [179] in terms of BER and SNR.

3.2.4.4 Example 4: Decoding the Information Bits

While decoding the information bits at communication receivers, they all use the same weight vectors and have access to a shared lookup table in advance. This helps ensure consistency in how signals are processed. The shape of the composite signal at the transmitted and received sides is depicted in Figure 3.19, showcasing the overall structure of the signal throughout the transmission process.

Furthermore, the FFT analysis reveals that both the transmitted and received signals have the same frequency content. Additionally, in Figure 3.20, each

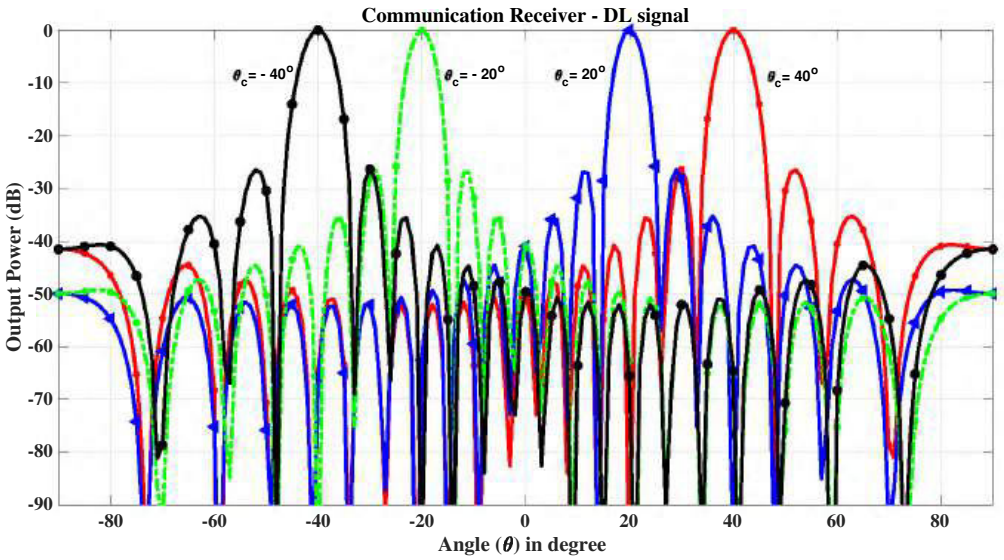

Figure 3.17: The communication receiver at $\theta_{c1} = 20^\circ$, $\theta_{c2} = 40^\circ$, $\theta_{c3} = -20^\circ$ and $\theta_{c4} = -40^\circ$.

bit is decoded accurately after going through a filtering process. This suggests that the system is effective at understanding and extracting information from the signals it receives.

3.2.4.5 Example 5: Security of the Communication Process against Intercepts

In this section, the concerns related to security in communication are discussed. The SNR for all angles used for transmission is calculated. It is clear from Figure 3.21 that interference at the desired angle, i.e., $\theta_c = -50^\circ$ is minimum while the rest of the angles suffer very high levels of interference. The total number of bits transmitted was 10^6. The SNR was fixed at 5 dB. The results are compared with beam pattern ASK and beam pattern PSK-based approaches. It is concluded that the performance of the proposed scheme is better than these methods at the same SNR.

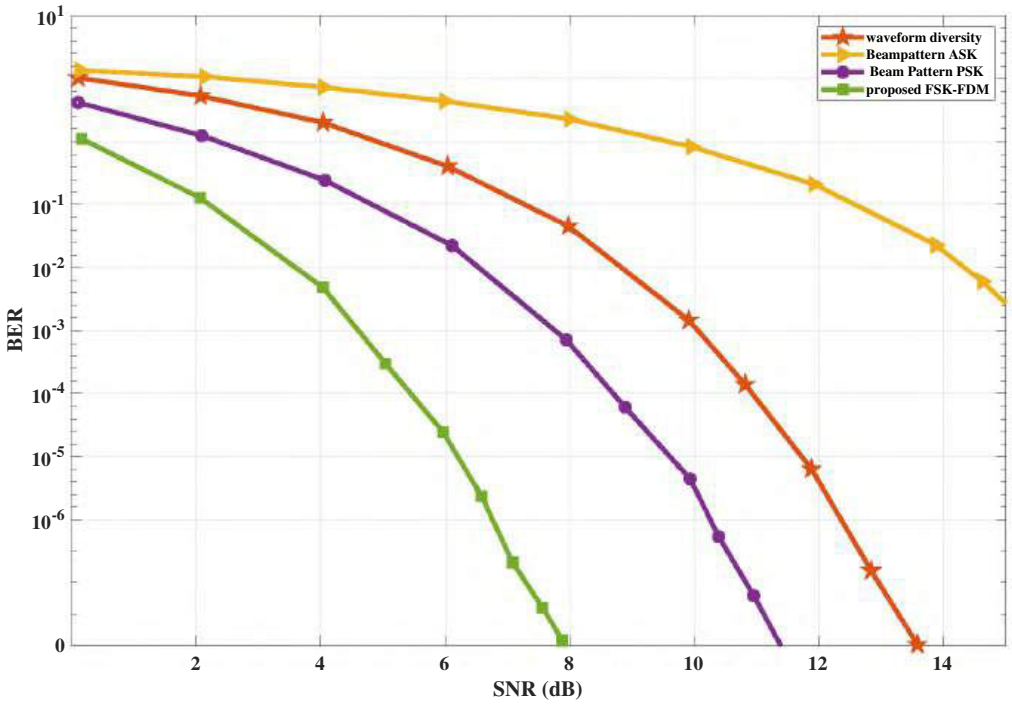

Figure 3.18: Example 3: The performance comparison of the proposed scheme with existing schemes.

3.2.4.6 Example 6: DoA Estimation Performance

The objective in this section is to assess the accuracy of DoA estimation for radar operation. A target is assumed to be located in the far field region at a distance of $\theta_r = 0^\circ$. It is assumed that the target reflection coefficients remain constant from pulse to pulse during the radar pulse period but will change pulse-to-pulse as they are drawn from a normal distribution. The number of radar receiver array elements is set to $M_R = 24$. The number of pulses used was $N = 100$, and 100 snapshots per pulse were used at the radar receiver to build the data covariance matrix. Bartlett beam-forming is used to estimate the DoA for all methods tested. Throughout the different scenarios, i.e., communication in the main and side lobes, no performance degradation was observed in terms of radar operation and DoA estimation. The results are presented in the form

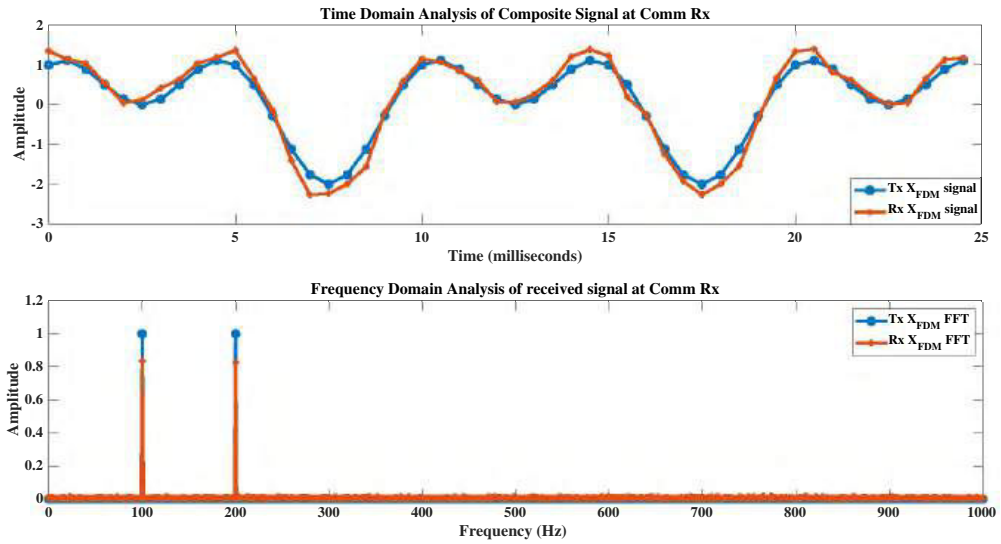

Figure 3.19: Example 4: The performance comparison of the transmitted and received FDM signals and their frequency response.

of power vs. SNR, as shown in Figure 3.22.

3.2.4.7 Example 7: Probability of Target Detection

In this subsection, the probability of target detection at different SNR levels is discussed. A single target is considered in this case, located at $\theta_r = 0^\circ$ with $M_R = 24$ antenna elements. The receiver operating characteristic (ROC) curves are calculated between the probability of detection $\mathbf{P}_d$ and the probability of a false alarm $\mathbf{P}_{FA}$ at different SNR levels.

Mathematically, ROC can be calculated as (3.24)

$$\mathbf{P}_d = \frac{1}{2}[erfc(erfc^{-1}(2P_{FA}) - \sqrt{\chi})]. \tag{3.24}$$

where χ is the SNR.

Figure 3.23 shows the detection probability at an SNR of -5 dB and 5 dB, providing insight into the system's performance under different signal-to-noise ratios. Finally, it is observed that embedding information into the radar emis-

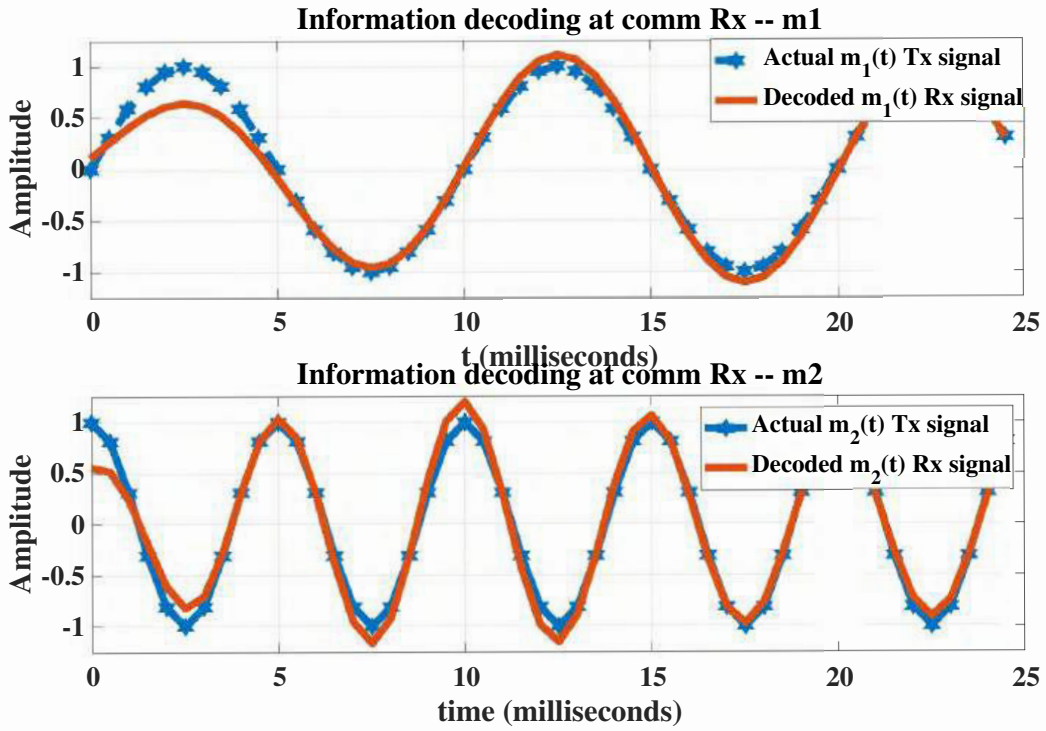

Figure 3.20: Decoding information bits at the communication receiver

sion does not affect radar operation, indicating that the communication and radar functions can coexist without interference.

A comparison of the proposed technique with other existing techniques in terms of BER vs. SNR is provided in Table 3.4.

Table 3.4: The effectiveness of the proposed technique over existing techniques in terms of BER vs. SNR.

	BER for information Embedding schemes (No. of Defected Bits)			
SNR	**Waveform Diversity**	**Beam pattern-ASK**	**Beam pattern PSK**	**FSK–FDM (Proposed)**
0	912	913	862	804
2	872	903	809	754
4	830	886	756	694
6	760	864	706	639
8	665	835	651	587
10	616	791	590	533

The comparison in Table 3.5 clearly demonstrates the superiority of the proposed technique over existing methods. The enhanced performance of the pro-

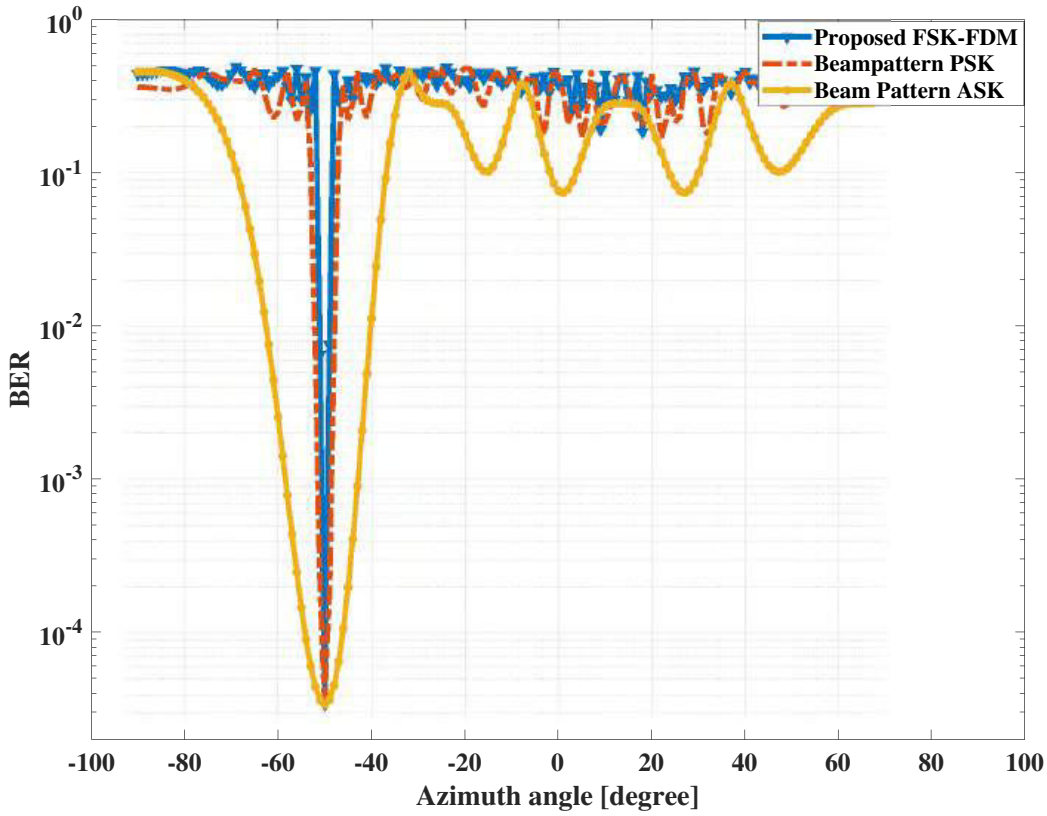

Figure 3.21: Example 5: The performance comparison against the intercepts at the communication receiver at $\theta_c = -50^\circ$.

posed technique is particularly evident when evaluated in terms of bit error rate (BER) versus security against interception at the communication receiver, analyzed to the beam width (measured in degrees) for $\theta_c = 50^\circ$. It is evident from the data presented in the table that the proposed scheme achieves a narrower beam width compared to traditional methods, further contributing to its enhanced security and efficiency in reducing interception risks.

When implementing an FSK–FDM-based DFRC transmitter, careful consideration of the SNR is essential as it directly influences the data rate. Simulation results reveal that the proposed scheme excels particularly at higher SNR values, showcasing its robust performance in varying conditions.

The proposed system achieves a better trade-off between jamming robust-

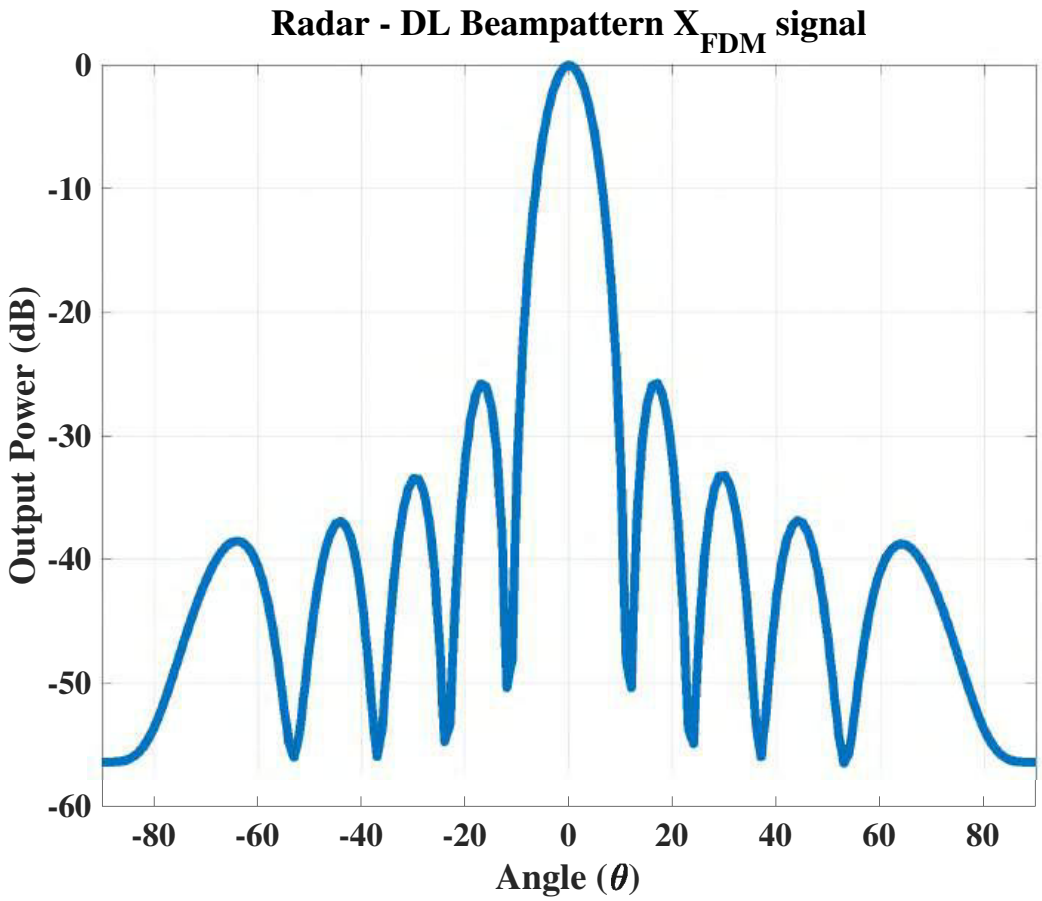

Figure 3.22: Example 6: The proposed composite FDM signal received at the radar receiver.

ness and data rate. It also has lower computational complexity, making it a cost-effective solution. Finally, it offers greater flexibility in terms of modulation format and data rate. Furthermore, the proposed system offers enhanced flexibility in terms of modulation format and data rate, providing adaptability to diverse communication environments and requirements. This versatility enhances its applicability across a range of scenarios, making it a compelling choice for practical implementation.

3.3 Summary

In this chapter, two new approaches were introduced for the dual-function radar-communication system by employing a frequency shift keying-based ar-

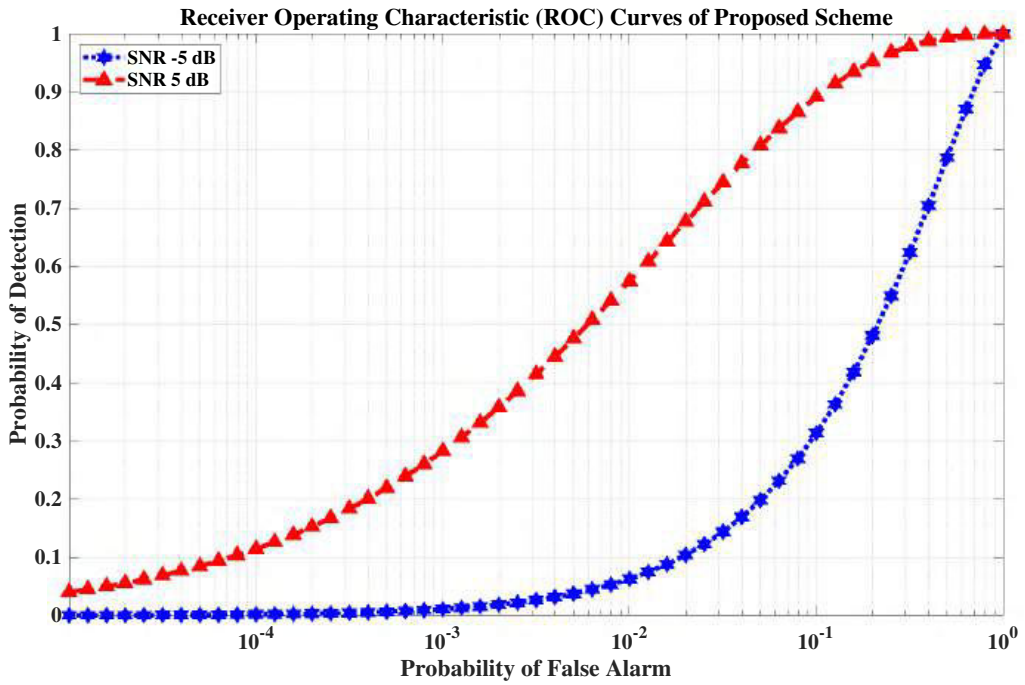

Figure 3.23: Example 7: The receiver operating characteristic curves of the proposed scheme.

Table 3.5: The effectiveness of the proposed technique over existing techniques in terms of bit error rate vs. security against intercept at the communication receiver (beam width in degrees) for $\theta_c = 50^o$.

	security against intercept (beam width in degrees)			
BER	**Waveform Diversity**	**Beam pattern-ASK**	**Beam pattern PSK**	**FSK–FDM (Proposed)**
10^{-1}	34	32	6	4
10^{-2}	24	22	4	3
10^{-3}	17	15	3	1.5
10^{-4}	10	8	1.5	1

chitecture. The first was based on using QAM symbols at different frequency levels and named Frequency QAM (FQAM). This proposed scheme works regardless of the main lobe and sidelobes and utilizes M-ary orthogonal frequency and QAM symbols to transmit binary information to each communication user. This technique doubles the PRF-based data rate, and radar operation remains uninterrupted. It is concluded that the proposed hybrid scheme performs well compared to standalone FSK and QAM. Similarly, the second proposed technique increased the data rate for the communication receiver. Moreover, it

delivers information to the communication receivers with an improved BER regardless of their location in the main or sidelobes of the radar beam. Next, orthogonal frequency and waveform-based combinations were used to transmit binary information to each communication user, facilitating double the PRF-based data rate with improved secrecy. Finally, diverse scenarios were considered, and extensive simulations were conducted to validate the effectiveness of the proposed technique.

Chapter 4

Deep Learning-Enabled Cognitive Design for DFRC

The dual-function radar and communication (DFRC) paradigm has recently emerged as a solution to spectrum congestion challenges. However, most research in this area depends on computationally complex likelihood-based methods for communication signals, using only a single waveform. It is important to note that using a single waveform for different scenarios, such as when a communication receiver is in the radar's main lobe or side lobe, can result in performance degradation in a DFRC system.

To address this issue, this thesis introduces a cognitive DFRC architecture that employs a variety of orthogonal waveforms at the transmitter. Specifically, based on a perception-action cycle, a PSK-based waveform is used for communication when both the radar target and communication receiver are within the main lobe, while a QAM-based waveform is used when the radar target is in the main lobe and the communication receiver is in the side lobes.

Furthermore, to improve feature-based estimation, the communication receiver uses a Convolutional Neural Network (CNN) that is designed to automatically learn and extract features from received signals at different SNR

levels. Additionally, the system's adaptive nature allows it to effectively identify the type of received signal and determine its corresponding SNR value. Moreover, in realistic scenarios with various channel impairments, deep learning techniques are applied to extract features from received signals, departing significantly from likelihood-based methods and reducing computational complexity. The proposed methodology's effectiveness is validated through Monte Carlo simulations, underscoring its potential to address challenges associated with DFRC under real-world conditions.

Reflecting on the aforementioned points, a communication receiver must be able to receive signals from multiple directions. In consequence, there is an inherent risk of multi-path fading, which leads to difficulties in detecting signals accurately. As a result, software-defined radio (SDR) and cognitive radio (CR) are becoming increasingly popular, as these devices can adapt their transmission parameters to suit the conditions, etc. Therefore, it is essential that the receiver can classify the signal without prior knowledge of the transmitter's parameters.

There has been considerable interest in the subject of spectrum congestion among researchers. Nevertheless, two broad categories of algorithms can be applied to received signals: likelihood-based (LB) and feature-based (FB). The first category applies spectral densities (PSD), calculating the probabilities ratio between the signals and applying matched filtering-related techniques, whereas, in the second category, features are extracted from the received signal and used to make a decision. The results of the LB-based approach are reliable and provide us with optimal solutions but the computation complexity is high. In contrast, the FB approach is easy to implement and gives us the freedom to ignore transmission schemes and the nature of devices. Furthermore, they are

robust enough to take account of channel mismatches.

4.0.1 Feature Based Estimation:

The feature-based estimation technique extracts multiple features from the received signal to estimate the characteristics of the transmitted signal, such as its range, velocity, amplitude, phase frequency, and modulation type [161]. By using FB estimation techniques, cognitive radio systems can determine if a signal is legitimate or not and thus help prevent false alarm detection [162]. Ultimately, FB estimation is essential for reliable spectrum sharing and efficient cognitive radio networks. Additionally, with improved communications performance and efficient spectrum exploitation, FB estimation can provide a valuable tool for interference avoidance in wireless networks [163]. The FB classification can be implemented by Combining with Kalman Filtering [164] or Hidden Markov Models (HMM) to improve the efficacy of results and prevent false detections [165].

The suboptimal Feature-based method is developed to classify signals by identifying useful features before the classification process [166]. These features can include instantaneously calculated values, transformed representations, statistical measures, or characteristics derived from constellation shapes. Extensive research has been conducted on both methods, revealing that the LB method offers the most effective solution but demands significant computational resources and prior knowledge of the signal. On the other hand, although less optimal in terms of accuracy, the FB method provides a faster response time due to its lack of dependence on prior information. In ML-based techniques, feature extraction becomes a task requiring expertise when employing these methods. To overcome this challenge in FB methods and enhance their

efficacy in recognizing complex patterns effectively compared to shallow models do deep learning approaches have drawn considerable attention for reducing reliance on traditional feature engineering methodologies. Due to the rapid advancements in DL technologies, numerous methods have been developed to self-learn the features, and DL is preferred because it requires large datasets, which are easily obtained from communication systems. The complexity of DL is a major concern since it involves training and testing phases, many applications have utilized depthwise convolutional networks. As a result of depth-wise convolutions, the model size is reduced significantly, but accuracy remains the same. Compared to conventional convolution, this model has fewer parameters, making it suitable for small devices in cognitive environments. In [167], authors applied a Markov-based decision process and Deep Q network to estimate the target parameters for cognitive radar. The main achievement is to minimize the interference between radar and the communication user. In [168] separable convolutional neural network (CNN) is applied to estimate features of the received signal at the communication receiver. The authors have applied CNN architecture to the signal received from a highly noise-impaired channel. Similarly, in [169] long short-term memory (LSTM) with a gated recurrent unit (GRU) layer is applied to obtain higher accuracy for B5G wireless networks and Internet of Things (IoT) networks. The efficacy of results is measured in terms of accuracy, training loss, and confusion matrix. The value of SNR is used between -20 dB to 20 dB. A few more models based on CNN architectures are studied in [170–172]mainly focusing on the extraction of features and calculating the computational complexity and accuracy of proposed models. In [173; 174], researchers skipped the features extraction step to further reduce the computational complexities. Similarly, to increase the performance while

keeping low computational complexities, the combination of CNN with recurrent neural network (RNN) is presented in [175; 176]. More details about the use of CNN, RNN, and other variants of DL algorithms have been widely discussed in literature by [177; 178].

In this investigation, a methodology is introduced that employs multiple orthogonal waveforms for information embedding, encompassing the following key aspects:

- Diverse Waveform Usage: A PSK-based waveform is chosen for communication when both the radar target and the communication receiver are positioned within the main lobe. Alternatively, a QAM-based waveform is employed when the radar target is within the main lobe and the communication receiver is situated in the side lobes.

- CNN-Based Feature Extraction: The CNN-based architecture presented in this study is meticulously designed to autonomously learn and extract features from received signals characterized by a specified SNR.

- Cognitive System Capabilities: This proposed cognitive system (based on the perception-action cycle) proficiently identifies both the type of received signal and its corresponding SNR value. Additionally, these acquired statistics are subsequently communicated to the DFRC fusion center through the communication receiver's uplink.

An impactful contribution of this research involves the successful implementation of a MATLAB model for signal classification using CNN. Demonstrating robust performance, the model achieves an accuracy rate surpassing 80%, showcasing its effectiveness in signal classification tasks. Moreover, the proposed CNN architecture approximates the received signal with minimal degra-

dation in performance, simultaneously achieving a significant enhancement in processing speed. By utilizing extended symbol-rate signals at low SNR, the proposed methodology establishes an end-to-end trainable system grounded in deep CNN architecture. Distinguishing itself from feature-based approaches, the proposed CNN architecture autonomously acquires features from raw signals, streamlining the overall system design. Additionally, the introduced approximation to the received signal enables concurrent processing and parallel execution, expediting the inference speed.

The subsequent sections of this chapter follow a structured arrangement. Section II provides insights into the conventional data model. Section III details the proposed architecture for Dual-Function Radar and Communication (DFRC). This section covers the discussion on the suggested information embedding methodology at the transmitter side, and the design aspects of both the radar receiver and the communication receiver. Additionally, a thorough examination of the deep learning-based architecture is presented, elucidating detailed information on the path leading to information decoding. Section IV is dedicated to the presentation and discussion of results, while Section V discusses the conclusion, presenting a synthesis of key findings and conclusive remarks drawn from the research.

4.1 Conventional Data Model

Consider the DFRC transmitter, which has a uniform linear array spaced half a wavelength apart. There is one communication receiver in the far field equipped with a uniform linear array (ULA). The radar receiver is placed next to the DFRC transmitter. This placement ensures that both the DFRC transmitter

and the radar receiver observe the same spatial angle. The receiver array at the communication receiver captures the signal from the DFRC transmitter, as shown in Figure (4.1) and discussed in [80].

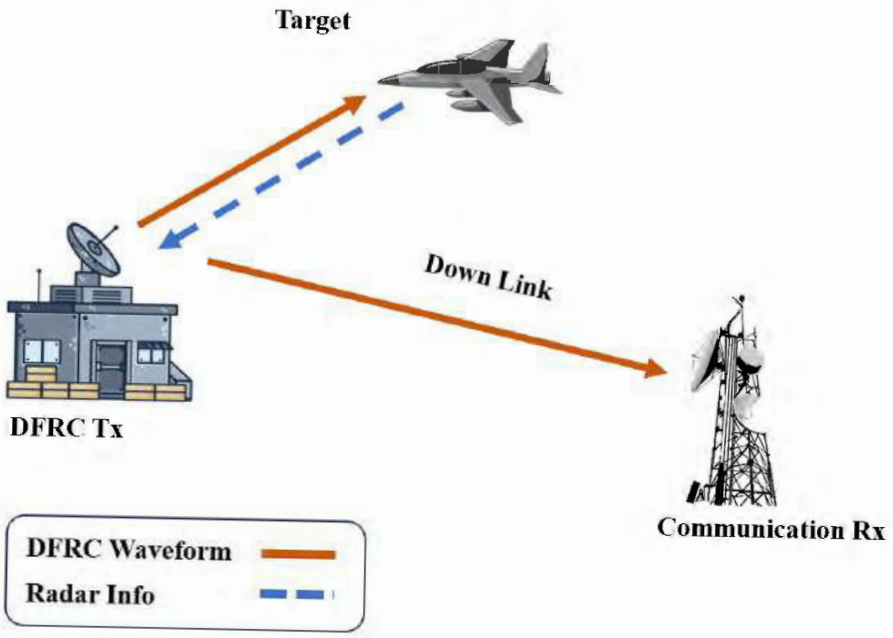

Figure 4.1: Data model of existing DFRC.

4.2 The proposed Architecture

The main goal of this data model is to develop cognition between the DFRC transmitter and the communication receiver. An uplink antenna array is added to the communication receiver to provide feedback to the cognitive feedback processor. This processor receives information from both the radar receiver and the communication receiver.

The first type of feedback provides geographical information about the target, such as the angle of arrival and signal-to-noise ratio (SNR). The second type of feedback comes from the communication receiver and includes details about the waveform and channel SNR, as shown in Figure (4.2).

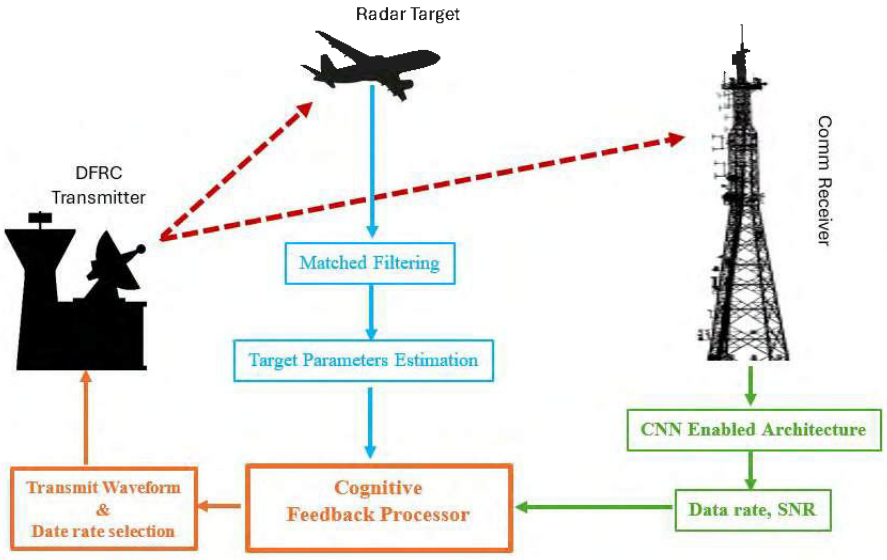

Figure 4.2: Flowchart of proposed System

The DFRC transmitter generates an omnidirectional waveform that strikes both the target and the communication receiver. The signal strikes back from both the radar receiver and the communication receiver which may or may not be partially overlapped. Alongside this, the communication receiver scans the entire environment and obtains the locations of the target and DFRC transmitter. The communication receiver sends the channel information to the DFRC receiver via the uplink path. Once the channel information is updated, the fusion center designs the DFRC transmit beamformer. When the target lies in the main lobe and the communication receiver lies in the side lobes, a QAM-based waveform will be used. Similarly, when both the target and communication receiver exist in the main lobe, a PSK-based waveform will be used.

More details about the radar and communication feedback processor are discussed in the communication receiver section. The entire activity is summarised in the following algorithm.

Table 4.1: Radar Target Search and Communication Channel Estimation

Algorithm:	Radar Target Search and Communication Channel Estimation.
Step 1 :	DFRC transmitter generates omnidirectional signal to search the target and communication receiver.
Step 2 :	Radar receiver receives the echo from target and estimates its angle and reflection coefficients.
Step 3 :	Communication receiver estimates the location of DFRC transmitter and target by using the MUSIC algorithm.
Step 4 :	Communication receiver decodes the information received in step 2 and sends feedback to DFRC transmitter via Uplink.
Step 5 :	DFRC receives the feedback from communication receiver and updates the waveform according to channel behavior.

4.2.1 DFRC Transmitter Design

In Figure (4.2), the initial module under discussion is the DFRC transmitter. The signal transmitted undergoes channel impairments and interacts with the target in the far-field, as well as the communication receiver. Subsequent sections develop a signal data model for the DFRC design, employing various modulation schemes. DFRC transmitters, radar receivers, and communication receivers are all equipped with uniform linear arrays (ULAs) utilizing M_T, M_R, N_T, and N_R antenna elements, respectively, for the transmission and reception of various signals. The spacing between each element in an array is generally half a wavelength, consistent across all arrays. It is assumed that the DFRC transmitter and radar receiver are positioned so closely that they receive the same angle of radiation. Detection and tracking of radar targets are primarily achieved with the transmitter array. Additionally, the transmitter array encapsulates communication bits without affecting radar operation. DFRC transmitting arrays steer power within the main beam, where radars operate, using this beam of radiation for object detection and location. The radar receiver then interprets the received signal, enabling the user to determine the object's location. At the

input of the transmit antenna, the $M_T \times 1$ vector form of the baseband signal for the τ^{th} pulse is

$$\mathbf{s}(t,\tau) = \mathbf{s}_{radar}(t,\tau) + \mathbf{s}_{com}(t,\tau) \tag{4.1}$$

In this formula, the signal transmitted from DFRC contains the information of both the radar signal and communication signal.

4.2.2 Proposed Information Embedding Methodology

Transmitted signals encapsulate binary data conveyed through waveform characteristics, encompassing amplitude, phase, and frequency. Both radar and communication receivers intercept these signals emanating from the DFRC transmitter. The radar receiver employs the MUSIC algorithm to obtain the object's direction of arrival (DOA) information, whereas the communication receiver deciphers the waveform information and channel SNR using CNN. On the transmitter side, a single symbol is transmitted within each pulse repetition interval. The choice of this symbol may vary from pulse to pulse, depending upon the characteristics of the channel. The lookup table comprises numerous waveforms and diverse modulation schemes, including BPSK, QPSK, 8 PSK, 16 QAM, and 64 QAM. Subsequently, the transmitter selects a singular symbol from the variety of available options for modulation, as illustrated in Figure (4.3). The communication receiver identifies the modulation scheme and corresponding waveform, facilitating the extraction of binary information.

The list of symbols, along with their dimensions and descriptions used in this chapter, for upcoming Equations, is provided in the table (4.2).

Table 4.2: List of symbols

Symbol	Dimensions	Description
$\psi_1(t)$	$M_T \times 1$	PSK based waveform
$\psi_2(t)$	$M_T \times 1$	QAM based waveform
$g(t)$	1×1	Pulse shaping filter
A_I	1×1	QAM amplitude information In phase
A_Q	1×1	QAM amplitude information Quadrature
t	1×1	Time period of each radar pulse
τ	1×1	Pulse number
A	1×1	Power assigned to each waveform
$\mathbf{w}$	$M_T \times 1$	Beamforming weights
$(\cdot)^*$	$M_T \times 1$	Complex conjugate operator
$\psi(t)$	$M_T \times 1$	orthogonal waveform
δ	1×1	kroneker delta
$\mathbf{h}(t)$	$N_R \times 1$	Channel impulse response
$(*)$	1×1	Convolutional operator
$\mathbf{n}(t)$	$M_R \times 1$	The AWGN vector
A_p	1×1	Received signal power
β_p	1×1	Reflection coefficient
$\mathbf{a}(\theta_p)$	$M_T \times 1$	Transmitter steering vector
θ_p	1×1	Direction of radar target
$\mathbf{s}(t,\tau)$	$M_T \times 1$	Transmitted baseband signal
$\mathbf{b}(\theta_p)$	$M_R \times 1$	Receiver array steering vector
$\mathbf{e}_r(t,\tau)$	$M_R \times 1$	interference encountered at the radar receiver
$\mathbf{n}_r(t,\tau)$	$M_R \times 1$	Additive white Gaussian noise
d	1×1	Inter element spacing
λ	1×1	Wavelength

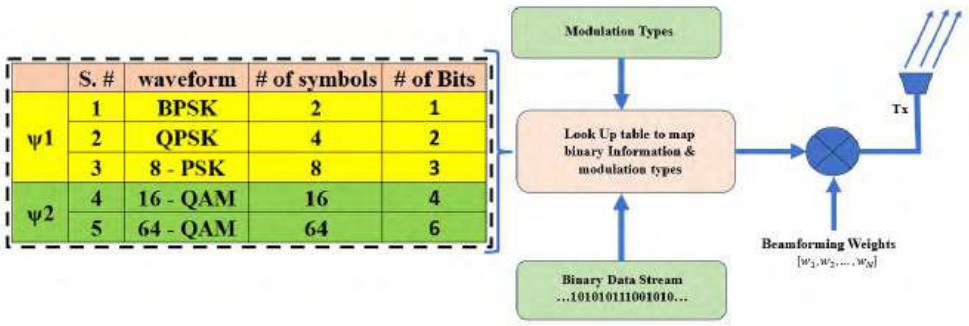

Figure 4.3: The proposed information embedding methodology at the DFRC transmitter.

It is important to note that orthogonal waveforms with large time-bandwidth product be used. Such waveform gives maximum detectable range and better resolution. The generalized waveform of $M-aryPSK$ and $M-aryQAM$ modulated signal is represented by [180]:

$$\begin{aligned} \psi_{1,j}(t) &= g(t)cos(2\pi f_c t + \theta_j) \\ \theta_j &= \frac{2\pi}{J}(j-1), j = 1,...,J. \end{aligned} \tag{4.2}$$

$$\begin{aligned} \psi_{2,j}(t) =& A_I g(t)cos(2\pi f_c t + \theta_j) - \\ & A_Q g(t)sin(2\pi f_c t + \theta_j) \\ \theta_j =& \frac{2\pi}{J}(j-1), j = 1,...,J. \end{aligned} \tag{4.3}$$

As depicted in Figure (4.3), the value of J for PSK-based waveforms is $2,4,8$ and for QAM-based waveforms, it is 16 and 64. Thus, at the input of the DFRC transmitter, the combined form of the signals is given by [71]

$$\mathbf{s}(t,\tau) = A(\tau)\mathbf{w}^*\psi(t) \tag{4.4}$$

The orthogonality of waveform can be written as :

$$\int_t \mid \psi(t) \mid^2 dt = 1 \tag{4.5}$$

and

$$\int_t \psi_k \psi_k^*(t) dt = \delta(k - k^{'}) \tag{4.6}$$

where δ is Kronecker delta.

Training data is transmitted over a multi-tap rician wireless channel after modulation. The signal passed through the wireless channel looks like

$$\mathbf{r}(t) = \mathbf{s}(t) * \mathbf{h}(t) + \mathbf{n}(t), \tag{4.7}$$

In matrix vector form

$$\mathbf{r}(t) = \mathbf{Hs} + \mathbf{n}(t), \tag{4.8}$$

where $\mathbf{H} = diag(\mathbf{h})$ with $\mathbf{h} = [h_1, h_2, ..., h_{M_R}]^T$ is $M_R \times 1$ vector containing channel information and $\mathbf{s} = [s_1, s_2, ..., s_{M_R}]^T$ contains the information in the form of amplitudes and phases. Furthermore, due to the multipath channel effect, the complexities of the received signal in Equation (4.7) increases as expressed mathematically,

$$\begin{aligned} r(t) = & (s(t - \Delta t) * \sum_{i=1}^{N} \rho_i \delta(t - t_i) e^{j(\phi_i + \Delta\phi)}) \\ & e^{j2\pi\Delta f t} + n(t) \end{aligned} \tag{4.9}$$

where, $s(t - \Delta t)$ accounts for timing offset, $e^{j(\phi_i + \Delta\phi)}$ represents the phase

offset added to each multipath component and $e^{j2\pi\Delta ft}$ accounts for the frequency offset. Moreover, $\sum_{i=1}^{N} \rho_i \cdot \delta(t-t_i) \cdot e^{j(\phi_i+\Delta\phi)}$ represents the multipath channel response with N multipath components. Each component includes a delay (t_i), complex attenuation (ρ_i), and phase shift (ϕ_i). These offsets are all introduced simultaneously, and their specific values will depend on the impairments introduced by the channel or other factors in the communication system. Consequently, as a result, the constellation image looks messy due to these channel-introduced impairments, which result in overlapping points. In such constellation images, it is extremely difficult to determine whether the modulation scheme selected is right or wrong.

4.2.3 Radar Receiver Design

Suppose there are P distant targets within the radar's main beam. The baseband signal received by the radar receiver can be represented in vector form as follows:

$$\begin{aligned}\mathbf{x}_{radar}(t,\tau) =& A_p \sum_{p=1}^{P} \beta_p(\mathbf{a}^T(\theta_p)\mathbf{s}(t,\tau))\mathbf{b}(\theta_p)+ \\ & \mathbf{e}_r(t,\tau)+\mathbf{n}_r(t,\tau)\end{aligned} \tag{4.10}$$

The steering vector for the radar receiver array can be written as

$$\mathbf{b}(\theta_p) = [1, e^{j\frac{2\pi}{\lambda}d\sin(\theta_p)}, \ldots, e^{j\frac{2\pi}{\lambda}d(M_R-1)\sin(\theta_p)}]^T \tag{4.11}$$

For enhanced clarity, Table 4.2 provides a thorough list of symbols, including their corresponding dimensions and descriptive explanations for Equation (4.10) and Equation (4.11).

4.2.4 Communication Receiver design

Considering J communication receivers, each is equipped with N_T antenna elements for uplink purposes and N_R antenna elements for downlink purposes, all located in the far field. To facilitate prior communication, each receiver has access to a lookup table that contains the dictionary of orthogonal symbols used by the dual-function transmitter. The proposed system extracts SNR information from the received signal. It then transmits this information back to the DFRC transmitter via an uplink antenna array. This technique is recognized in the literature as uplink channel estimation [181]. Assuming that the j^{th} communication receiver, which is equipped with N_R antenna elements arranged in a uniform linear configuration, receives the following signal:

$$\mathbf{x}_{com}(t,\tau) = A_j \alpha_j (\mathbf{a}^T(\phi_j)\mathbf{s}(t,\tau))\mathbf{c}_j(\phi_j) + \mathbf{n}_j(t,\tau) \tag{4.12}$$

The received power at the communication receiver is denoted by A_j. The parameter α_j represents the constant channel coefficient originating from the transmitter array towards the j^{th} communication receiver, summarizing the propagation characteristics. On the other hand, $\mathbf{a}(\phi_j)$ corresponds to the steering vector in the direction of θ_j for the communication receiver from the dual-function transmitter. Moreover, $\mathbf{s}(t,\tau)$ represents the baseband signal carrying actual information. The $\mathbf{c}_j(\phi_j)$ characterizes the steering vector from the receive array, which is related to the communication receiver's location. The noise component $\mathbf{n}_j(t,\tau)$ is an additive white Gaussian noise vector with a zero mean and variance $\sigma^2\mathbf{I}$. Furthermore, (ϕ_j) designates the direction associated with the kth communication receiver.

The steering vector of communication receiver ULA can be written as

$$\mathbf{c}(\theta) = [1, e^{j\frac{2\pi}{\lambda}d\sin(\theta_j)}, ..., e^{j\frac{2\pi}{\lambda}d(N_R-1)\sin(\theta_j)}]^T \tag{4.13}$$

In the initial stage, beamforming is applied to the received signal. This operation isolates the steering vector by employing beamforming weights at the communication receiver. Consequently, the desired signal can be extracted from the received signal, allowing the receiver to focus on the desired signal's direction while mitigating interference from other directions. This reduction in interference enhances the signal-to-noise ratio (SNR) at the receiver. The beamforming operation is mathematically expressed by Equation (4.12). The received signal is comprehensive and contains information on received power, channel impairments, noise, and modulation scheme. These parameters have both deterministic and stochastic nature. More details about the signal parameters are shown below:

$$\mathbf{x}_{com}(t) = \hat{A}e^{j(2\pi\Delta f t+\phi_j)}\eta^{k,i}g(t-nT_s) \tag{4.14}$$

The amplitude, phase offset, and residual of carrier frequency are represented by $\hat{A}$, ϕ_j, and Δf, whereas symbol interval is written as T_s and g(t) is the pulse shaping. $\eta^{k,i}$ is the modulated symbol with k^{th} waveform and i^{th} constellation.

4.2.4.1 Spectrogram Image Diagrams

A spectrogram is a visual representation of the frequencies present in a signal over time. To generate a spectrogram image, a time-domain signal received in Equation (4.14) is used. The process involves converting the time-domain signals into frequency-time representations by short-term Fourier transform

(STFT), which can then be fed into a neural network for classification. To analyze the signal over short time intervals, the signal is multiplied by a window function. Common window functions include the Hamming window or Gaussian window. The windowed signal is denoted as $x_w(t)$

$$\mathbf{x}_w(t) = \mathbf{x}_{com} \cdot \mathbf{w}(t) \tag{4.15}$$

Furthermore, the windowed signal is sampled down and FFT is applied to it as

$$\mathbf{X}_d = FFT\{\mathbf{x}_w[n]\} \tag{4.16}$$

$\mathbf{X}_d$ represents the complex spectrum matrix of the signal at a given frequency. The spectrogram can be mathematically described as a $2D$ matrix:

$$\mathbf{S}(t,f) = |\mathbf{X}_d(f,t)|^2 \tag{4.17}$$

where, $\mathbf{S}(t,f)$ represents the magnitude of the spectral content at time t and frequency f.

It's worth noting that the implementation of neural networks varies depending on the complexity of the modulation schemes and the size of the dataset. The main objective of using CNN-based architecture is to recognize the unique spectral patterns and temporal characteristics associated with different modulation schemes, enabling it to classify unknown modulation signals accurately.

4.2.4.2 Proposed Convolutional Neural Network Design

In the proposed method, data is effectively classified with the assistance of CNNs. Unlike other classification algorithms, CNNs do not necessitate extensive preprocessing. Convolutional architectures are available in both 2D and

3D, depending on the user's requirements. The structure comprises four layers. The first layer is the convolution layer, responsible for receiving input data and extracting features. This layer performs the convolution operation between the filter and the input map. The second layer is a pooling layer, which reduces the dimensionality of the feature map. Compressing the output of the convolution layer is sometimes necessary, and pooling achieves this by down-sampling the feature map. This enhances feature robustness when there are positional changes. Common methods for pooling include average pooling and maximum pooling. The third layer is fully connected, and tasked with classifying the data. Every neuron in each layer is connected with specific weights and activations to the neurons in the layer above. The fourth layer is the output layer, which delivers the final result. An activation function is utilized to calculate the probability response at the output layer. The overall flow chart of the study is illustrated in Figure (4.4). The CNN architecture is improved by incorporating a fully connected layer and a Softmax classifier layer to enhance its effectiveness. This model finds application in various domains, providing detailed feature mapping, robust predictions, automated modeling, and semi-supervised learning. The following hyperparameters for the CNN are optimized: learning rate, dropout rate, filter size, number of filters, and network width.

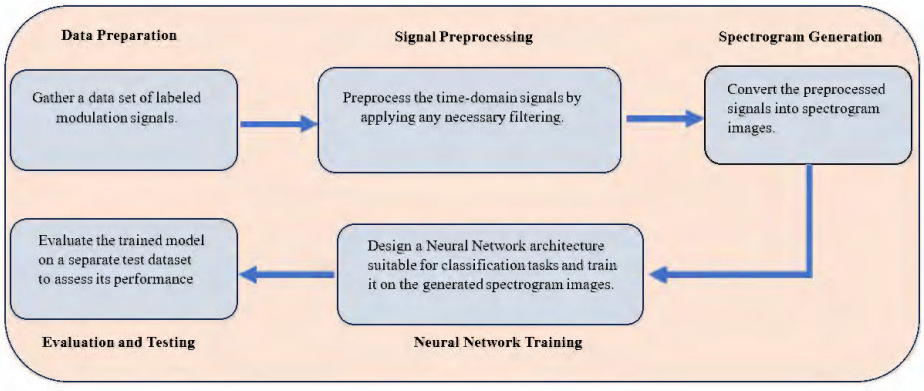

Figure 4.4: Flowchart of CNN

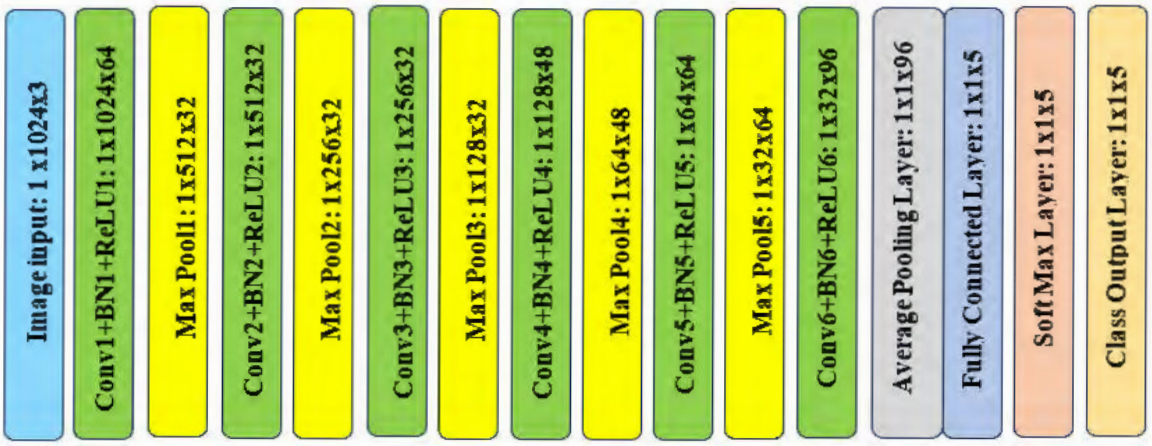

Figure 4.5: The proposed CNN architecture.

The proposed network, illustrated in Figure (4.5), takes spectrogram images as input with dimensions of $1 \times 1024 \times 3$. A variety of spatial filters, each with several learnable parameters, are employed in the convolutional layers of the proposed design. This facilitates the efficient and rapid learning of spatial properties and other pertinent high-level features. In each convolutional layer, the input undergoes convolution with the filters and is subsequently passed through activation functions. The mathematical description of a the convolutional layer is as follows:

$$\mathbf{G}_{conv} = \zeta(\mathbf{S} \cdot \mathbf{K} + b_{conv}), \tag{4.18}$$

where, ζ is the activation function, $\mathbf{K}$ is Convolutional layer kernel matrix, $\mathbf{S}$ is the raw output images obtained by spectrogram and b_{conv} is the bias of for symbol decoding. Furthermore, the samples extracted from convolutional layers are fed to pooling layer for dimensions reduction and feature extraction. The output of the pooling layer can be written as:

$$\mathbf{D}_{pooling} = \urcorner(\mathbf{G}_{conv} + b_{pooling}) \tag{4.19}$$

in Equation (4.19), $\urcorner$ represents the pooling layer activation function. There are three different types of pooling operations available, i.e. max pooling, average pooling, and $L2-Norm$ pooling. Furthermore, a fully connected layer is responsible for the detection of data and it gives us the final answer. Max pooling takes the maximum value within each pooling window, helping to retain the most significant features. Furthermore, when dealing with multi-class classification problems, the softmax activation function is applied element-wise to the output vector $\mathbf{D}$ obtained after the pooling layer. Given an input vector z, the softmax function is defined as:

$$\mathbf{z}_{output} = Softmax(\mathbf{D}) \tag{4.20}$$

The output of the softmax function is a probability distribution over the classes, and it's commonly used in the final layer of a neural network for classification tasks.

4.2.5 Proposed Cognitive Design and Adaptive Modulation

The design and implementation of a cognitive communication system with adaptive modulation and SNR thresholding present a sophisticated approach to addressing the dynamic nature of communication channels. The system incorporates a cognitive feedback loop that continuously monitors key parameters, such as SNR, channel quality, and interference levels, through a dedicated sensing module. This real-time feedback informs an intelligent decision-making algorithm, enabling the system to dynamically adjust its configuration based on changing channel conditions. The integration of SNR thresholding establishes predefined thresholds for different modulation schemes $(M-PSK\&M-QAM)$, allowing the system to select the most suitable modulation scheme at

any given moment. This ensures optimal utilization of available bandwidth while balancing the trade-off between data rate and reliability. The adaptive modulation module seamlessly switches between modulation schemes based on the determined SNR thresholds, while rate adaptation mechanisms adjust data rates accordingly. Thorough testing and optimization are essential to fine-tune the system's parameters, ensuring robust performance across diverse communication scenarios. This cognitive communication system represents a sophisticated and dynamic solution for addressing the challenges posed by variable channel conditions. The SNR thresholding for the communication receiver to be in the main lobe and the side lobes are given in Table 4.3.

Table 4.3: SNR threshold for main lobe and side lobes

Main Lobe		**Side Lobes**	
-15dB to -5dB	BPSK	-15dB to 5dB	16QAM
-5dB to 5dB	QPSK		
5dB to 15dB	8PSK	5dB to 15dB	64QAM
15dB and above	16 PSK		

Similarly, Figure (4.6) embodies the selection of waveform and data rates based on the channel statistics and value of SNR.

4.2.6 UP Link Communication Channel

Similarly, the signal generated by the communication receiver and transmitted by using ULA having dimension $N_T \times 1$ towards DFRC transmitter or fusion center can be written as:

$$\mathbf{s}_{UL}(t,\tau) = A_{UL}(\tau)\mathbf{w}_{UL}^{*}\psi_{UL}(t) \tag{4.21}$$

where, A_{UL} is the signal power, $\mathbf{w}_{UL}$ is the UL steering vector from the communication receiver towards the DFRC transmitter and $\psi_{UL}(t)$ is the desired

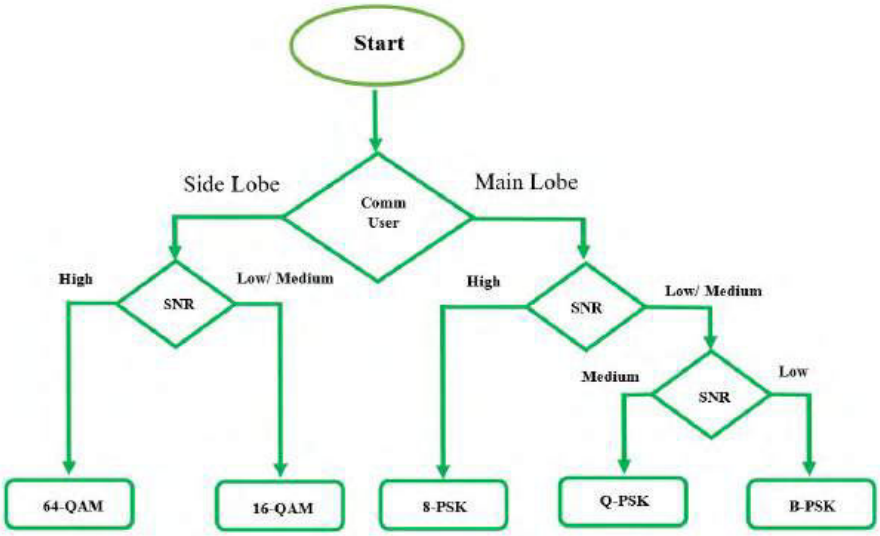

Figure 4.6: The internal mechanism of proposed radar and communication feedback processor

waveform contains snr level information.

4.3 Simulation Results

For any learning task, it is recommended to start by plotting the input data. This helps to identify prominent features. If a clear pattern emerges from the visualization, using a neural network may be unnecessary or even suboptimal. To generate the constellation diagram, the receiver must precisely recover the received signal's timing, carrier frequency, phase, and waveform. Communications systems cannot eliminate channel effects due to their inherent nondeterministic nature. In real-time communication scenarios, factors such as increased thermal noise, oscillator drift and temperature variations at the DFRC transmitter, and symbol timing offset may arise. Additionally, sample rate degradation and carrier frequency offsets contribute to performance deterioration. Owing to these impairments, accurately identifying the true modulation and transmitted symbol becomes exceedingly challenging.

Furthermore, Multipath fading further degrades signal quality, leading to

data loss. This data loss then worsens the performance of the transmission system. More details about the channel parameters are provided in the table 4.4.

Table 4.4: Wireless Channel parameters

Parameter Name	**Parameter Value**
Modulation Schemes	5
Samples of each modulation	1000
Signal Dimension	$1 \times 1024 \times 3$
Duration of each input frame	$5ms$
Center Frequency	902 MHz
SNR Range	-30 dB to $+30$ dB
Sampling Rate	200 kHz
Symbols of each waveform	1024
Samples per symbol	8
Doppler spread	5 Hz
Maximum Clock Offset	5 ppm
Channel profile	Rician
Fading K factor	4
Fading delay ratio	$0, 1.8, 3.4$
Path Gains	$0, -2, -10$dB
Maximum Doppler Shift	4

In this received signal classification task, at the receiver, 1000 received samples were collected to make a spectrogram diagram in image format by applying short-term Fourier transform (STFT). The generated image is then fed to a CNN-based classifier for classification. The classification result is a probability vector that indicates the probability of the received constellation being a particular modulation scheme.

In the next section, the performance of the proposed CNN-based system is presented. The proposed system has been evaluated based on classification

accuracy and miss classification error over a wide range of SNRs.

4.3.1 Proposed CNN Classification Performance

In the subsequent section, the CNN-based received signal classifier, its constellation diagram, and the training procedure will be examined. Throughout the CNN training process, various parameters of the optimizer and training algorithm require adjustment to enhance both the training speed and classification accuracy. Specifically, batch processing is adapted during training, employing batches of 10000 images for each iteration. To facilitate effective learning, the CNN underwent training for 1000 iterations. Additional details regarding the diverse training parameters of the CNN are provided in Table 4.5.

Table 4.5: CNN Parameters.

Parameter Name	**Parameter Value**
Percent Training Samples	80%
Percent Validation Samples	10%
Percent Test Samples	10%
Mini batch size	10
Initial learning rate	0.0001
Iteration per epoch	500
Validation frequency	3
Max epochs	10
Solver name	Adam

Training was done on a standard Intel 11^{th} Gen Intel(R) Core(TM) $i5$ $1135G7$, with $2.40GHz$ and $2.42GHz$ processors, having 8 GB ram and Intel Iris Xe Graphics $G780EUs(400-1300MHz)$ GPU cards that took $3hours10minutes$ approximately.

The details of the CNN network layer parameters are comprehensively dis-

Table 4.6: CNN Layers Details

Layers Name	**Layer Dimensions**	**Filter size**	**No. of Filters**
Input Layer	$1 \times 1024 \times 3$		
Conv. Layer 1	$1 \times 1024 \times 32$	3×3	32
BN. Layer 1	$1 \times 1024 \times 32$	1×32	2
Conv. Layer 2	$1 \times 512 \times 32$	3×3	32
BN. Layer 2	$1 \times 512 \times 32$	1×32	2
Conv. Layer 3	$1 \times 256 \times 32$	3×3	32
BN. Layer 3	$1 \times 256 \times 32$	1×32	2
Conv. Layer 4	$1 \times 128 \times 48$	1×8	48
BN. Layer 4	$1 \times 128 \times 48$	1×8	2
Conv. Layer 5	$1 \times 64 \times 64$	1×8	64
BN. Layer 5	$1 \times 64 \times 64$	1×8	2
Conv. Layer 6	$1 \times 32 \times 96$	1×8	96
BN. Layer 6	$1 \times 32 \times 96$	1×8	2
Average Pooling Layer	$1 \times 1 \times 96$	1×1	32
Fully Connected Layer	$1 \times 1 \times 5$	5×96	
Softmax Layer	$1 \times 1 \times 5$		
Class output Layer	$1 \times 1 \times 5$		

cussed in Table 4.6. This encompasses essential information, including the filter size and the number of filters utilized in each layer. Subsequently, each convolutional layer is succeeded by a batch normalization layer, followed by a Rectified Linear Unit (ReLU) activation function and a Max pooling layer.

This proposed architectural configuration enhances training speed, promotes generalization, and yields improved performance.

Case 1: Radar in the Main lobe, Communication receiver in the Side lobes

The QAM-based waveform is utilized in the 1^{st} case when the radar target is in the main lobe while the communication user is in the side lobes. The results in Table 4.7 show performance accuracy at $-7dB$ using the confusion matrix. These values show that for lower SNR values, the modulation accuracy of less data rate is very high.

Table 4.7: Confusion matrix of Proposed CNN at snr -7 dB.

16 QAM	82	17	1	0	0	82 %
64 QAM	14	84	1	0	1	84 %
8 PSK	3	1	76	0	20	76 %
QPSK	6	0	8	86	06	86 %
BPSK	0	0	0	0	100	100 %
	16 QAM	64 QAM	8 PSK	QPSK	BPSK	Accuracy (%)

Case 2: Both the Radar and the communication receiver are in the Main lobe

In the second case, where both radar and communication receivers are positioned within the main lobe, the proposed system achieves an overall accuracy of 92.6%. Notably, BPSK modulation reaches 100% accuracy at $0dB$, while QPSK achieves 98% accuracy at higher data rates. However, classification accuracy degrades for higher-order modulations, such as 16-QAM and 64-QAM, due to identical constellation diagrams.

To mitigate the risk of encountering local minima during training, the Adam optimization algorithm is employed for the Convolutional Neural Network (CNN). The advantages of Adam over stochastic gradient descent (SGD) include improved computational complexity and the efficient calculation of both mean and variance for each parameter's moving average. In conjunction with the softmax layer, a cross-entropy loss function is utilized to quantify the disparities between the detected class and the true class. Therefore, the integration of softmax activation with the cross-entropy loss function is performed to accomplish the classification task.

Table 4.8 shows performance accuracy at $0dB$. The overall accuracy achieved is 94%. Similarly, the performance of BPSK is 100% while the 16QAM is 94%.

Figure (4.7) shows the scatter plot image of the received modulated sig-

Table 4.8: Confusion matrix of proposed CNN at snr 0 dB.

16 QAM	92	6	0	0	2		94 %
64 QAM	1	91	0	8	0		91 %
8 PSK	4	0	94	0	2		94 %
QPSK	1	0	1	98	0		98 %
BPSK	0	0	0	0	100		100 %
	16 QAM	64 QAM	8 PSK	QPSK	BPSK		Accuracy(%)

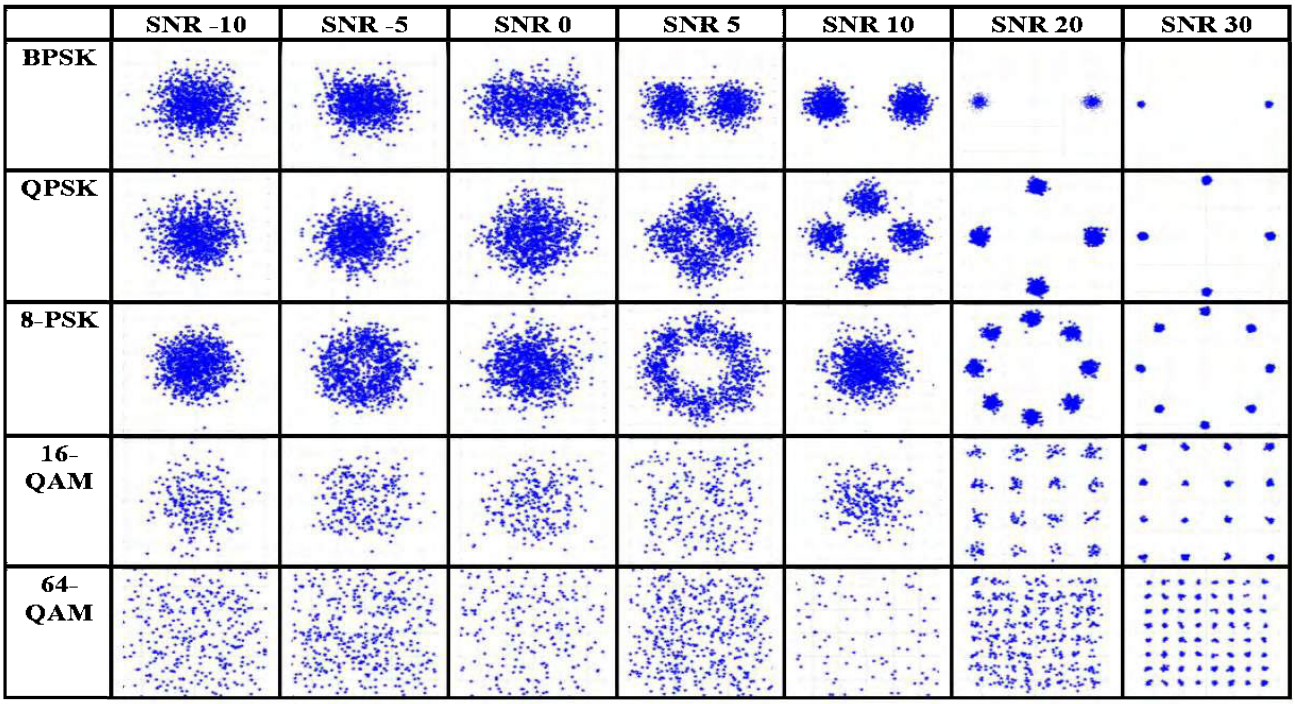

Figure 4.7: The Constellation diagrams for digital modulation types of the received signal from SNR = -10dB to SNR= 30dB,

nal, where the x-axis shows the In phase while the y-axis shows the quadrature component. These constellations are obtained for $BPSK$, $QPSK$, $8-PSK$, $16-QAM$ and $64-QAM$ at snr -10 dB, $-5dB$, 0dB, 5dB, 10dB, and 20dB respectively. Furthermore, the Figure (4.8) shows the time domain representation. The x-axis shows the time duration while the y-axis shows the amplitude. These observations help us to study the behavior of channels, ease of filtering, and efficient utilization of bandwidth.

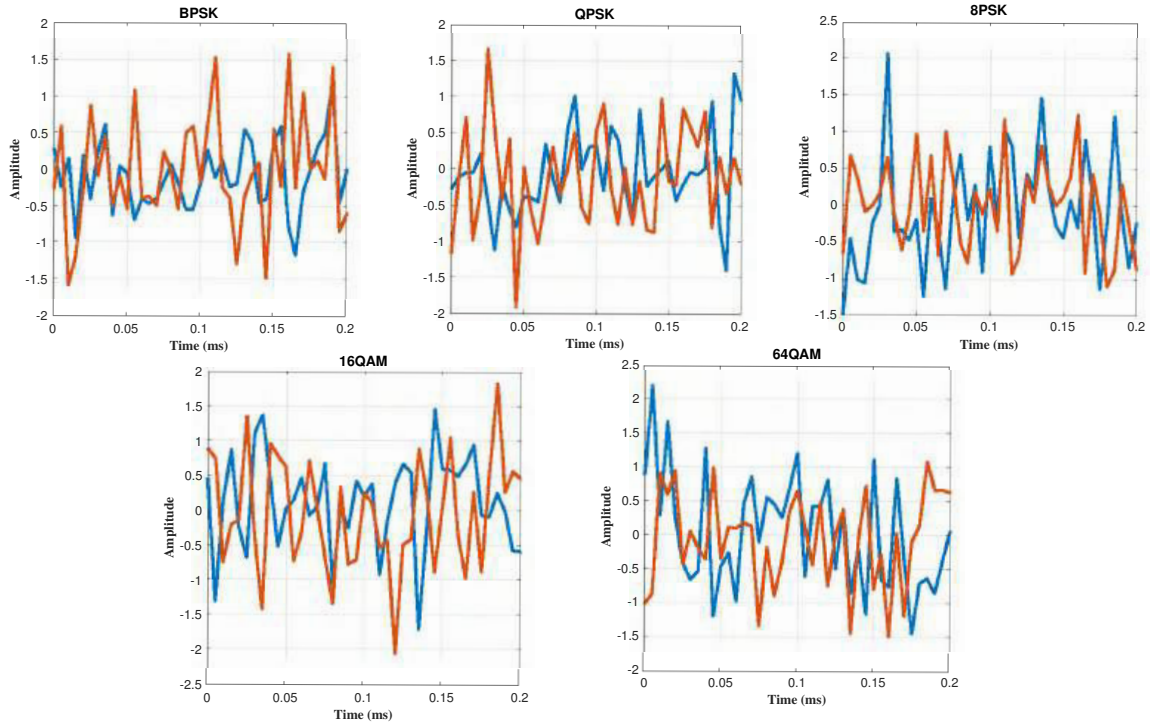

Figure 4.8: The I & Q time domain representation of the signal at SNR = 20dB

The spectrogram image was generated using raw signals modulated with BPSK, QPSK, 8PSK, 16 QAM, and 64QAM, each consisting of 1024 samples per waveform. The central frequency employed for modulation is 902MHz, and each sample has a duration of 5ms. Owing to the influence of the channel, a Doppler spread of 5Hz is observed. This comprehensive representation allows for the analysis of signal characteristics across different modulation schemes under specific channel conditions. The detailed spectrogram provides insights into the temporal and frequency dynamics, offering a valuable resource for understanding the impact of channel effects on various modulation signals as shown in Figure (4.9).

The training accuracy of the proposed system in terms of SNR is compared with the Zhou [166], Ali [182], Krzystone[183] and Kim [184] as depicted in the Table 4.9.

The computational complexities of the convolutional layer, fully connected

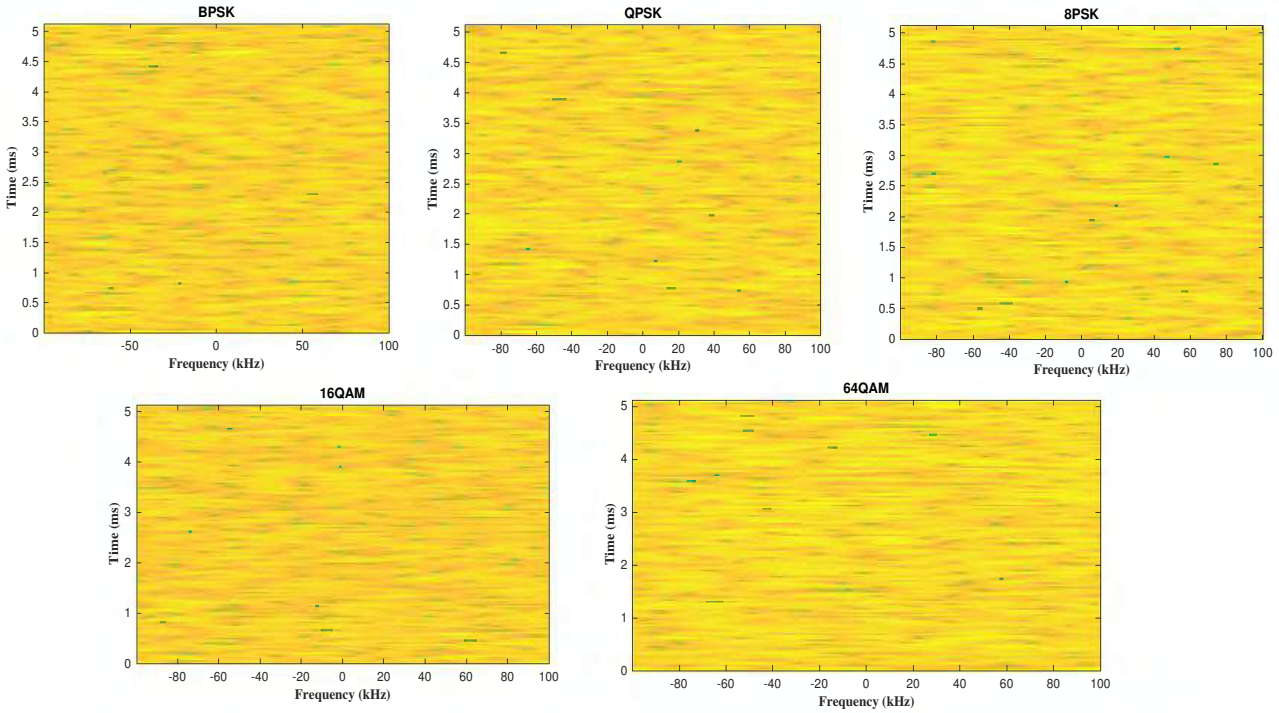

Figure 4.9: The spectrogram representation of the signal at SNR = 20dB. Time is given by the vertical axis while frequency is along the horizontal axis.

Table 4.9: Comparison of training Accuracy vs SNR

SNR(dB) / Accuracy(%)	-20	-15	-10	-5	0	5	10	15
Zhou [166]	14	15	20	35	65	75	83	87
Krzy [183]	13	14	28	34	60	75	82	88
Ali [182]	12	13	20	36	66	77	84	92
Kim [184]	11	12	21	36	65	74	81	93
Proposed	10	14	22	37	67	78	84	94

layer, and the pooling layer of the proposed system, as well as existing models, can be calculated using the following equations:

$$Para_{(conv)} = [(K \times K) \times (C_{in}) + (B_n)] \times (C_{out}) \tag{4.22}$$

$$Para_{(BN)} = 2 \times (C_{out}) \tag{4.23}$$

$$Para_{(fully)} = (C_{in} \times C_{out}) + C_{out} \tag{4.24}$$

whereas, In a convolutional layer, the parameters consist of learnable filters and biases. Each filter, typically of size $K \times K$ has dimensions based on the number of input channels C_{in}, C_{out} is the number of filters applied in the current layer while B_n is the bais of each filter. Similarly, in the batch normalization layer, each feature map has two learnable parameters: a scaling factor and a shifting factor, also called as the gamma and the beta. These parameters play a key role in stabilizing the training process by normalizing the inputs, which helps improve the overall performance of the network. Pooling layers (e.g., max pooling, average pooling) do not have learnable parameters, so they contribute 0 to the parameter count. For a fully connected layer, the number of parameters is given by the number of input units times the number of output units, plus one bias term for each output unit. In the end, we add up the parameters from all the convolutional layers and batch normalization layers to get the total number of parameters.

In this study, it has been observed that deeper architectures are most effective with more complex datasets. Furthermore, there is a notable relationship between the number of dense layers, the number of neurons, and the dataset complexity. The number of convolutional and dense layers directly impacts the model's runtime. While using lower filter sizes and higher batch sizes can enhance the model's performance, it also increases the computational cost. Additionally, a lower batch size yields better results when the learning rate is low. For models with a greater number of layers, maintaining a lower learning rate leads to improved outcomes as mentioned in the Table 4.10.

These insights are critical for selecting appropriate waveforms based on the expected noise conditions in communication systems. For scenarios with high noise levels, BPSK and QPSK are preferable due to their robustness and high

Table 4.10: Comparison of Time Complexity

Model	Total Layers	Parameters	Epocs	Optimizer
Zhou [166]	22	5,71,695	40	SDGM
Krzy [183]	13	27,49,275	72	ADAM
Ali [182]	49	4,27,484	60	ADAM
Kim [184]	22	1,43,760	45	SDGM
Proposed	28	1,41,432	10	ADAM

accuracy. For environments with lower noise levels, more complex modulation schemes like 16 QAM and 64 QAM can be considered to achieve higher data rates while maintaining acceptable accuracy.

4.3.2 Radar Performance Evaluation

In this section, we highlight the performance of the radar receiver. In the first case, the radar target is positioned at an angle of $\theta_r = 0^\circ$, while the communication receiver is placed at $\theta_c = 5^\circ$. A PSK-based waveform is used in this example. In the second case, the radar target remains at $\theta_r = 0^\circ$, but the communication receiver is positioned at $\theta_c = 30^\circ$, using a QAM waveform. The target reflection coefficient is assumed to follow the swirling 2 model. It changes from pulse to pulse but remains constant throughout each pulse. A ULA with 10 sensors, spaced half a wavelength apart, is used for the radar receiver array. Data is collected using 1000 pulses to build the covariance matrix. The MUSIC algorithm is then applied at the radar receiver for DOA estimation. The target resolution is achieved by [185].

$$|\theta - \theta_i| \leqslant \frac{|\theta_1 - \theta_2|}{2}, i = 1, 2 \tag{4.25}$$

Figure 4.10 illustrates the radar performance for both scenarios discussed earlier. Meanwhile, Figure 4.11 displays the radar receiver's performance under a high SNR value.

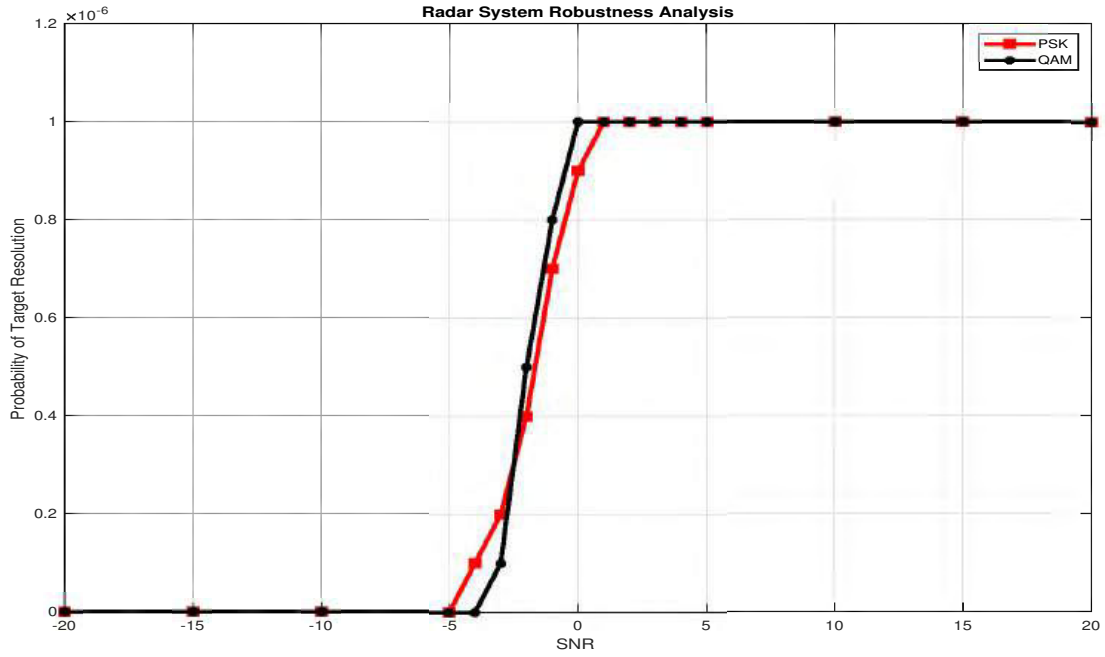

Figure 4.10: The Robustness of radar receiver in terms of Target separation vs SNR

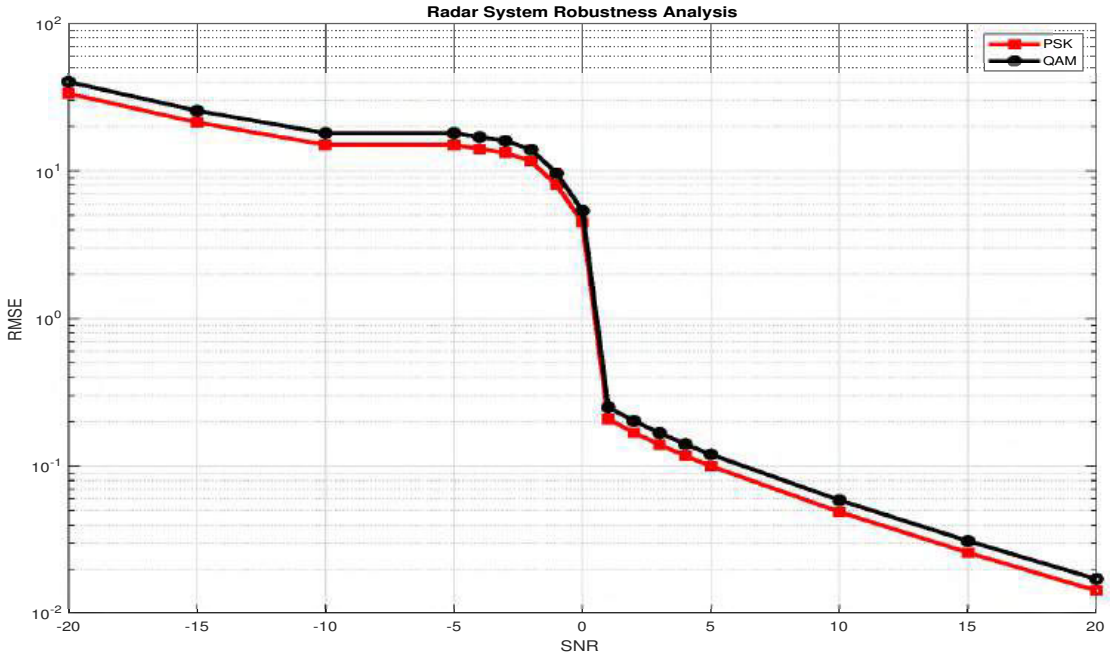

Figure 4.11: The Robustness of radar receiver in terms of RMSE and SNR

4.3.3 Statistical Analysis

Moreover, the Friedman test is applied to evaluate the training accuracy of various CNN models across a range of SNR values on the given datasets. The significance of the p-value $(p < 0.005)$ was assessed for all models, and the proposed model demonstrated statistical significance, passing all test parameters. For each SNR value, the performance (training accuracy) of each CNN model was ranked. The Friedman test was then used to determine if there were significant differences in performance among the models. The Friedman test statistic (χ_F^2) is calculated using the formula:

$$\chi_F^2 = \frac{12}{nk(k+1)} \sum_{j=1}^{k} R_j^2 - 3n(k+1) \tag{4.26}$$

where: n is the number of observations (e.g., different SNR levels), k is the number of groups (e.g., different CNN models), Rj is the sum of ranks for group j. The proposed CNN model showed a statistically significant improvement in training accuracy across the range of SNR values, as evidenced by the Friedman test. The p-value was found to be below the threshold for significance, indicating that the proposed model's performance is significantly different from that of the other models tested.

4.4 Summary

In this work, Cognitive architecture for DFRC for a variety of five communication schemes and two different waveforms have been presented. With the aid of deep learning techniques, features are extracted from received signals at the communication receiver. Its accuracy is simulated over a broad range of SNR. In this, a CNN-based image classifier is employed to categorize images

depicting various constellation schemes. In comparison with existing modulation classification algorithms for received signals, this CNN-based approach demonstrates superior classification accuracy and avoids the need for manual feature selection. The algorithm exhibits robustness against carrier frequency variations, phase offset, timing errors, and phase jitter. Moreover, this classifier does not rely on noise variance for classification. Simulations indicate that the proposed CNN-based received signal classification achieves an average classification accuracy of 90.22% and 92.44% for five modulation schemes at $-7dB$ and $0dB$ SNR, respectively.

Chapter 5

Conclusion and Future Work

5.1 Conclusions

This doctoral research focused on integrating radar and communication functionalities within a unified system to improve data rates, spectrum efficiency, and interference mitigation in dual-function radar and communication (DFRC) systems. A novel hybrid technique, FQAM, combining Frequency Shift Keying (FSK) with Quadrature Amplitude Modulation (QAM), was proposed to enhance communication data rates by embedding information in both frequency and constellation number. Extensive simulations demonstrated that FQAM significantly improves spectral efficiency and reduces interference compared to existing methods. Additionally, a deep learning-based approach was developed to optimize communication performance and mitigate interference using the perception-action cycle for real-time signal identification and adaptive waveform selection. This method improved data rates and reduced bit error rates (BER) by adjusting to the relative positions of radar targets and communication receivers. Simulation results validated its effectiveness across diverse conditions. These contributions advance DFRC systems by integrating innovative modulation techniques with deep learning, enhancing spectrum utilization,

radar target tracking, and overall system performance, thereby paving the way for next-generation multi-functional radar and communication systems.

5.2 Future Work

5.2.1 Future work in uplink for Communication in DFRC and limitation in Data Rate

Given the current literature and contributions to DFRC systems regarding information embedding, there remains significant potential to further enhance the system's performance by focusing on advancements in uplink channel estimation and multi-user interference mitigation. Integrating sophisticated algorithms for error detection and correction is essential to achieve more robust and reliable system performance [9; 35; 186; 187].

5.2.2 Future work in Interference Mitigation

The interference mitigation can be overcome by fast time coding, polarization, cognitive designs based on information feedback, improved range-angle dependent target focusing, etc. Moreover, channel coding schemes are to be used in waveforms to mask the communication data from the intercepts. The SNR needed for combating channel interference must be examined because of the radar equation and power requirements[9; 35; 186; 187].

5.3 Bibliography

[1] H. Griffiths, S. Blunt, L. Cohen, and L. Savy, "Challenge problems in spectrum engineering and waveform diversity," in *2013 IEEE Radar Conference (RadarCon13)*. IEEE, 2013, pp. 1–5.

[2] H. Griffiths, L. Cohen, S. Watts, E. Mokole, C. Baker, M. Wicks, and S. Blunt, "Radar spectrum engineering and management: Technical and regulatory issues," *Proceedings of the IEEE*, vol. 103, no. 1, pp. 85–102, 2014.

[3] C. Baylis, M. Fellows, L. Cohen, and R. J. Marks II, "Solving the spectrum crisis: Intelligent, reconfigurable microwave transmitter amplifiers for cognitive radar," *IEEE Microwave Magazine*, vol. 15, no. 5, pp. 94–107, 2014.

[4] H. Hayvaci and B. Tavli, "Spectrum sharing in radar and wireless communication systems: A review," in *2014 International Conference on Electromagnetics in Advanced Applications (ICEAA)*. IEEE, 2014, pp. 810–813.

[5] S. Kumar, G. Costa, S. Kant, B. F. Flemming, N. Marchetti, and P. Mogensen, "Spectrum sharing for next generation wireless communication networks," in *2008 First International Workshop on Cognitive Radio and Advanced Spectrum Management*. IEEE, 2008, pp. 1–5.

[6] F. Liu, C. Masouros, A. Li, and T. Ratnarajah, "Robust mimo beamforming for cellular and radar coexistence," *IEEE Wireless Communications Letters*, vol. 6, no. 3, pp. 374–377, 2017.

[7] A. Basit, W.-Q. Wang, S. Y. Nusenu, and S. Zhang, "Range-angle-dependent beampattern synthesis with null depth control for joint radar communication," *IEEE Antennas and Wireless Propagation Letters*, vol. 18, no. 9, pp. 1741–1745, 2019.

[8] A. Basit, W.-Q. Wang, and S. Y. Nusenu, "Adaptive transmit array sidelobe control using FDA-MIMO for tracking in joint radar-communications," *Digital Signal Processing*, vol. 97, p. 102619, 2020. [Online]. Available: https://www.sciencedirect.com/science/article/pii/S1051200419301733

[9] L. Han and K. Wu, "Joint wireless communication and radar sensing systems-state of the art and future prospects," *IET Microwaves, Antennas & Propagation*, vol. 7, no. 11, pp. 876–885, 2013.

[10] S. Quan, W. Qian, J. Guq, and V. Zhang, "Radar-communication integration: An overview," in *The 7th IEEE/International Conference on Advanced Infocomm Technology*. IEEE, 2014, pp. 98–103.

[11] A. Dimas, B. Li, M. Clark, K. Psounis, and A. Petropulu, "Spectrum sharing between radar and communication systems: Can the privacy of the radar be preserved?" in *2017 51st Asilomar Conference on Signals, Systems, and Computers*. IEEE, 2017, pp. 1285–1289.

[12] L. LI, G.-j. LI, and C.-q. LI, "A communication system based on active phased-array radar," *Journal of China Academy of Electronics and Information Technology*, vol. 2, 2008.

[13] D. Ma, N. Shlezinger, T. Huang, Y. Liu, and Y. C. Eldar, "Automotive dual-function radar communications systems: An overview," in *2020*

IEEE 11th Sensor Array and Multichannel Signal Processing Workshop (SAM), 2020, pp. 1–5.

[14] A. R. Chiriyath, B. Paul, and D. W. Bliss, "Radar-communications convergence: Coexistence, cooperation, and co-design," *IEEE Transactions on Cognitive Communications and Networking*, vol. 3, no. 1, pp. 1–12, 2017.

[15] G. C. Tavik, C. L. Hilterbrick, J. B. Evins, J. J. Alter, J. G. Crnkovich, J. W. de Graaf, W. Habicht, G. P. Hrin, S. A. Lessin, D. C. Wu *et al.*, "The advanced multifunction RF concept," *IEEE transactions on microwave theory and techniques*, vol. 53, no. 3, pp. 1009–1020, 2005.

[16] D. Ma, T. Huang, Y. Liu, and X. Wang, "A novel joint radar and communication system based on randomized partition of antenna array," in *2018 IEEE International Conference on Acoustics, Speech and Signal Processing (ICASSP)*. IEEE, 2018, pp. 3335–3339.

[17] C. Aydogdu, M. F. Keskin, N. Garcia, H. Wymeersch, and D. W. Bliss, "Radchat: Spectrum sharing for automotive radar interference mitigation," *IEEE Transactions on Intelligent Transportation Systems*, vol. 22, no. 1, pp. 416–429, 2019.

[18] C. Sturm, Y. L. Sit, M. Braun, and T. Zwick, "Spectrally interleaved multi-carrier signals for radar network applications and multi-input multi-output radar," *IET Radar, Sonar & Navigation*, vol. 7, no. 3, pp. 261–269, 2013.

[19] M. Bică and V. Koivunen, "Multicarrier radar-communications waveform design for RF convergence and coexistence," in *ICASSP 2019-2019*

IEEE International Conference on Acoustics, Speech and Signal Processing (ICASSP). IEEE, 2019, pp. 7780–7784.

[20] B. Paul, A. R. Chiriyath, and D. W. Bliss, "Survey of rf communications and sensing convergence research," *IEEE Access*, vol. 5, pp. 252–270, 2016.

[21] C. Aydogdu, M. F. Keskin, N. Garcia, H. Wymeersch, and D. W. Bliss, "RadChat: Spectrum sharing for automotive radar interference mitigation," *IEEE Transactions on Intelligent Transportation Systems*, vol. 22, no. 1, pp. 416–429, 2021.

[22] A. Herschfelt and D. W. Bliss, "Spectrum management and advanced receiver techniques (smart): Joint radar-communications network performance," in *2018 IEEE Radar Conference (RadarConf18)*. IEEE, 2018, pp. 1078–1083.

[23] R. Saruthirathanaworakun, J. M. Peha, and L. M. Correia, "Opportunistic primary-secondary spectrum sharing with a rotating radar," in *2012 International Conference on Computing, Networking and Communications (ICNC)*. IEEE, 2012, pp. 1025–1030.

[24] R. Saruthira thanaworakun, J. M. Peha, and L. M. Correia, "Performance of data services in cellular networks sharing spectrum with a single rotating radar," in *2012 IEEE International Symposium on a World of Wireless, Mobile and Multimedia Networks (WoWMoM)*. IEEE, 2012, pp. 1–6.

[25] S.-S. Raymond, A. Abubakari, and H.-S. Jo, "Coexistence of power-

controlled cellular networks with rotating radar," *IEEE Journal on Selected Areas in Communications*, vol. 34, no. 10, pp. 2605–2616, 2016.

[26] D. Ciuonzo, A. De Maio, G. Foglia, and M. Piezzo, "Intrapulse radar-embedded communications via multiobjective optimization," *IEEE Transactions on Aerospace and Electronic Systems*, vol. 51, no. 4, pp. 2960–2974, 2015.

[27] A. Khawar, A. Abdelhadi, and T. C. Clancy, "A mathematical analysis of cellular interference on the performance of S-band military radar systems," in *2014 Wireless Telecommunications Symposium*. IEEE, 2014, pp. 1–8.

[28] E. Obregon, K. W. Sung, and J. Zander, "On the sharing opportunities for ultra-dense networks in the radar bands," in *2014 IEEE International Symposium on Dynamic Spectrum Access Networks (DYSPAN)*. IEEE, 2014, pp. 215–223.

[29] M. J. Marcus, "Sharing government spectrum with private users: opportunities and challenges," *IEEE Wireless Communications*, vol. 16, no. 3, pp. 4–5, 2009.

[30] L. Wang, J. McGeehan, C. Williams, and A. Doufexi, "Radar spectrum opportunities for cognitive communications transmission," in *2008 3rd International Conference on Cognitive Radio Oriented Wireless Networks and Communications (CrownCom 2008)*. IEEE, 2008, pp. 1–6.

[31] M. Tercero, K. W. Sung, and J. Zander, "Temporal secondary access opportunities for wlan in radar bands," in *2011 The 14th International*

Symposium on Wireless Personal Multimedia Communications (WPMC). IEEE, 2011, pp. 1–5.

[32] J. T. Johnson, C. J. Baker, H. Wang, L. Ye, and C. Zhang, "Assessing the potential for spectrum sharing between communications and radar systems in the L-band portion of the rf spectrum allocated to radar," in *2014 International Conference on Electromagnetics in Advanced Applications (ICEAA)*. IEEE, 2014, pp. 331–334.

[33] F. Liu, A. Garcia-Rodriguez, C. Masouros, and G. Geraci, "Interfering channel estimation for radar and communication coexistence," in *2019 IEEE 20th International Workshop on Signal Processing Advances in Wireless Communications (SPAWC)*, 2019, pp. 1–5.

[34] J. A. Mahal, A. Khawar, A. Abdelhadi, and T. C. Clancy, "Spectral coexistence of MIMO radar and MIMO cellular system," *IEEE Transactions on Aerospace and Electronic Systems*, vol. 53, no. 2, pp. 655–668, 2017.

[35] B. Li and A. P. Petropulu, "Joint transmit designs for coexistence of MIMO wireless communications and sparse sensing radars in clutter," *IEEE Transactions on Aerospace and Electronic Systems*, vol. 53, no. 6, pp. 2846–2864, 2017.

[36] F. Liu, C. Masouros, A. Li, T. Ratnarajah, and J. Zhou, "MIMO radar and cellular coexistence: A power-efficient approach enabled by interference exploitation," *IEEE Transactions on Signal Processing*, vol. 66, no. 14, pp. 3681–3695, 2018.

[37] F. Liu, A. Garcia-Rodriguez, C. Masouros, and G. Geraci, "Interfering channel estimation for radar and communication coexistence," in *2019*

IEEE 20th International Workshop on Signal Processing Advances in Wireless Communications (SPAWC). IEEE, 2019, pp. 1–5.

[38] P. Si, E. Sun, R. Yang, and Y. Zhang, "Cooperative and distributed spectrum sharing in dynamic spectrum pooling networks," in *The 19th Annual Wireless and Optical Communications Conference (WOCC 2010)*. IEEE, 2010, pp. 1–5.

[39] Y. Yao, X. Li, and L. Wu, "Cognitive frequency-hopping waveform design for dual-function mimo radar-communications system," *Sensors*, vol. 20, no. 2, p. 415, 2020.

[40] R. Saruthirathanaworakun, J. M. Peha, and L. M. Correia, "Gray-space spectrum sharing between multiple rotating radars and cellular network hotspots," in *2013 IEEE 77th Vehicular Technology Conference (VTC Spring)*. IEEE, 2013, pp. 1–5.

[41] Z. Geng, H. Deng, and B. Himed, "Adaptive radar beamforming for interference mitigation in radar-wireless spectrum sharing," *IEEE Signal Processing Letters*, vol. 22, no. 4, pp. 484–488, 2014.

[42] Z. Junhui, Y. Tao, G. Yi, W. Jiao, and F. Lei, "Power control algorithm of cognitive radio based on non-cooperative game theory," *China Communications*, vol. 10, no. 11, pp. 143–154, 2013.

[43] N. Gatsis and G. B. Giannakis, "Power control with imperfect exchanges and applications to spectrum sharing," *IEEE transactions on signal processing*, vol. 59, no. 7, pp. 3410–3423, 2011.

[44] I. Kim and D. Kim, "Minimizing source-sum-power consumption in

multi-sensor single-relay networks," *IEEE transactions on communications*, vol. 59, no. 9, pp. 2362–2366, 2011.

[45] A. Goldsmith, S. A. Jafar, I. Maric, and S. Srinivasa, "Breaking spectrum gridlock with cognitive radios: An information theoretic perspective," *Proceedings of the IEEE*, vol. 97, no. 5, pp. 894–914, 2009.

[46] Y. Chen, G. Yu, Z. Zhang, H.-H. Chen, and P. Qiu, "On cognitive radio networks with opportunistic power control strategies in fading channels," *IEEE Transactions on wireless communications*, vol. 7, no. 7, pp. 2752–2761, 2008.

[47] S. Srinivasa and S. A. Jafar, "Soft sensing and optimal power control for cognitive radio," *IEEE Transactions on Wireless Communications*, vol. 9, no. 12, pp. 3638–3649, 2010.

[48] V. Asghari and S. Aissa, "Adaptive rate and power transmission in spectrum-sharing systems," *IEEE Transactions on Wireless Communications*, vol. 9, no. 10, pp. 3272–3280, 2010.

[49] S. Wang, F. Huang, and Z.-H. Zhou, "Fast power allocation algorithm for cognitive radio networks," *IEEE Communications Letters*, vol. 15, no. 8, pp. 845–847, 2011.

[50] A. Liu, Z. Huang, M. Li, Y. Wan, W. Li, T. X. Han, C. Liu, R. Du, D. K. P. Tan, J. Lu *et al.*, "A survey on fundamental limits of integrated sensing and communication," *IEEE Communications Surveys & Tutorials*, vol. 24, no. 2, pp. 994–1034, 2022.

[51] S. D. Blunt, P. Yatham, and J. Stiles, "Intrapulse radar-embedded com-

munications," *IEEE Transactions on Aerospace and Electronic Systems*, vol. 46, no. 3, pp. 1185–1200, 2010.

[52] M. Nowak, M. Wicks, Z. Zhang, and Z. Wu, "Co-designed radar-communication using linear frequency modulation waveform," *IEEE Aerospace and Electronic Systems Magazine*, vol. 31, no. 10, pp. 28–35, 2016.

[53] D. Gaglione, C. Clemente, C. V. Ilioudis, A. R. Persico, I. K. Proudler, J. J. Soraghan, and A. Farina, "Waveform design for communicating radar systems using fractional fourier transform," *Digital Signal Processing*, vol. 80, pp. 57–69, 2018.

[54] Y. Liu, G. Liao, J. Xu, Z. Yang, and Y. Zhang, "Adaptive ofdm integrated radar and communications waveform design based on information theory," *IEEE Communications Letters*, vol. 21, no. 10, pp. 2174–2177, 2017.

[55] A. Hassanien, M. G. Amin, Y. D. Zhang, and F. Ahmad, "Signaling strategies for dual-function radar communications: An overview," *IEEE Aerospace and Electronic Systems Magazine*, vol. 31, no. 10, pp. 36–45, 2016.

[56] C. Avdogdu, N. Garcia, and H. Wymeersch, "Improved pedestrian detection under mutual interference by fmcw radar communications," in *2018 IEEE 29th Annual International Symposium on Personal, Indoor and Mobile Radio Communications (PIMRC)*. IEEE, 2018, pp. 101–105.

[57] X. Wang, S. Mao, and M. X. Gong, "An overview of 3GPP cellular

vehicle-to-everything standards," *GetMobile: Mobile Computing and Communications*, vol. 21, no. 3, pp. 19–25, 2017.

[58] C. Sahin, J. Jakabosky, P. M. McCormick, J. G. Metcalf, and S. D. Blunt, "A novel approach for embedding communication symbols into physical radar waveforms," in *2017 IEEE Radar Conference (RadarConf)*. IEEE, 2017, pp. 1498–1503.

[59] D. Ma, T. Huang, N. Shlezinger, Y. Liu, X. Wang, and Y. C. Eldar, "A DFRC system based on multi-carrier agile FMCW MIMO radar for vehicular applications," in *2020 IEEE International Conference on Communications Workshops (ICC Workshops)*. IEEE, 2020, pp. 1–7.

[60] D. Ma, N. Shlezinger, T. Huang, Y. Shavit, M. Namer, Y. Liu, and Y. C. Eldar, "Spatial modulation for joint radar-communications systems: Design, analysis, and hardware prototype," *IEEE Transactions on Vehicular Technology*, vol. 70, no. 3, pp. 2283–2298, 2021.

[61] K. Wu, J. A. Zhang, X. Huang, Y. J. Guo, and R. W. Heath, "Waveform design and accurate channel estimation for frequency-hopping mimo radar-based communications," *IEEE Transactions on Communications*, vol. 69, no. 2, pp. 1244–1258, 2020.

[62] D. Ma, N. Shlezinger, T. Huang, Y. Liu, and Y. C. Eldar, "Joint radar-communication strategies for autonomous vehicles: Combining two key automotive technologies," *IEEE signal processing magazine*, vol. 37, no. 4, pp. 85–97, 2020.

[63] C. S. Pappu and T. L. Carroll, "Quasi-FM waveform using chaotic os-

cillator for joint radar and communication systems," *Chaos, Solitons & Fractals*, vol. 152, p. 111449, 2021.

[64] S. H. Dokhanchi, B. S. Mysore, K. V. Mishra, and B. Ottersten, "A mmwave automotive joint radar-communications system," *IEEE Transactions on Aerospace and Electronic Systems*, vol. 55, no. 3, pp. 1241–1260, 2019.

[65] C. B. Barneto, T. Riihonen, M. Turunen, L. Anttila, M. Fleischer, K. Stadius, J. Ryynänen, and M. Valkama, "Full-duplex OFDM radar with lte and 5G NR waveforms: Challenges, solutions, and measurements," *IEEE Transactions on Microwave Theory and Techniques*, vol. 67, no. 10, pp. 4042–4054, 2019.

[66] L. Gaudio, M. Kobayashi, G. Caire, and G. Colavolpe, "On the effectiveness of OTFS for joint radar parameter estimation and communication," *IEEE Transactions on Wireless Communications*, vol. 19, no. 9, pp. 5951–5965, 2020.

[67] M. A. Richards, J. A. Scheer, W. A. Holm, B. Beckley, P. Mark, A. Richards *et al.*, "Principles of modern radar volume i-basic principles," 2010.

[68] P. M. McCormick, S. D. Blunt, and J. G. Metcalf, "Simultaneous radar and communications emissions from a common aperture, part i: Theory," in *2017 IEEE Radar Conference (RadarConf)*. IEEE, 2017, pp. 1685–1690.

[69] A. Hassanien, M. G. Amin, Y. D. Zhang, and F. Ahmad, "Phase-

modulation based dual-function radar-communications," *IET Radar, Sonar & Navigation*, vol. 10, no. 8, pp. 1411–1421, 2016.

[70] G. N. Saddik, R. S. Singh, and E. R. Brown, "Ultra-wideband multifunctional communications/radar system," *IEEE Transactions on Microwave Theory and Techniques*, vol. 55, no. 7, pp. 1431–1437, 2007.

[71] A. Hassanien, M. G. Amin, Y. D. Zhang, and F. Ahmad, "Dual-function radar-communications: Information embedding using sidelobe control and waveform diversity," *IEEE Transactions on Signal Processing*, vol. 64, no. 8, pp. 2168–2181, 2015.

[72] A. R. Al-Salehi, I. M. Qureshi, A. N. Malik, Z. Khan, and W. Khan, "Throughput enhancement for dual-function radar-embedded communications using two generalized sidelobe cancellers," *IEEE Access*, vol. 7, pp. 91 390–91 398, 2019.

[73] A. Hassanien, M. G. Amin, Y. D. Zhang, and B. Himed, "A dual-function mimo radar-communications system using PSK modulation," in *2016 24th European Signal Processing Conference (EUSIPCO)*. IEEE, 2016, pp. 1613–1617.

[74] A. Hassanien, M. G. Amin, Y. D. Zhang, F. Ahmad, and B. Himed, "Non-coherent PSK-based dual-function radar-communication systems," in *2016 IEEE Radar Conference (RadarConf)*. IEEE, 2016, pp. 1–6.

[75] T. Huang, N. Shlezinger, X. Xu, Y. Liu, and Y. C. Eldar, "MAJoRCom: A dual-function radar communication system using index modulation," *IEEE transactions on signal processing*, vol. 68, pp. 3423–3438, 2020.

[76] E. Basar, "Index modulation techniques for 5G wireless networks," *IEEE Communications Magazine*, vol. 54, no. 7, pp. 168–175, 2016.

[77] T. Huang, X. Xu, Y. Liu, N. Shlezinger, and Y. C. Eldar, "A dual-function radar communication system using index modulation," in *2019 IEEE 20th International Workshop on Signal Processing Advances in Wireless Communications (SPAWC)*, 2019, pp. 1–5.

[78] X. Wang, A. Hassanien, and M. G. Amin, "Dual-function MIMO radar communications system design via sparse array optimization," *IEEE Transactions on Aerospace and Electronic Systems*, vol. 55, no. 3, pp. 1213–1226, 2018.

[79] T. Huang, N. Shlezinger, X. Xu, D. Ma, Y. Liu, and Y. C. Eldar, "Multi-carrier agile phased array radar," *IEEE Transactions on Signal Processing*, vol. 68, pp. 5706–5721, 2020.

[80] F. Liu, C. Masouros, A. P. Petropulu, H. Griffiths, and L. Hanzo, "Joint radar and communication design: Applications, state-of-the-art, and the road ahead," *IEEE Transactions on Communications*, vol. 68, no. 6, pp. 3834–3862, 2020.

[81] T. W. Tedesso and R. Romero, "Code shift keying based joint radar and communications for EMCON applications," *Digital Signal Processing*, vol. 80, pp. 48–56, 2018.

[82] C.-Y. Chen and P. Vaidyanathan, "MIMO radar ambiguity properties and optimization using frequency-hopping waveforms," *IEEE Transactions on Signal Processing*, vol. 56, no. 12, pp. 5926–5936, 2008.

[83] G. Sharma, P. Srihari, and K. R. Rajeswari, "MIMO radar ambiguity analysis of frequency hopping pulse waveforms," in *2014 IEEE Radar Conference*. IEEE, 2014, pp. 1241–1246.

[84] K. Han and A. Nehorai, "Jointly optimal design for MIMO radar frequency-hopping waveforms using game theory," *IEEE Transactions on Aerospace and Electronic Systems*, vol. 52, no. 2, pp. 809–820, 2016.

[85] A. Hassanien, B. Himed, and B. D. Rigling, "A dual-function MIMO radar-communications system using frequency-hopping waveforms," in *2017 IEEE Radar Conference (RadarConf)*. IEEE, 2017, pp. 1721–1725.

[86] Y. Yao, X. Li, and L. Wu, "Cognitive frequency-hopping waveform design for dual-function mimo radar-communications system," *Sensors*, vol. 20, no. 2, 2020. [Online]. Available: https://www.mdpi.com/1424-8220/20/2/415

[87] I. P. Eedara, "Novel signal embedding strategies for mimo dual function radar communication systems," Ph.D. dissertation, VILLANOVA UNIVERSITY, 2021.

[88] A. Hassanien, M. G. Amin, Y. D. Zhang, and F. Ahmad, "Dual-function radar-communications: Information embedding using sidelobe control and waveform diversity," *IEEE Transactions on Signal Processing*, vol. 64, no. 8, pp. 2168–2181, 2016.

[89] T. Huang, N. Shlezinger, X. Xu, Y. Liu, and Y. C. Eldar, "MAJoRCom: A dual-function radar communication system using index modulation," *IEEE Transactions on Signal Processing*, vol. 68, pp. 3423–3438, 2020.

[90] P. Striano, C. V. Ilioudis, C. Clemente, and J. J. Soraghan, "Fractional fourier transform based joint radar communication system for multi-user automotive applications," in *2019 IEEE Radar Conference (RadarConf)*, 2019, pp. 1–6.

[91] D. Gaglione, C. Clemente, C. V. Ilioudis, A. R. Persico, I. K. Proudler, J. J. Soraghan, and A. Farina, "Waveform design for communicating radar systems using fractional fourier transform," *Digital Signal Processing*, vol. 80, pp. 57–69, 2018. [Online]. Available: https://www.sciencedirect.com/science/article/pii/S1051200418302070

[92] M. Jamil, H.-J. Zepernick, and M. I. Pettersson, "On integrated radar and communication systems using oppermann sequences," in *MILCOM 2008-2008 IEEE Military Communications Conference*. IEEE, 2008, pp. 1–6.

[93] E. J. Kaminsky and L. Simanjuntak, "Chirp slope keying for underwater communications," in *Sensors, and Command, Control, Communications, and Intelligence (C3I) Technologies for Homeland Security and Homeland Defense IV*, E. M. Carapezza, Ed., vol. 5778, International Society for Optics and Photonics. SPIE, 2005, pp. 894 – 905. [Online]. Available: https://doi.org/10.1117/12.605426

[94] S. Xu, Y. Chen, and P. Zhang, "Integrated radar and communication based on DS-UWB," in *2006 3rd International Conference on Ultrawideband and Ultrashort Impulse Signals*. IEEE, 2006, pp. 142–144.

[95] M. Roberton and E. Brown, "Integrated radar and communications based on chirped spread-spectrum techniques," in *IEEE MTT-S International Microwave Symposium Digest, 2003*, vol. 1. IEEE, 2003, pp. 611–614.

[96] F. Hu, G. Cui, W. Ye, L. Kong, Y. Huang, and L. Yuan, "Integrated radar and communication system based on stepped frequency continuous waveform," in *2015 IEEE Radar Conference (RadarCon)*. IEEE, 2015, pp. 1084–1087.

[97] Q. Zhang, X. Wang, Z. Li, and Z. Wei, "Design and performance evaluation of joint sensing and communication integrated system for 5G mmwave enabled cavs," *IEEE Journal of Selected Topics in Signal Processing*, 2021.

[98] G. Saddik and E. Brown, "Towards a multifunctional LFM waveform communication radar system: Single-crystal AIN-on-sic SAW filters for x-band," in *GOMAC Tech. Conf.*, 2005, pp. 399–402.

[99] P. Rocca, F. Yang, L. Poli, and S. Yang, "Time-modulated array antennas–theory, techniques, and applications," *Journal of Electromagnetic Waves and Applications*, vol. 33, no. 12, pp. 1503–1531, 2019.

[100] R. S. Dixon, "Argus: a next-generation omnidirectional powerful radiotelescope," *Acta Astronautica*, vol. 35, no. 9-11, pp. 745–752, 1995.

[101] J. Bregains, J. Fondevila-Gomez, G. Franceschetti, and F. Ares, "Signal radiation and power losses of time-modulated arrays," *IEEE Transactions on Antennas and Propagation*, vol. 56, no. 6, pp. 1799–1804, 2008.

[102] P. Rocca, G. Oliveri, R. J. Mailloux, and A. Massa, "Unconventional phased array architectures and design methodologies—a review," *Proceedings of the IEEE*, vol. 104, no. 3, pp. 544–560, 2016.

[103] S. S. Holland and M. N. Vouvakis, "The planar ultrawideband modular

antenna (PUMA) array," *IEEE Transactions on Antennas and Propagation*, vol. 60, no. 1, pp. 130–140, 2011.

[104] G. Li, S. Yang, Y. Chen, and Z. Nie, "A hybrid analog-digital adaptive beamforming in time-modulated linear arrays," *Electromagnetics*, vol. 30, no. 4, pp. 356–364, 2010.

[105] G. Li, S. Yang, Y. Chen, and Z.-P. Nie, "A novel electronic beam steering technique in time modulated antenna array," *Progress In Electromagnetics Research*, vol. 97, pp. 391–405, 2009.

[106] R. Maneiro-Catoira, J. C. Bregains, J. A. Garcia-Naya, and L. Castedo, "Enhanced time-modulated arrays for harmonic beamforming," *IEEE Journal of Selected Topics in Signal Processing*, vol. 11, no. 2, pp. 259–270, 2016.

[107] G. Bogdan, Y. Yashchyshyn, and M. Jarzynka, "Time-modulated antenna array with lossless switching network," *IEEE Antennas and Wireless Propagation Letters*, vol. 15, pp. 1827–1830, 2016.

[108] L. Poli, P. Rocca, G. Oliveri, and A. Massa, "Harmonic beamforming in time-modulated linear arrays," *IEEE Transactions on Antennas and Propagation*, vol. 59, no. 7, pp. 2538–2545, 2011.

[109] R. Maneiro-Catoira, J. C. Brégains, J. A. Garcia-Naya, L. Castedo, P. Rocca, and L. Poli, "Performance analysis of time-modulated arrays for the angle diversity reception of digital linear modulated signals," *IEEE Journal of Selected Topics in Signal Processing*, vol. 11, no. 2, pp. 247–258, 2016.

[110] C. Shan, Y. Ma, H. Zhao, and J. Shi, "Joint radar-communications design based on time modulated array," *Digital Signal Processing*, vol. 82, pp. 43–53, 2018.

[111] O. Gassab, A. Azrar, and S. Bouguerra, "Time modulated linear array (TMLA) design," in *Advanced Radio Frequency Antennas for Modern Communication and Medical Systems*. IntechOpen, 2020.

[112] J. Euziere, R. Guinvarc'h, M. Lesturgie, B. Uguen, and R. Gillard, "Dual function radar communication time-modulated array," in *2014 International Radar Conference*. IEEE, 2014, pp. 1–4.

[113] M. M. Sahin, I. G. Erol, E. Arslan, E. Basar, and H. Arslan, "OFDM-IM for joint communication and radar-sensing: A promising waveform for dual functionality," *Frontiers in Communications and Networks*, p. 34.

[114] P. Kumari, D. H. Nguyen, and R. W. Heath, "Performance trade-off in an adaptive IEEE 802.11 ad waveform design for a joint automotive radar and communication system," in *2017 IEEE International Conference on Acoustics, Speech and Signal Processing (ICASSP)*. IEEE, 2017, pp. 4281–4285.

[115] K. V. Mishra, M. B. Shankar, V. Koivunen, B. Ottersten, and S. A. Vorobyov, "Toward millimeter-wave joint radar communications: A signal processing perspective," *IEEE Signal Processing Magazine*, vol. 36, no. 5, pp. 100–114, 2019.

[116] P. Kumari, S. A. Vorobyov, and R. W. Heath, "Adaptive virtual waveform design for millimeter-wave joint communication–radar," *IEEE Transactions on Signal Processing*, vol. 68, pp. 715–730, 2019.

[117] B. Kihei, J. A. Copeland, and Y. Chang, "Design considerations for vehicle-to-vehicle IEEE 802.11 p radar in collision avoidance," in *2015 IEEE Global Communications Conference (GLOBECOM)*. IEEE, 2015, pp. 1–7.

[118] V. Petrov, G. Fodor, J. Kokkoniemi, D. Moltchanov, J. Lehtomaki, S. Andreev, Y. Koucheryavy, M. Juntti, and M. Valkama, "On unified vehicular communications and radar sensing in millimeter-wave and low terahertz bands," *IEEE Wireless Communications*, vol. 26, no. 3, pp. 146–153, 2019.

[119] C. D. Ozkaptan, E. Ekici, O. Altintas, and C.-H. Wang, "OFDM pilot-based radar for joint vehicular communication and radar systems," in *2018 IEEE Vehicular Networking Conference (VNC)*. IEEE, 2018, pp. 1–8.

[120] D. H. Nguyen and R. W. Heath, "Delay and doppler processing for multi-target detection with IEEE 802.11 OFDM signaling," in *2017 IEEE International Conference on Acoustics, Speech and Signal Processing (ICASSP)*. IEEE, 2017, pp. 3414–3418.

[121] S. Ghafoor, N. Boujnah, M. H. Rehmani, and A. Davy, "MAC protocols for terahertz communication: A comprehensive survey," *IEEE Communications Surveys & Tutorials*, vol. 22, no. 4, pp. 2236–2282, 2020.

[122] W. Yi, Y. Liu, Y. Deng, A. Nallanathan, and R. W. Heath, "Modeling and analysis of mmwave V2X networks with vehicular platoon systems," *IEEE Journal on Selected Areas in Communications*, vol. 37, no. 12, pp. 2851–2866, 2019.

[123] P. Popovski, O. Simeone, F. Boccardi, D. Gündüz, and O. Sahin, "Semantic-effectiveness filtering and control for post-5G wireless connectivity," *Journal of the Indian Institute of Science*, vol. 100, no. 2, pp. 435–443, 2020.

[124] M. L. Rahman, J. A. Zhang, K. Wu, X. Huang, Y. J. Guo, S. Chen, and J. Yuan, "Enabling joint communication and radio sensing in mobile networks–a survey," *arXiv preprint arXiv:2006.07559*, 2020.

[125] Y. Luo, J. A. Zhang, X. Huang, W. Ni, and J. Pan, "Multibeam optimization for joint communication and radio sensing using analog antenna arrays," *IEEE Transactions on Vehicular Technology*, vol. 69, no. 10, pp. 11 000–11 013, 2020.

[126] H. Elayan, O. Amin, B. Shihada, R. M. Shubair, and M.-S. Alouini, "Terahertz band: The last piece of RF spectrum puzzle for communication systems," *IEEE Open Journal of the Communications Society*, vol. 1, pp. 1–32, 2019.

[127] E. Grossi, M. Lops, L. Venturino, and A. Zappone, "Opportunistic radar in IEEE 802.11 ad networks," *IEEE Transactions on Signal Processing*, vol. 66, no. 9, pp. 2441–2454, 2018.

[128] Y. Yang and R. S. Blum, "MIMO radar waveform design based on mutual information and minimum mean-square error estimation," *IEEE Transactions on Aerospace and Electronic Systems*, vol. 43, no. 1, pp. 330–343, 2007.

[129] Y. Gu and Y. D. Zhang, "Information-theoretic pilot design for downlink

channel estimation in FDD massive MIMO systems," *IEEE Transactions on Signal Processing*, vol. 67, no. 9, pp. 2334–2346, 2019.

[130] Y. Liu, G. Liao, J. Xu, Z. Yang, and Y. Zhang, "Adaptive OFDM integrated radar and communications waveform design based on information theory," *IEEE Communications Letters*, vol. 21, no. 10, pp. 2174–2177, 2017.

[131] B. Donnet and I. Longstaff, "Combining MIMO radar with OFDM communications," in *2006 European radar conference*. IEEE, 2006, pp. 37–40.

[132] A. De Maio and M. Lops, "Design principles of MIMO Radar detectors," *IEEE Transactions on Aerospace and Electronic Systems*, vol. 43, no. 3, pp. 886–898, 2007.

[133] R. Xu, L. Peng, W. Zhao, and Z. Mi, "Radar mutual information and communication channel capacity of integrated radar-communication system using MIMO," *ICT Express*, vol. 1, no. 3, pp. 102–105, 2015, special Issue on Next Generation (5G/6G) Mobile Communications. [Online]. Available: https://www.sciencedirect.com/science/article/pii/S2405959515300527

[134] A. R. Chiriyath, B. Paul, G. M. Jacyna, and D. W. Bliss, "Inner bounds on performance of radar and communications co-existence," *IEEE Transactions on Signal Processing*, vol. 64, no. 2, pp. 464–474, 2015.

[135] Y. Yang and R. S. Blum, "MIMO radar waveform design based on mutual information and minimum mean-square error estimation," *IEEE Trans-*

actions on Aerospace and Electronic Systems, vol. 43, no. 1, pp. 330–343, 2007.

[136] B. Luo, Q. Cui, H. Wang, and X. Tao, "Optimal joint water-filling for coordinated transmission over frequency-selective fading channels," *IEEE Communications Letters*, vol. 15, no. 2, pp. 190–192, 2010.

[137] "[ofdm-based joint radar-communication system: Optimal sub-carrier allocation and power distribution by exploiting mutual information."

[138] E. Başar, Ü. Aygölü, E. Panayırcı, and H. V. Poor, "Orthogonal frequency division multiplexing with index modulation," *IEEE Transactions on signal processing*, vol. 61, no. 22, pp. 5536–5549, 2013.

[139] E. Basar, M. Wen, R. Mesleh, M. Di Renzo, Y. Xiao, and H. Haas, "Index modulation techniques for next-generation wireless networks," *IEEE access*, vol. 5, pp. 16 693–16 746, 2017.

[140] E. Arslan, A. T. Dogukan, and E. Basar, "Index modulation-based flexible non-orthogonal multiple access," *IEEE Wireless Communications Letters*, vol. 9, no. 11, pp. 1942–1946, 2020.

[141] A. T. Dogukan and E. Basar, "Super-mode OFDM with index modulation," *IEEE Transactions on Wireless Communications*, vol. 19, no. 11, pp. 7353–7362, 2020.

[142] E. Arslan, A. T. Dogukan, and E. Basar, "Sparse-encoded codebook index modulation," *IEEE Transactions on Vehicular Technology*, vol. 69, no. 8, pp. 9126–9130, 2020.

[143] E. Başar, "OFDM with index modulation using coordinate interleaving," *IEEE Wireless Communications Letters*, vol. 4, no. 4, pp. 381–384, 2015.

[144] P. Kumari, N. Gonzalez-Prelcic, and R. W. Heath, "Investigating the IEEE 802.11 ad standard for millimeter wave automotive radar," in *2015 IEEE 82nd Vehicular Technology Conference (VTC2015-Fall)*. IEEE, 2015, pp. 1–5.

[145] L. Yan, X. Fang, H. Li, and C. Li, "An mmwave wireless communication and radar detection integrated network for railways," in *2016 IEEE 83rd Vehicular Technology Conference (VTC Spring)*. IEEE, 2016, pp. 1–5.

[146] V. Va and R. W. Heath, "Performance analysis of beam sweeping in millimeter wave assuming noise and imperfect antenna patterns," in *2016 IEEE 84th Vehicular Technology Conference (VTC-Fall)*. IEEE, 2016, pp. 1–5.

[147] P. Kumari, J. Choi, N. González-Prelcic, and R. W. Heath, "IEEE 802.11 ad-based radar: An approach to joint vehicular communication-radar system," *IEEE Transactions on Vehicular Technology*, vol. 67, no. 4, pp. 3012–3027, 2017.

[148] J. A. Zhang, X. Huang, Y. J. Guo, J. Yuan, and R. W. Heath, "Multi-beam for joint communication and radar sensing using steerable analog antenna arrays," *IEEE Transactions on Vehicular Technology*, vol. 68, no. 1, pp. 671–685, 2019.

[149] B. D. Van Veen and K. M. Buckley, "Beamforming: A versatile approach to spatial filtering," *IEEE assp magazine*, vol. 5, no. 2, pp. 4–24, 1988.

[150] C. Sturm and W. Wiesbeck, "Waveform design and signal processing aspects for fusion of wireless communications and radar sensing," *Proceedings of the IEEE*, vol. 99, no. 7, pp. 1236–1259, 2011.

[151] A. K. Singh, S. E. Avirah, and P. Kumar, "Multi Beam Antenna System for portable 3-D Surveillance Radar," in *The Second European Conference on Antennas and Propagation, EuCAP 2007*. IET, 2007, pp. 1–4.

[152] W. Hong, Z. H. Jiang, C. Yu, J. Zhou, P. Chen, Z. Yu, H. Zhang, B. Yang, X. Pang, M. Jiang, Y. Cheng, M. K. T. Al-Nuaimi, Y. Zhang, J. Chen, and S. He, "Multibeam Antenna Technologies for 5G Wireless Communications," *IEEE Transactions on Antennas and Propagation*, vol. 65, no. 12, pp. 6231–6249, 2017.

[153] Y. A. Atesal, B. Cetinoneri, K. M. Ho, and G. M. Rebeiz, "A two-channel 8–20-GHz SiGe BiCMOS receiver with selectable IFs for multibeam phased-array digital beamforming applications," *IEEE Transactions on Microwave Theory and Techniques*, vol. 59, no. 3, pp. 716–726, 2011.

[154] C. T. Gregory, H. Charles, E. James *et al.*, "The advanced multifunction RF concept," *IEEE Transactions on microwave theory and techniques*, vol. 53, no. 3, pp. 1009–1020, 2005.

[155] G. Trunk, I. Hughes, L. PK *et al.*, "Advanced multifunction RF system (AMRFS) preliminary design considerations," *NRL, Washington, DC, Formal Rep*, pp. 5300–01, 2001.

[156] G. Tavik, "Advanced multifunction radio frequency (amrf) concept testbed overview," in *Government Microcircuit Application Conf. Dig., Mar. 2001*, 2001, pp. 100–102.

[157] L. J. WU DC, "Advanced ECM transmitter advanced technology demonstration," NRL, Washington, DC, Rep NRL/FR/5740-02-10033, Tech. Rep., 2002.

[158] D. H. Schaubert, "Wide-band phased arrays of vivaldi notch antennas," in *Tenth International Conference on Antennas and Propagation (Conf. Publ. No. 436)*, vol. 1. IET, 1997, pp. 6–12.

[159] S. Lindenmeier, J.-F. Luy, and P. Russer, "A multifunctional antenna for terrestrial and satellite radio applications," in *2001 IEEE MTT-S International Microwave Sympsoium Digest (Cat. No. 01CH37157)*, vol. 1. IEEE, 2001, pp. 393–396.

[160] P. W. Moo and D. J. DiFilippo, "Multifunction RF systems for naval platforms," *Sensors*, vol. 18, no. 7, p. 2076, 2018.

[161] A. Krayani, A. S. Alam, M. Calipari, L. Marcenaro, A. Nallanathan, and C. Regazzoni, "Automatic Modulation Classification in Cognitive-IoT Radios using Generalized Dynamic Bayesian Networks," in *2021 IEEE 7th World Forum on Internet of Things (WF-IoT)*, 2021, pp. 235–240.

[162] R. Gupta, S. Kumar, and S. Majhi, "Blind Modulation Classification for Asynchronous OFDM Systems Over Unknown Signal Parameters and Channel Statistics," *IEEE Transactions on Vehicular Technology*, vol. 69, no. 5, pp. 5281–5292, 2020.

[163] R. Bibi, Y. Saeed, A. Zeb, T. M. Ghazal, T. Rahman, R. A. Said, S. Abbas, M. Ahmad, and M. A. Khan, "Edge AI-based automated detection and classification of road anomalies in VANET using deep learning," *Computational intelligence and neuroscience*, vol. 2021, pp. 1–16, 2021.

[164] F. Song, Y. Li, W. Cheng, L. Dong, M. Li, and J. Li, "An improved kalman filter based on long short-memory recurrent neural network for

nonlinear radar target tracking," *Wireless Communications and Mobile Computing*, vol. 2022, 2022.

[165] F. Gao, T. Huang, J. Wang, J. Sun, A. Hussain, and H. Zhou, "A novel multi-input bidirectional lstm and hmm based approach for target recognition from multi-domain radar range profiles," *Electronics*, vol. 8, no. 5, p. 535, 2019.

[166] S. Zhou, Z. Yin, Z. Wu, Y. Chen, N. Zhao, and Z. Yang, "A robust modulation classification method using convolutional neural networks," *EURASIP Journal on Advances in Signal Processing*, vol. 2019, pp. 1–15, 2019.

[167] M. Kozy, J. Yu, R. M. Buehrer, A. Martone, and K. Sherbondy, "Applying deep-q networks to target tracking to improve cognitive radar," in *2019 IEEE Radar Conference (RadarConf)*. IEEE, 2019, pp. 1–6.

[168] M. Usman and J.-A. Lee, "AMC-IoT: automatic modulation classification using efficient convolutional neural networks for low powered IoT devices," in *2020 International Conference on Information and Communication Technology Convergence (ICTC)*. IEEE, 2020, pp. 288–293.

[169] C. Roy, S. S. Yadav, V. Pal, M. Singh, S. K. Patra, G. Sinha *et al.*, "An Ensemble Deep Learning Model for Automatic Modulation Classification in 5G and Beyond IoT Networks," *Computational Intelligence and Neuroscience*, vol. 2021, 2021.

[170] T. J. O'Shea, J. Corgan, and T. C. Clancy, "Convolutional radio modulation recognition networks," in *Engineering Applications of Neural*

Networks: 17th International Conference, EANN 2016, Aberdeen, UK, September 2-5, 2016, Proceedings 17. Springer, 2016, pp. 213–226.

[171] D. Hong, Z. Zhang, and X. Xu, "Automatic modulation classification using recurrent neural networks," in *2017 3rd IEEE International Conference on Computer and Communications (ICCC)*. IEEE, 2017, pp. 695–700.

[172] D. Zhang, W. Ding, B. Zhang, C. Xie, H. Li, C. Liu, and J. Han, "Automatic modulation classification based on deep learning for unmanned aerial vehicles," *Sensors*, vol. 18, no. 3, p. 924, 2018.

[173] L. Xie and Q. Wan, "Cyclic feature-based modulation recognition using compressive sensing," *IEEE Wireless Communications Letters*, vol. 6, no. 3, pp. 402–405, 2017.

[174] J. C. Clement, N. Indira, P. Vijayakumar, and R. Nandakumar, "Deep learning based modulation classification for 5G and beyond wireless systems," *Peer-to-peer networking and applications*, vol. 14, pp. 319–332, 2021.

[175] S. Peng, H. Jiang, H. Wang, H. Alwageed, Y. Zhou, M. M. Sebdani, and Y.-D. Yao, "Modulation classification based on signal constellation diagrams and deep learning," *IEEE Transactions on Neural Networks and Learning Systems*, vol. 30, no. 3, pp. 718–727, 2019.

[176] D. Zhang, W. Ding, B. Zhang, C. Xie, H. Li, C. Liu, and J. Han, "Automatic modulation classification based on deep learning for unmanned aerial vehicles," *Sensors*, vol. 18, no. 3, 2018.

[177] D. Hong, Z. Zhang, and X. Xu, "Automatic modulation classification using recurrent neural networks," in *2017 3rd IEEE International Conference on Computer and Communications (ICCC)*, 2017, pp. 695–700.

[178] F. Meng, P. Chen, L. Wu, and X. Wang, "Automatic modulation classification: A deep learning enabled approach," *IEEE Transactions on Vehicular Technology*, vol. 67, no. 11, pp. 10 760–10 772, 2018.

[179] A. Hassanien, M. G. Amin, E. Aboutanios, and B. Himed, "Dual-function radar communication systems: A solution to the spectrum congestion problem," *IEEE Signal Processing Magazine*, vol. 36, no. 5, pp. 115–126, 2019.

[180] J. G. Proakis, *Digital communications*. McGraw-Hill, Higher Education, 2008.

[181] J.-M. Kang, C.-J. Chun, and I.-M. Kim, "Deep Learning Based Channel Estimation for MIMO Systems With Received SNR Feedback," *IEEE Access*, vol. 8, pp. 121 162–121 181, 2020.

[182] A. H. Shah, A. H. Miry, and T. M. Salman, "Automatic modulation classification based deep learning with mixed feature." *International Journal of Electrical & Computer Engineering (2088-8708)*, vol. 13, no. 2, 2023.

[183] J. Krzyston, R. Bhattacharjea, and A. Stark, "Complex-valued convolutions for modulation recognition using deep learning," in *2020 IEEE International Conference on Communications Workshops (ICC Workshops)*. IEEE, 2020, pp. 1–6.

[184] S.-H. Kim, J.-W. Kim, W.-P. Nwadiugwu, and D.-S. Kim, "Deep

learning-based robust automatic modulation classification for cognitive radio networks," *IEEE access*, vol. 9, pp. 92 386–92 393, 2021.

[185] H. L. Van Trees, *Optimum array processing: Part IV of detection, estimation, and modulation theory*. John Wiley & Sons, 2002.

[186] M. F. Munir, A. Basit, W. Khan, A. Saleem, and A. Al-salehi, "A comprehensive study of past, present, and future of spectrum sharing and information embedding techniques in joint wireless communication and radar systems," *Wireless Communications and Mobile Computing*, vol. 2022, 2022.

[187] A. Hassanien, M. G. Amin, E. Aboutanios, and B. Himed, "Dual-function radar communication systems: A solution to the spectrum congestion problem," *IEEE Signal Processing Magazine*, vol. 36, no. 5, pp. 115–126, 2019.